

**Determination of clouds in MSG data  
for the validation of clouds in a regional  
climate model**

Zur Erlangung des akademischen Grades eines  
DOKTORS DER NATURWISSENSCHAFTEN  
der Fakultät für Physik der  
Universität Karlsruhe (TH)

genehmigte

DISSERTATION

von

Dipl.-Met. Roger Huckle  
aus Lindau (Bodensee)

Tag der mündlichen Prüfung: 22.05.2009

Referent Prof. Dr. H. Fischer

Korreferent Prof. Dr. Ch. Kottmeier



## Abstract

On numerous occasions, e.g. the IPCC reports or the Stern report, the imminent anthropogenic climate change has been brought to a wide public attention. Regional climate models can help to assess the influence of such a climate change on the different regions of the earth. The validation of these models with measurements is very important. Satellite data are of great benefit in this case, as data on a global scale and high temporal resolution (if necessary) is available.

The satellites of the METEOSAT series have continuously measured the state of the atmosphere as well as the land and sea surfaces over the past 30 years. With the second generation (MSG) in operation and the third generation (MTG) in preparation another 30 years of consistent measurements can be expected. This unique data set is ideal for climate analysis and for the validation of climate models.

In this work an automated cloud mask for the detection of cloud filled pixels in the MSG data was developed. This cloud mask was compared to other MSG cloud masks. The results showed a good agreement between the IMK cloud mask, the cloud mask from EUMETSAT's Now Casting SAF and the cloud mask from the FU Berlin.

At the IMK research work with the climate version of the regional weather prediction model ('Lokal Model' (LM)) from the DWD has been in progress for some years. For the year 2005 the model was run with a 7 km horizontal resolution for an area including all of Germany and the Alps. The IMK cloud mask was used to validate the cloud cover in the CLM data.

A number of comparisons between IMK cloud mask and CLM cloud data was performed. A special interest was on convective situations, especially convection developing in southwest Germany. The detection of convective clouds in satellite data is good, due to cold cloud tops and high reflection of sunlight. Current numerical models have problems modelling convection correctly, one of the reasons being the horizontal resolution which is mostly larger than the initial convective processes. The validation results for convective days therefore is lower than for non convective days.

The comparison on pixel by pixel basis has its drawbacks, as only a slight shift in time and space between model and measurement results in a disagreement, even if the modelled data represent the current situation in an adequate way. Therefore an object based analysis was introduced.

The clouds in the MSG data were classified using an object based image analysis (OBIA). Special interest again was on convective clouds. Automated cloud classification algorithms were developed enabling the analysis of large data sets. The results of the MSG classification were used to validate the CLM data this time on an object basis. A better validation is possible, also detecting the 'wrong' type of clouds in model data.



# Zusammenfassung

Bei zahlreichen Gelegenheiten, z.B. dem IPCC Report oder dem Stern Report, wurde der drohende anthropogene Klimawandel ins öffentliche Bewusstsein gerückt. Regionale Klimamodelle können helfen, den Einfluss eines solchen Klimawandels auf verschiedene Regionen der Erde abzuschätzen. Die Validierung dieser Modelle mit Messungen ist sehr wichtig. Satellitendaten sind in diesem Fall von großem Nutzen, da diese in einem globalem Maßstab und (wenn nötig) in einer hohen zeitlichen Auflösung vorliegen.

Die Satelliten der METEOSAT Reihe haben den Zustand der Atmosphäre, sowie der Land- und Meeresoberflächen kontinuierlich über die vergangenen 30 Jahre gemessen. Mit der zweiten Generation (METEOSAT Second Generation - MSG) im operationellen Betrieb und der dritten Generation (MTG, in Planung) sind weitere 30 Jahre konsistente Messungen zu erwarten. Dieser einmalige Datensatz ist ideal für Klimaanalysen und die Validierung von Klimamodellen.

In dieser Arbeit wurde eine automatisierte Wolkenmaske für die Erkennung bewölkter Pixel in den MSG Daten entwickelt. Diese Wolkenmaske wurde mit anderen MSG Wolkenmasken verglichen. Die Ergebnisse zeigen eine gute Übereinstimmung zwischen der IMK Wolkenmaske und den Wolkenmasken der FU Berlin bzw. von EUMETSATs Now Casting SAF.

Am IMK wurde in den vergangenen Jahren intensiv mit der Klimaversion des Lokal Modells des DWD gearbeitet. Für das Jahr 2005 wurde das Modell mit einer Auflösung von 7x7 km in der Horizontalen betrieben. Das Gebiet umfasste ganz Deutschland, Teile der angrenzenden Länder und die komplette Alpenregion. Die IMK Wolkenmaske wurde für die Validierung der Wolkenbedeckung im CLM verwendet.

Eine Reihe von Vergleichen zwischen IMK Wolkenmaske und CLM Wolkenbedeckung wurde durchgeführt. Ein besonderes Augenmerk lag auf konvektiven Situationen, insbesondere Konvektion die in Südwestdeutschland ihren Ursprung hatte. Die Erkennung von Konvektion, in Satellitendaten ist gut möglich, da die Wolkenoberseiten kalt sind und das Sonnenlicht gut reflektieren. Aktuelle numerische Modelle haben Probleme mit der korrekten Modellierung von Konvektion. Einer der Gründe ist die im Vergleich mit den konvektiven Prozessen recht große horizontale Auflösung. Die Validierungsergebnisse der konvektiven Tage sind daher auch geringer als an Tagen ohne Konvektion.

Der Vergleich auf Pixelbasis hat seine Nachteile, da zum Beispiel schon eine kleine horizontale Verschiebung zwischen Modell und Messung zu einem schlechten Validierungsergebnis führt, selbst wenn die Abweichungen nur minimal sind. Daher bietet sich eine Objektbasierte Analyse an.

Die Wolken in den MSG Daten wurden mit Hilfe einer Objektbasierten Bildanalyse (OBIA) klassifiziert. Wiederum waren konvektive Wolken im Mittelpunkt des Interesses. Eine automatisierte Wolkenanalyse wurde entwickelt, welche die Analyse großer

Datenmenge ermöglicht. Die Ergebnisse der MSG Klassifizierung wurden auch verwendet, um die CLM Daten zu validieren, diesmal auf Objektbasis. Dies erlaubt auch die Validierung der modellierten Wolkenart.

# Contents

<b>1</b>	<b>Introduction</b>	<b>1</b>
<b>2</b>	<b>Basic Radiation Principles</b>	<b>4</b>
2.1	Black Body Laws . . . . .	5
2.2	Radiative Transfer . . . . .	6
2.3	Atmospheric Windows . . . . .	8
<b>3</b>	<b>METEOSAT Second Generation (MSG)</b>	<b>12</b>
3.1	Spinning Enhanced Visible and Infrared Imager (SEVIRI) . . . . .	13
<b>4</b>	<b>CLM - a Regional Climate Model</b>	<b>17</b>
<b>5</b>	<b>Areas of interest</b>	<b>20</b>
5.1	Development area for MSG cloud mask . . . . .	20
5.2	Regional climate model (CLM) area . . . . .	20
<b>6</b>	<b>Automated cloud mask for MSG</b>	<b>22</b>
6.1	Dynamic threshold in IR 10.8 $\mu\text{m}$ channel . . . . .	23
6.2	Dynamic threshold in VIS 0.6 $\mu\text{m}$ channel . . . . .	28
6.3	Thin cirrus detection . . . . .	29
6.4	Fog detection during night . . . . .	31

6.5	Use of the channel difference $IR_{039} - IR_{108}$ . . . . .	31
6.6	Snow detection . . . . .	32
6.7	Special meteorological situations . . . . .	32
6.8	Further possibilities of cloud detection . . . . .	35
6.9	Detection of dust clouds, sun glint and other special cases . . . . .	35
<b>7</b>	<b>Validation of the IMK cloud mask</b>	<b>38</b>
7.1	Validation with MSG cloud mask from FU Berlin . . . . .	38
7.2	Validation with Now Casting SAF cloud mask . . . . .	44
<b>8</b>	<b>Comparison between MSG and CLM data</b>	<b>55</b>
8.1	Convective situations . . . . .	58
8.1.1	Monthly analysis . . . . .	59
8.1.2	Point comparison . . . . .	62
8.2	Spatial averaging . . . . .	67
8.3	Day and Night comparisons . . . . .	68
8.4	Special case: June and July 2005 . . . . .	70
<b>9</b>	<b>Cloud types</b>	<b>74</b>
<b>10</b>	<b>Object Based Image Analysis</b>	<b>79</b>
10.1	Cloud analysis . . . . .	81
10.1.1	Cumulonimbus (Cb) . . . . .	81
10.1.2	Thin Cirrus (Ci) . . . . .	83
10.1.3	High and low Cumulus (Cu) . . . . .	86
10.1.4	Thunderstorms and fields of Cumuli . . . . .	87
10.1.5	Non convective clouds . . . . .	89
10.2	Object based comparison of MSG and CLM . . . . .	89

<i>CONTENTS</i>	III
<b>11 Conclusions</b>	<b>95</b>
<b>12 Literature</b>	<b>99</b>



# Chapter 1

## Introduction

Perhaps the biggest challenge for human society in the next decades is the imminent climate change. The effects on every day life can be significant (Stern, 2006). How big the impact is depends on the region and industrial and technical development of the society. To quantify the climate change for a specific region, the use of a regional climate model is advisable.

Out of the 'Lokal Modell' (LM) from the German Weather Service (DWD) a regional climate model, the CLM, was developed. With this non-hydrostatic model the climate changes can be modelled on a regional scale.

As with every model the validation of the model results is very important for the quality and further development of the model. One value of the model output, the cloud cover, will be validated in this thesis. For the validation data from EUMETSAT's METEOSAT Second Generation (MSG) satellite METEOSAT-8 was used.

Clouds are perhaps the most prominent part of the atmospheric water cycle. Clouds can easily be detected by humans from the ground. From space the detection of most clouds is also possible. An automated cloud detection in satellite data is not trivial, therefore threshold tests and spectral analysis were generated. The effects of the possible climate change on the atmospheric water cycle can be manifold. In general a higher air temperature would enable the atmosphere to carry more water. Higher temperatures also mean a higher energy level. More and more severe thunderstorms can be the result. Also the distribution and intensity of precipitation can change. What exactly will happen when temperatures rise is still uncertain.

The satellites of the METEOSAT series have continuously measured the state of the atmosphere as well as the land and sea surfaces over the past 30 years. With the second generation in operation and the third generation (MTG) in preparation another 30 years of consistent measurements can be expected. This unique data set is ideal for climate analysis.

For the validation of the CLM data a cloud detection algorithm on pixel basis was developed. This cloud mask for MSG data uses data from seven channels from the SEVIRI instrument onboard MSG. The majority of the clouds is detected in the infrared and visible part of the spectrum with dynamic thresholds for every individual pixel that are calculated using solely MSG data. For every 15 minute time slot a 30 day gliding window at that specific time is used to calculate statistical values which are then used to generate a diurnal cycle for every pixel. Further tests if a pixel is cloudy include channel differences to detect thin cirrus clouds or fog at night.

Every pixel marked as cloudy is later checked if the pixel really contains clouds or if snow covered ground is detected. For this the near infrared channel is used. At  $1.6\mu m$  the reflective characteristics of snow and water droplets in clouds are very different. Water droplets reflect the sun light just as good as in the visible part of the spectrum, but snow does not. Snow appears 'black' in the near infrared. The difficulty is now to determine whether the snow or ice is on the ground or in the air (ice topped clouds).

To verify the functionality of the cloud mask, it was compared with two other cloud masks for MSG. One was from the FU Berlin, the other from EUMETSAT's Now Casting SAF. The cloud mask from Berlin has a similar physical approach using only MSG data and creating dynamic thresholds for the analysis of the IR channels. The SAF cloud mask uses next to the MSG data also data from weather prediction models to generate an expected clear sky radiance with which the measured value is then compared. The advantage is that also for untypical weather situations or for areas with a high amount of clouds a reliable threshold can be found for the infrared channels. The disadvantage, on the other hand, is that the cloud detection is dependant on external data. For the specific task of validating the regional climate model data against measured satellite data, the use of an different numerical model as a major contributor to to the cloud detection algorithm is not adequate.

A major aspect for the comparison between CLM and MSG cloud mask was the performance of the CLM during convective situations. For this purpose a number of 28 days between March and October 2005 were picked on which convective clouds developed in the region of southwest Germany. These convective clouds developed in the absence of frontal systems only due to the heating of the ground or the overflow of the mountain ridges. The modelling of convection is difficult, many processes have not yet been fully understood and the model resolution is often too coarse to describe the triggering of convection. Numerous field campaigns have taken place in the area of the Black Forest and the Swabian Alb, to obtain more information concerning convection over complex terrain.

The pixel by pixel comparison between the cloud mask and the CLM data has the disadvantage that the model does not necessarily model the clouds exactly at the right pixel at the right time. A small shift in time and space does not imply that the model does not work. Especially for climate issues the exact position of a cloud is not so important. More important is the ability of the CLM to model the correct amount of clouds over a certain area within a certain time, for example the developing convection

over the Black Forest. A pixel based comparison can not show these time and spatial shifts appropriately.

The use of object based image analysis (OBIA) can help solve some of these problems. In OBIA neighbouring pixels with similar spectral characteristics are grouped together to form meaningful objects. In addition to the spectral values a single pixel has, an object also has statistical values (mean, standard deviation, etc.) as well as geometrical features, e.g. area, border length or length to width ratio. Performing this object creation on different scales, i.e. creating levels with different sized objects, a hierarchical component is introduced. When analysing images on an object basis more information is available and a better classification can be achieved.

The object based image analysis is used to classify clouds in MSG image, but also to compare CLM and MSG data on object basis. This enables a better validation of the CLM clouds because here the amount of clouds in an image object can be compared, thus spatial shifts between the two data sets do not come into play.

For the development of the cloud mask and the comparison between the different data sets, measurements from March to October 2005 was used.

# Chapter 2

## Basic Radiation Principles

Remote sensing is based on the principle of gathering information about an object without having direct physical contact. The simplest form of remote sensing is looking. The eye (sensor) sees things by way of electromagnetic radiance emitted or reflected by an object. The use of electromagnetic waves for remote sensing is by far the most common but the use of other carrier medium (e.g. sound) is also possible. The METEOSAT second generation (MSG) satellites measure in the 'visible', 'near infrared' and 'infrared' part of the electromagnetic spectrum (see chapter 3 for details). The source of the electromagnetic waves is either reflected sun light or emitted terrestrial radiation from the surface and/or from atmosphere volumes. Satellite sensors measure 'Top Of Atmosphere' (TOA) radiances in the IR. These radiances can be expressed in Brightness Temperature (BT). The emitted radiances from the earth's surface are modulated on their way to the sensor by the atmosphere, in some cases (e.g. clouds) the surface radiation is completely absorbed and the source of the measured radiation is the top of the cloud. In order to retrieve information close to the surface from TOA radiances the influence of the atmosphere has to be extracted (Dash et al., 2002; Cracknell and Hayes, 1991).

The electromagnetic spectrum can be divided up into several parts (Tab. 2.1). Most important for us is the visible part, enabling us to see, mostly reflected light. For scientific purposes the other parts of the spectrum have great importance. In the infrared part terrestrial radiation is dominant and transports information about the earth's surface and the atmosphere. At microwave wavelength the penetration through clouds and into the ground with active sensors is possible. The use of passive microwave instruments can also be an important source of information. Depending on the scientific area the naming of these intervals can vary.

**Table 2.1:** *Principal Division of the Electromagnetic Spectrum (after Campbell, 2002 and Meschede, 2006)*

Division	Limits
Gamma rays	< 0.03 nm
X-rays	0.03-300 nm
Ultraviolet radiation	0.30 – 0.38 $\mu\text{m}$
Visible light	0.38 – 0.72 $\mu\text{m}$
Infrared radiation	
Near infrared	0.72 – 5.0 $\mu\text{m}$
Mid infrared	5 – 40 $\mu\text{m}$
Far infrared	40 – 1000 $\mu\text{m}$
Microwave radiation	1 mm-30 cm
Radio	$\geq$ 30 cm

## 2.1 Black Body Laws

A black body is defined as an object where absorption is complete. Emission by a black body is the converse of absorption. The emitted energy of a black body in relation to wavelength and temperature is given by the **Planck function** (Liou, 2002):

$$B_{\lambda}(T) = \frac{2hc^2}{\lambda^5} \cdot \frac{1}{\exp\left(\frac{hc}{K\lambda T}\right) - 1} \quad (2.1)$$

$$\begin{aligned} K &= 1,3806 \cdot 10^{-23} \frac{J}{K} && \text{Boltzmann's constant} \\ c &= 2,998 \cdot 10^8 \frac{m}{s} && \text{speed of light in vacuum} \\ h &= 6,626 \cdot 10^{-34} Js && \text{Planck constant} \end{aligned}$$

When plotting the black body radiance (Planck function) for different temperatures as a function of the wavelength (see Fig. 2.1) a peak radiation shows up. The black body radiation increases with temperature and the wavelength of maximum intensity decreases with increasing temperature. Towards short wavelengths a steep decrease and towards long wavelengths a slower and longer decrease can be observed. Integrating the Planck function over the entire spectrum we receive the flux density for a black body, the **Stefan-Boltzmann law**:

$$F = \pi \int_0^{\infty} B_{\lambda}(T) d\lambda = \sigma T^4 \quad (2.2)$$

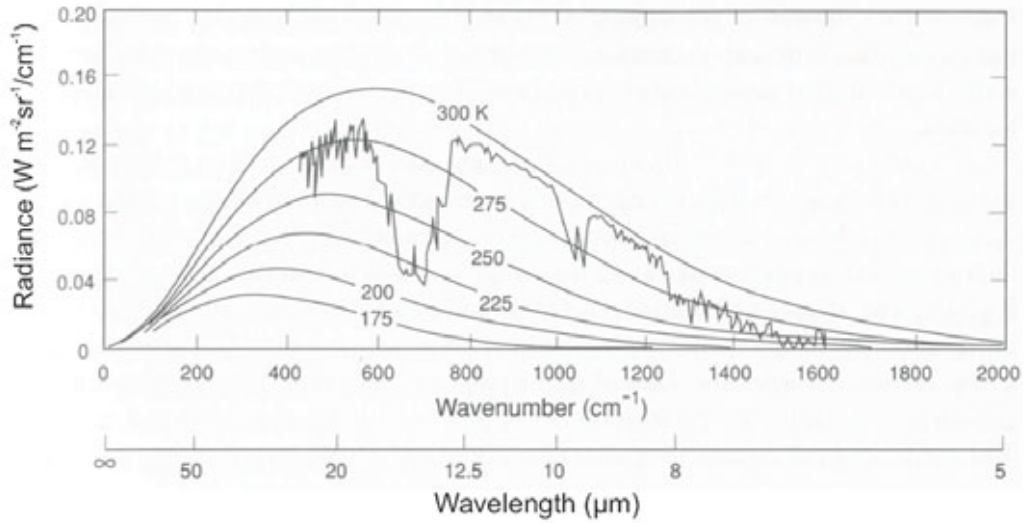


**Figure 2.1:** *Theoretical Planck radiance curves for a number of the earth’s atmospheric temperatures as a function of wave number and wavelength. Also shown is a thermal infrared emission spectrum observed from the Nimbus 4 satellite based on an infrared interferometer spectrometer (Liou, 2002).*

where  $\sigma = 5.67 \cdot 10^{-8} \text{Wm}^{-2}\text{K}^{-4}$  is the Stefan-Boltzmann constant. The statement of Equation 2.2 that the flux density is proportional to the fourth power of the absolute temperature is fundamental to the analysis of broadband infrared radiative transfer.

The wavelength of the maximum intensity of black body radiation can be found by differentiation of Eq. 2.1 with respect to the wavelength. The wavelength of the maximum  $\lambda_{max}$  results to:

$$\lambda_{max} = \frac{2897,8 \mu\text{mK}}{T}. \quad (2.3)$$

This Equation states that with higher temperature the maximum of the radiation moves to shorter wavelengths, this is in accordance to Figure 2.1. The temperature of a black body can be determined by measuring the maximum monochromatic intensity. Equation 2.3 is **Wien’s displacement law**.

## 2.2 Radiative Transfer

Radiation emitted at the earth surface travelling upwards through the atmosphere is subject to modification by the atmosphere. Absorption and scattering will attenuate

the radiation, on the other hand emission and scattering into the pathway will enhance the radiation intensity. The channel radiance for a non scattering atmosphere measured by a satellite sensor at the top of the atmosphere is given by the radiative transfer equation (RTE):

$$\begin{aligned}
 L_{\Delta\lambda} = \varepsilon_{\Delta\lambda} B_{\Delta\lambda}(T_s) \tau_{\Delta\lambda}(0, H^\infty) &+ \int_0^{H^\infty} B_{\Delta\lambda}(T(H)) \frac{\delta\tau_{\Delta\lambda}(H, H^\infty)}{\delta H} dH \\
 &+ (1 - \varepsilon_{\Delta\lambda}) \tau_{\Delta\lambda}(0, H^\infty) \int_{H^\infty}^0 B_{\Delta\lambda}(T(H)) \frac{\delta\tau_{\Delta\lambda}(H, H^\infty)}{\delta H} dH
 \end{aligned} \tag{2.4}$$

$L_{\Delta\lambda}$	:	received radiance by the detector in the spectral interval $\Delta\lambda$
$\Delta\lambda$	:	spectral interval
$\varepsilon_{\Delta\lambda}$	:	spectral emissivity of the earth surface
$\tau_{\Delta\lambda}(0, H^\infty)$	:	spectral transmissivity of the atmosphere
$\tau_{\Delta\lambda}(H, H^\infty)$	:	spectral transmissivity of the atmosphere between the height $H$ and the top of the atmosphere
$H$	:	height
$B(T)$	:	temperature dependant Planck function
$T_s$	:	surface temperature

Equation 2.4 defines the radiance along a vertical pencil beam through the atmosphere from  $H = 0$  (earth's surface) to  $H = H^\infty$  (top of atmosphere), for a slant beam the path length has to be taken into account. The first term on the right hand side in Eq. 2.4 denotes the temperature dependant black body radiation of the earth's surface multiplied by the surface emissivity and the transmissivity of the atmosphere between the point of emission and the sensor. The second term stands for the radiance emitted from the atmosphere in direction of the sensor. In the third term the downward emitted part of the atmospheric radiation, which is reflected in direction of the sensor is described. To solve the equation, the surface emissivity and the atmospheric transmissivity is necessary.

In the case of clouds the surface radiation is altered significantly. For optical thick clouds the absorption is complete and no information from the earth's surface is transmitted through the cloud. This is not the case for optically thin clouds, here radiation from the earth's surface is modulated, some weakening takes place and radiation emitted by the cloud top is added. This is described by the following equation, neglecting atmospheric emission/absorption above the cloud and scattering within the cloud the radiance at a frequency  $\nu$  in the atmospheric window for thin clouds is (Saunders and Kriebel, 1988 and Platt (1975)):

$$L_\nu = (1 - \varepsilon_c(\nu, \theta, \phi))L_\nu^{CLR} + \varepsilon_c(\nu, \theta, \phi)B_\nu(T_c) \quad (2.5)$$

where  $\varepsilon_c$  is the emissivity of the cloud top. Variations in  $\varepsilon_c$  with frequency will lead to differences between different channels for the same cloud. This can be used for the detection of clouds (see chapter 6).

## 2.3 Atmospheric Windows

The atmosphere consist of a mixture of several gases, some with a homogeneous distribution (e.g. O<sub>2</sub>) others vary considerably in time and space (e.g. H<sub>2</sub>O)(see Table 2.2). Every gas has different characteristics in terms of absorption of radiation, i.e. each gas has individual spectral intervals in which it absorbs radiation. The combination of all gases in the earth's atmosphere leads to areas in the electromagnetic spectrum, where absorption is complete and others, where modulation of radiation (upwelling or downwelling) is only very small. In these areas, the so called 'atmospheric windows', the transmittance is high and absorption by the cloud free atmosphere low. In the short wavelength part of the spectrum the most important atmospheric window ranges from 0.35  $\mu\text{m}$  to 0.9  $\mu\text{m}$  (Fig. 2.2). Towards the shorter wavelengths stratospheric ozone absorbs all radiation. Within the short wave atmospheric window Rayleigh scattering on air molecules takes place, also extinction due to scattering on aerosols and absorption due to water vapour happens. The maximum of the solar radiation is at 0.55  $\mu\text{m}$ , exactly in the atmospheric window, hence most of the suns radiation reaches the earth's surface. Sensors on satellites measuring the earth's surface reflectance therefore have their channels in this atmospheric window.

In the infrared part of the electromagnetic spectrum two main atmospheric windows exist. One ranges from 3.0  $\mu\text{m}$  to 4.2  $\mu\text{m}$  and the other from 8.0  $\mu\text{m}$  to 13.0  $\mu\text{m}$ . For a surface temperature of 300 K the maximum of terrestrial radiation lies at approx. 9.7  $\mu\text{m}$  (Eq. 2.3). Again this is in the atmospheric window, allowing most of the terrestrial radiation to escape into space. Due to the increase of CO<sub>2</sub> in the last decades, the atmospheric windows in the infrared have become less transparent, resulting in a greenhouse effect, letting in the solar radiation, but trapping the terrestrial radiation thus increasing the temperature of the earths atmosphere. Researching the effects of climate change on the atmospheric water cycle is one of the main aims of this project.

For measuring the reflectance of the solar radiation from the earth into space, the reflection intensity is important. The suns surface has a temperature of approx. 5800 K. The fraction of the solar irradiance from the sun ( $S_{Sun}$ ) that reaches the Earth's surface depends on the opening angle  $\alpha$  at the Sun's disc ( $\alpha = 0.267$ ), part of which is homogeneously reflected over the halfspace  $S_{half}$  ( $S_{half} = 2\pi \cdot sr$ ). The amount of solar irradiance reaching the earth's surface (only from the sky geometry; the atmospheric effect is not considered) is determined by  $S_{Sun}/S_{half}$ . Figure 2.3 shows the geometry

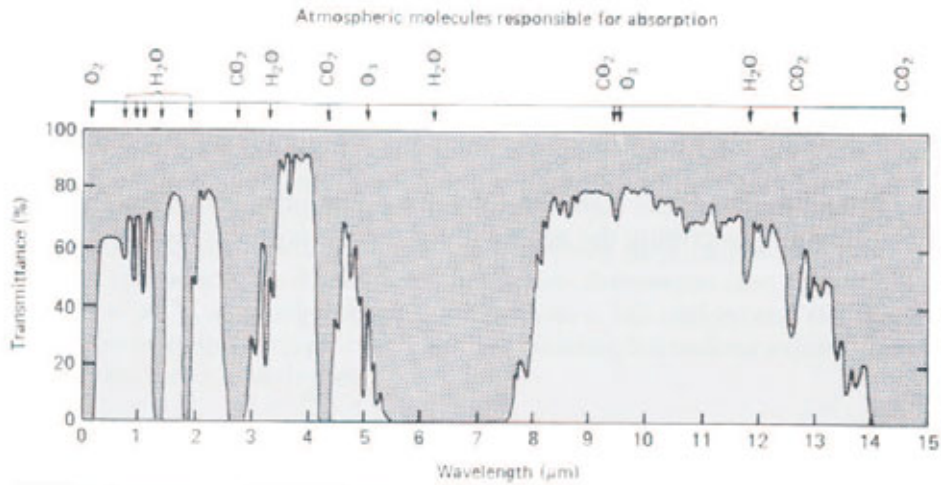


**Figure 2.2:** Transparency of the atmosphere and main absorbing molecules. The most important atmospheric windows range from  $0.35 \mu\text{m}$  to  $0.9 \mu\text{m}$  (corresponding to the peak solar irradiation) and from  $8.0 \mu\text{m}$  to  $13.0 \mu\text{m}$  (maximum of terrestrial radiation).

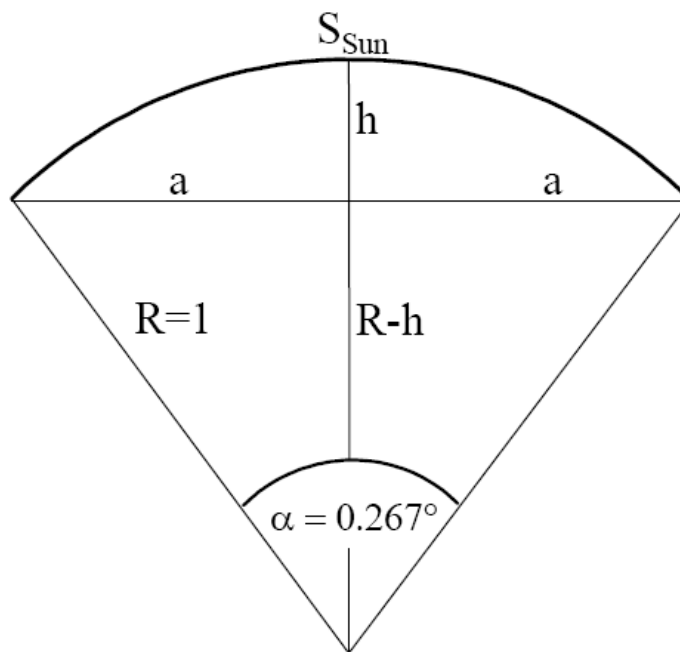


**Figure 2.3:** Geometry for deriving the fraction of Sun's irradiance that reaches Earth's surface. With sun radius  $R$  and an opening angle  $\alpha = 0.267^\circ$ .

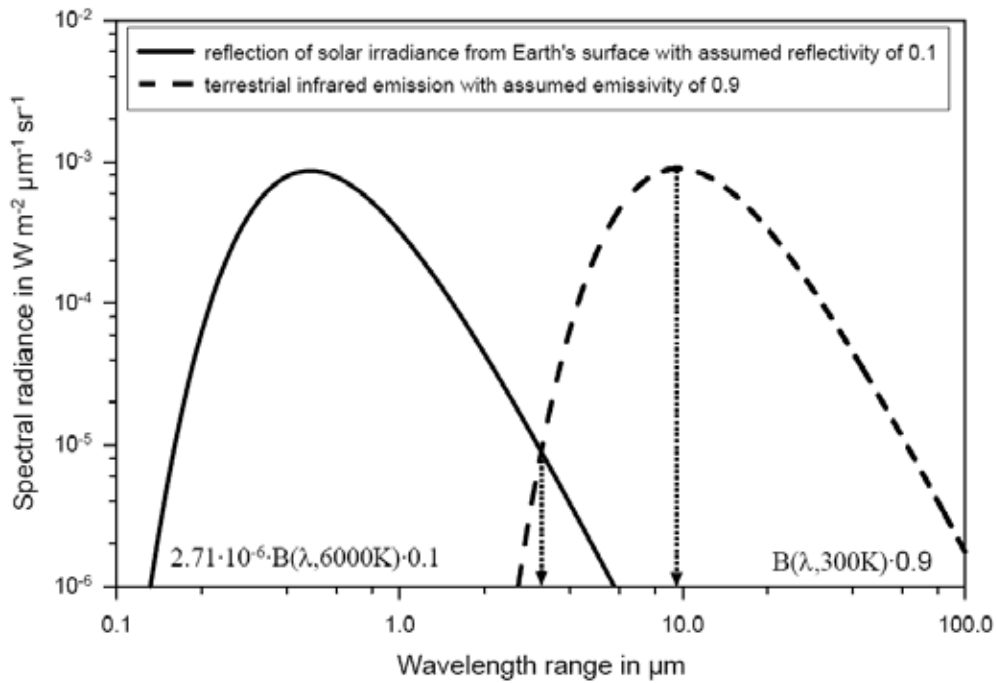


**Figure 2.4:** Reflection of solar irradiance from Earth's surface with assumed reflectivity of 0.1 (solid line), and infrared terrestrial emission with assumed emissivity of 0.9 (dashed line). The terrestrial emission is maximum at about  $9.7\mu\text{m}$ , and reflection of solar irradiance and terrestrial emission are of same order of magnitude at about  $3.8\mu\text{m}$ .

used to derive the fraction of solar irradiance reaching the earth's surface.  $S_{Sun}$  denotes the segment of the sky covered by the Sun on a unit sphere centered on the earth's surface.  $S_{Sun}$  is determined by the opening angle  $\alpha = 0.267^\circ$  (exaggerated in the figure). Using the relation  $S_{Sun} = \pi \cdot (h^2 + a^2)$ ,  $a = \sin(\alpha/2)$ , and  $h = 1 - \cos(\alpha/2)$ , yields  $(S_{Sun}/S_{half}) = 1.7 \cdot 10^{-5}/2\pi = 2.71 \cdot 10^{-6}$  which is the factor multiplied by total solar irradiance for deriving the fraction reaching the Earth.

This leads to a spectral intensity distribution, as shown in Fig. 2.4. The dashed line represents the terrestrial emission with an assumed emissivity of 0.9. At  $3.8\mu\text{m}$  the two curves cross. Therefore the MSG channel  $IR_{039}$  is sensitive to solar and terrestrial radiation (see chapters 3.1 and 6.5).

**Table 2.2:** *The chemical composition of the atmosphere (after U.S. Standard Atmosphere (1976) with modifications) (Liou, 2002). <sup>a</sup> Concentration near earth's surface.*

Permanent constituents		Variable constituents	
Constituent	% by volume	Constituent	% by volume
Nitrogen(N <sub>2</sub> )	78.084	Water vapour (H <sub>2</sub> O)	0 - 4
Oxygen (O <sub>2</sub> )	20.948	Ozone (O <sub>3</sub> )	0-12 · 10 <sup>-4</sup>
Argon (Ar)	0.934	Sulfur dioxide (SO <sub>2</sub> ) <sup>a</sup>	0.001 · 10 <sup>-4</sup>
Carbon dioxide (CO <sub>2</sub> )	0.036	Nitrogen dioxide (NO <sub>2</sub> ) <sup>a</sup>	0.001 · 10 <sup>-4</sup>
Neon (Ne)	18.18 · 10 <sup>-4</sup>	Ammonia (NH <sub>3</sub> ) <sup>a</sup>	0.004 · 10 <sup>-4</sup>
Helium (He)	5.24 · 10 <sup>-4</sup>	Nitric oxide (NO) <sup>a</sup>	0.0005 · 10 <sup>-4</sup>
Krypton (Kr)	1.14 · 10 <sup>-4</sup>	Hydrogen sulfide (H <sub>2</sub> S) <sup>a</sup>	0.00005 · 10 <sup>-4</sup>
Xenon (Xe)	0.089 · 10 <sup>-4</sup>	Nitric acid vapour (HNO <sub>3</sub> )	Trace
Hydrogen (H <sub>2</sub> )	0.5 · 10 <sup>-4</sup>	Chlorflouorocarbons	Trace
Methane (CH <sub>4</sub> )	1.7 · 10 <sup>-4</sup>	(CFCl <sub>3</sub> , CF <sub>2</sub> Cl <sub>2</sub>	
Nitrous oxide (N <sub>2</sub> O)	0.3 · 10 <sup>-4</sup>	CH <sub>3</sub> CCl <sub>3</sub> , CCl <sub>4</sub> , etc.)	
Carbon monoxide (CO)	0.08 · 10 <sup>-4</sup>		

# Chapter 3

## METEOSAT Second Generation (MSG)

Satellites enable the continuous observation of the earth's atmosphere and surface. Depending on the satellite orbit (geostationary or polar orbiting) and the instruments being carried, this observation can have anything in between a high temporal resolution (e.g. METEOSAT 15 minutes) or a high spatial resolution (e.g. QuickBird 61cm or IKONOS 1m). The detection of processes on different temporal and spatial scales is possible. Short lived and rapid developments such as a thunderstorm, can be observed as well as slow changes in land use and cover over several years. Depending on their purpose, passive satellite sensors can measure reflected solar radiation, solar radiation modulated by passing through the atmosphere, emitted terrestrial radiation in the infrared and also at microwave length. Also active sensors like radar and lidar are flown on satellites and measure the state of the earth (radar even being able to penetrate into the upper layers of the earth itself and through clouds).

The METEOSAT satellites series started operation in 1977 with METEOSAT-1, leading to global coverage of the earth by a total of five geostationary satellites. The seven satellites of the first generation were stationed in a geostationary orbit at  $0^\circ$  E over the equator. After being replaced some were moved over the Indian Ocean and continued service at  $63^\circ$  E, currently METEOSAT-7 is in operation there. The first satellite of METEOSAT Second Generation (MSG) was launched on August 28, 2002. From January 29, 2004 MSG-1, now called METEOSAT-8, took up service at  $0^\circ$  E. On December 22, 2005, MSG-2 (later named METEOSAT-9) was launched and replaced METEOSAT-8 as the prime operational satellite in April 2007.

The development from the first to the second generation was quite significant. The repeat cycle was reduced from 30 minutes to 15 minutes. The number of channels was increased from 3 to 12 and the resolution in the sub satellite point was enhanced from  $5 \times 5$  km to  $3 \times 3$  km for 11 channels and even to  $1 \times 1$  km for the High Resolution Visible (HRV) channel. The MSG satellites are in a geostationary orbit 35800 km above the

**Table 3.1:** Spectral channel characteristics of SEVIRI in terms of central, minimum and maximum wavelength of the channels and whether the channel is an absorption or a window channel (Schmetz et al., 2002).

Channel no.	Characteristics of spectral band ( $\mu m$ )			Main gaseous absorber or window
	$\lambda_{cen}$	$\lambda_{min}$	$\lambda_{max}$	
1 VIS0.6	0.635	0.56	0.71	Window
2 VIS0.8	0.81	0.74	0.88	Window
3 NIR1.6	1.64	1.50	1.78	Window
4 IR3.9	3.90	3.48	4.36	Window
5 WV6.2	6.25	5.35	7.15	Water vapor
6 WV7.3	7.35	6.85	7.85	Water vapor
7 IR8.7	8.70	8.30	9.10	Window
8 IR9.7	9.66	9.38	9.94	Ozone
9 IR10.8	10.80	9.80	11.80	Window
10 IR12.0	12.00	11.00	13.00	Window
11 IR13.4	13.40	12.40	14.40	Carbon dioxide
12 HRV	Broadband (0.4 - 1.1 $\mu m$ )			Window/water vapor

equator with the prime operational satellite at  $0^\circ$  E (currently METEOSAT-9) and the backup system nominal at  $3.4^\circ$  W (currently METEOSAT-8). Since May 2008 however METEOSAT-8 is operating in a rapid scan mode at  $9.5^\circ$  E, scanning from  $15^\circ$  N to  $70^\circ$  N in a 5 minute interval, but still being in position for backup operation.

One MSG satellite has a height of 2.4 m and the diameter of the cylindrical body is 3.2 m. The power demand of 150 W is supplied by solar cells on the satellite. The expected lifetime (fuel for flight corrections) is 7 years. The expected end of MSG is scheduled for 2018, with the third generation (MTG) in orbit from 2015.

### 3.1 Spinning Enhanced Visible and Infrared Imager (SEVIRI)

The main payload on MSG is the Spinning Enhanced Visible and Infrared Imager (SEVIRI)(Schmid, 2005), an optical imaging radiometer. SEVIRI has a 50 cm diameter aperture. The scanning radiometer provides data in two Visible (VIS), one Near InfraRed (NIR), eight InfraRed (IR), two of them in the Water Vapor (WV) absorption band and one High Resolution broadband channel in the Visible and near infrared (HRV)(for details see Table3.1).

The HRV channel contains 9 broad band detection elements to scan the Earth with 1 km sampling distance in the sub satellite point (SSP). All other channels have 3 narrow band detection elements per channel to scan with a 3 km sampling distance.

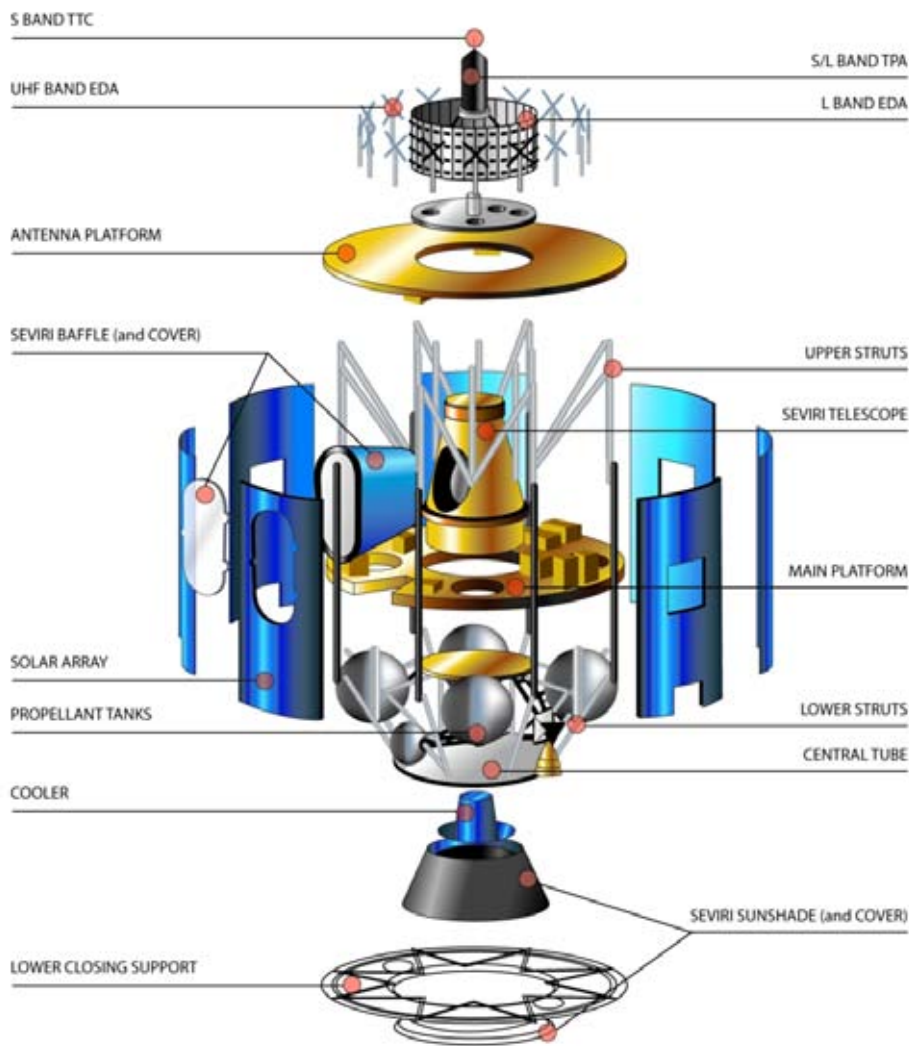


**Figure 3.1:** Schematic drawing of SEVIRI (EUMETSAT, 2006).

The sampling takes place from south to north with a step of 125.8 micro radians of the scanning mirror, corresponding to 9 km in the SSP. To cover the whole earth disc 1250 scan lines are required, with a satellite spin of 100 rpm, it takes 12.5 min to do one scan of the Earth disc. Another 2.5 min are required to move the scan mirror back to its initial position. During this time the on-board black body is inserted into the optical path for about 2 seconds for calibration. This leads to an overall repeat cycle of 15 minutes.

The IR detectors are made of Mercury Cadmium Telluride, the VIS detectors are of Silicone and the NIR are made of Indium Gallium Arsenide. In Figure 3.2 the spectral response function for MSG SEVIRI IR<sub>108</sub> is displayed (EUMETSAT, 2007). The responses are non-linear and may change over the lifetime of an instrument, making it necessary to make corrections for these changes after launch, when producing images from the system. The accuracy of pre-launch spectral response characterisation, and

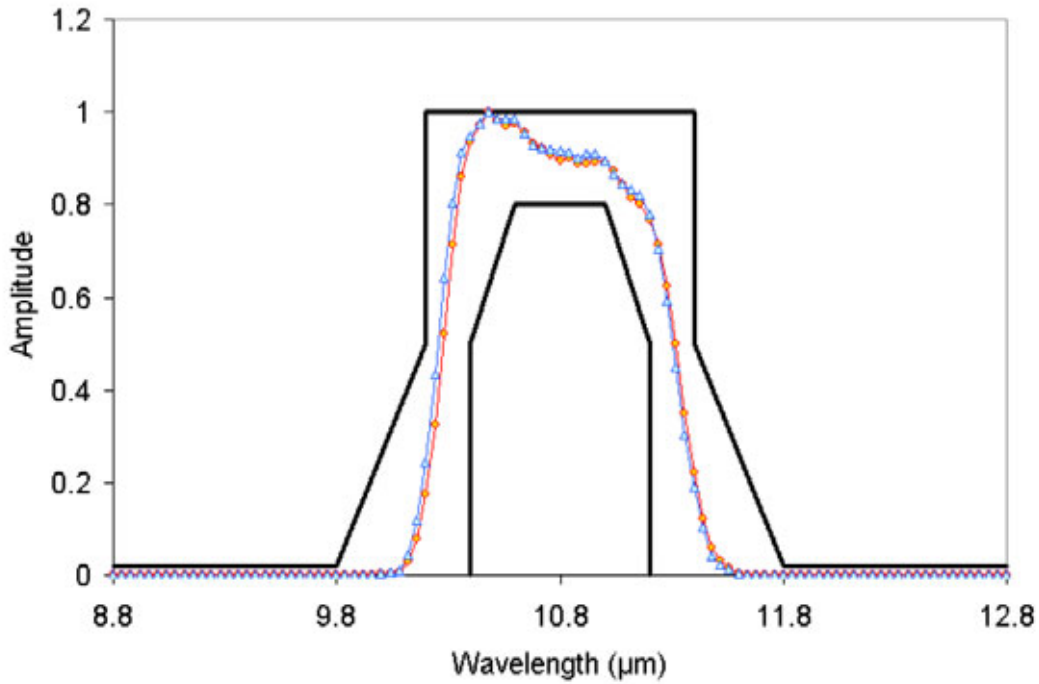


**Figure 3.2:** Spectral response function of MSG SEVIRI channel  $IR_{108}$ . Solid line is the specific template, dots are the Flight Model values at 95K, triangles are for 85K.

how well the on-orbit changes are understood, directly affects calibration accuracy and the quality of the data products. Even within the same satellite series, spectral response sometimes varies quite dramatically from instrument to instrument. In fact, spectral response often varies from detector to detector on the same instrument.

The spectral response function is defined as:

$$\tau(\lambda_c) = \frac{C(L0\lambda_c) - C(0)}{\frac{2}{\Delta\lambda_0} \cdot \int_{\lambda} [C(L0\lambda) - C(0)] \cdot d\lambda} \quad (3.1)$$

where:

$\lambda_c$  centre wavelength corresponding to the elementary spectral band  $c$ .

$\tau(\lambda_c)$  spectral response function at  $\lambda = \lambda_c$ , normalized to its peak value over the characterization bandwidth.

$C(0)$  fixed offset.

$C(L0\lambda_c)$  mean output signal at the radiance  $L0\lambda_c$  corresponding to the constant and uniform monochromatic scene at wavelength  $\lambda_c$ , given by:

$$C(L0\lambda_c) = \frac{\sum_{c,r} C(c,r)}{npix} \quad (3.2)$$

with:

$C(\mathbf{c},\mathbf{r})$  pixel counts at column position  $c$  and row position  $r$ .

**npix** total number of pixels in the image.

The recorded data is sent to the ground station in Darmstadt, Germany. Before redistributing the data to the users via the EUMETCast network the data is line corrected and rectified to nominal position and then sent out as level 1.5 data. One image contains 3712x3712 pixels, only the HRV has more (5568 x 11136 pixels). Each image is split up into 8 segments (HRV: 24) containing 464 lines.

# Chapter 4

## CLM - a Regional Climate Model

The necessity of regional climate simulations for climate impact studies has been recognized since the end of the 1980s. At that time, general circulation models (GCM) had a resolution of about 300 - 500 km and it was therefore not possible to use GCM results for regional climate impact studies (Houghton et al., 1990).

Regional climate models (RCM) are limited area models and therefore need driving data at their lateral boundaries. Generally, GCM results are used as driving data and this process is called nesting a RCM into a GCM. Normally, one-way nesting is applied. This means that the RCM takes the GCM results as driving data at its lateral boundaries but the results obtained by the RCM are not fed back to the GCM simulation. RCMs should not merely interpolate GCM results but they should be able to simulate local atmospheric feedback mechanisms that cannot be resolved by the coarse grid size of GCMs.

Forecasts of GCMs or reanalysis data sets can be used as driving data for the RCM. Reanalysis data sets are produced by running GCMs for past decades with assimilated observations. Therefore, they can be considered as the best method of interpolating observations to a regular grid. In general, reanalysis data is better suited to drive a RCM than forecast GCM data (Rojas and Seth, 2003).

In 1999 the German Weather service DWD started the operational use of the Local Model (LM) for its European weather forecast. Since then many institutions have participated in the further development of the LM. In 2007 the LM was renamed to COSMO, reflecting the joint effort of 10 European meteorological services participating in the Consortium for Small-scale Modelling (COSMO). Several modes of the model have been developed such as the COSMO-EU, used by the DWD for operational forecasts for Europe and the COSMO-DE for short range forecasting for Germany. The COSMO-CLM (in the following only CLM), is the climate mode of the model with no prescribed horizontal resolution or simulation area, with updated vegetation parameters and with no data assimilation. The data from the CLM version 3.19 were used for

comparison with the MSG cloud data. As driving data reanalysis from the GME (the global model from the DWD) were used.

The equations, non-hydrostatic and fully compressible, for the climate version are the same as in the basic model. The main difference is in the pre- and post-processing, enabling a longer run of the model. Additionally, it uses a deeper reaching ground model than the original version (Kücken and Hauße, 2002). The first CLM version was developed in 2001 based on the LM version 2.19. Since then the development has been parallel to the basic version of the LM integrating new developments from the LM.

The CLM has no set grid spacing, neither in horizontal nor in vertical dimensions, these parameters can be set individually for each run. For this work a horizontal resolution of 7 km was used.

The CLM model uses the basic conservation laws for momentum, mass and heat:

$$\rho \frac{d\mathbf{v}}{dt} = -\nabla p + \rho \mathbf{g} - 2\boldsymbol{\Omega} \times (\rho \mathbf{v}) - \nabla \underline{\mathbf{t}}, \quad (4.1)$$

$$\frac{d\rho}{dt} = -\rho \nabla \cdot \mathbf{v}, \quad (4.2)$$

$$\rho \frac{dq^x}{dt} = -\nabla \cdot \mathbf{J}^x + \mathbf{I}^x, \quad (4.3)$$

$$\rho \frac{de}{dt} = -p \nabla \cdot \mathbf{v} - \nabla \cdot (\mathbf{J}_e + \mathbf{R}) + \varepsilon. \quad (4.4)$$

Bold symbols are used to represent vectors and bold underlined symbols indicate dyadic tensors. Scalar and vector products are indicated by  $\cdot$  and  $\times$  respectively.

The following symbols are used:

$t$ : time	$p$ : pressure
$T$ : temperature	$\rho^x$ : partial density of mixture constituent $x$
$\rho$ : total density of air mixture	$q^x$ : mass fraction (specific content) of constituent $x$
$e$ : specific internal energy	$\mathbf{v}$ : barycentric velocity (relative to the rotating earth)
$\mathbf{I}^x$ : sources/sinks of constituent $x$	$\mathbf{J}_e$ : diffusion flux of internal energy
$\mathbf{J}^x$ : diffusion flux of constituent $x$	$\mathbf{R}$ : flux density of solar and thermal radiation
$\underline{\mathbf{t}}$ : stress tensor due to viscosity	$\varepsilon$ : kinetic energy dissipation due to viscosity
$\mathbf{g}$ : apparent acceleration of gravity	$\boldsymbol{\Omega}$ : constant angular velocity of earth rotation
$\nabla$ : gradient (Nabla) operator	$\frac{d}{dt}$ : total (Lagrangian) time derivative operator

A typical use of the CLM covers an area of some million square kilometres (e.g. see chapter 5.2), which makes it necessary to take curvature of the Earth into account. Therefore the model equations are written in spherical coordinates. When using spherical coordinates, two problems arise. Firstly the 'pole problem', which means that the geographical poles represent a singularity due to convergence of the meridians, and

therefore special measures have to be taken when the pole lies within the modelling domain. Secondly, and more often, varying horizontal resolution with latitude away from the equator are encountered. A suitable way to avoid both problems is realised in the CLM: the rotated grid. The computational spherical coordinate system is rotated in such a way that the intersection of the equator and the prime meridian of the new system passes through the simulation domain, thus avoiding the pole problem and providing minimal convergence of the meridians at the same time. The necessary coordinate transformations are performed during pre and postprocessing.

Further information concerning the dynamics and numerics of the LM can be found in Doms and Schättler (2002).

# Chapter 5

## Areas of interest

### 5.1 Development area for MSG cloud mask

The subset for the development of the cloud mask for the MSG data was centred around the Mediterranean. It includes the northern part of Africa, the Middle East, Turkey, all of Western and Central Europe, reaching as far north as Denmark and as far East as the Ukraine and the western parts of Russia. The area processed reaches from  $26^{\circ} 22' N$  to  $55^{\circ} 1' N$  and from  $10^{\circ} 1' W$  to  $41^{\circ} 55' E$  (Fig. 5.1).

As described in chapter 3.1, the MSG data comes in tiles. The channels used for the cloud mask have 8 tiles each. For data handling and process time limitation during the development phase, the area used was reduced to that described above. The chosen area includes different climatic regions, reaching from sandy deserts over elevated planes, irrigated crop land, broad leaf and coniferous forest to alpine glacial regions. Also water bodies, from lakes to rivers and oceans are included. The choice of this area enables the development of a diverse cloud mask, which works automatically in many different regions. For global use only minor adjustments should be necessary. One feature missing, but which is very important for global use is the blanking out of the 'sun glint' effect over water in the visible spectrum.

In order to be in a better position to compare the MSG cloud mask to the model output data from the CLM, the MSG data was re-projected to an equidistant latitude longitude grid, with a spatial resolution of approx. 5 km. The data was processed by the 2met! software from VCS.

### 5.2 Regional climate model (CLM) area

The area of interest is in Southwest Germany, it contains the Black Forest, the Swabian Alp, the Upper Rhine Valley and the Vosges Mountains in France. Many field cam-

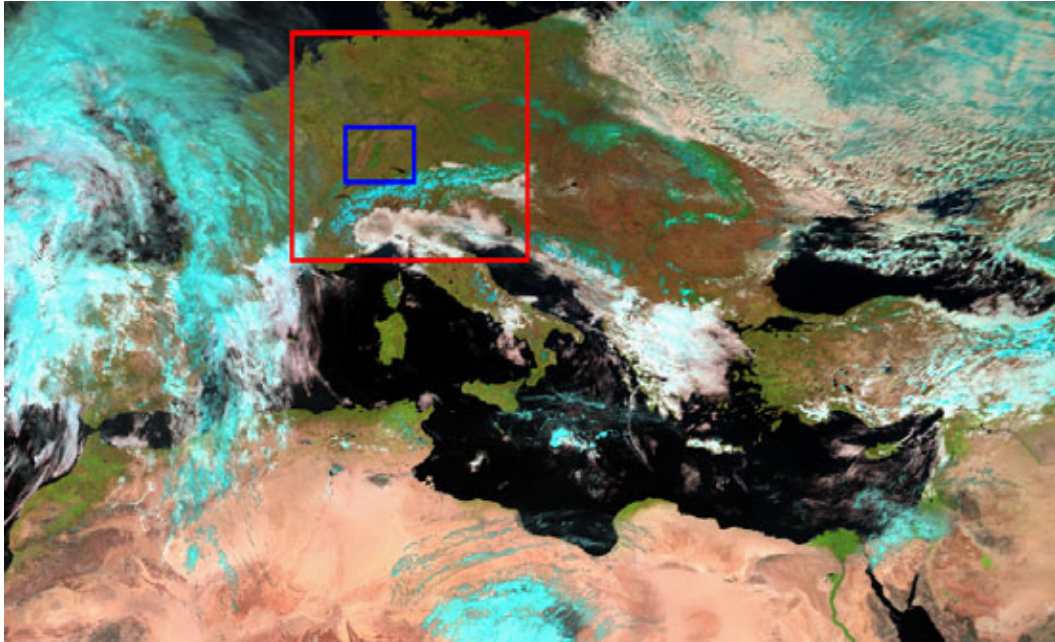


**Figure 5.1:** Area which was used to develop the MSG cloud mask. Red box: area of the CLM, blue box: area of special interest, named A1. Comparison and CLM cloud data validation was concentrated on this area.

paigns have taken place in this area. Some were interested in the regional climate (MESOKLIP (Fiedler and Prenosil, 1980; Vogel et al., 1986), REKLIP (Fiedler and Zimmermann, 1992)), others investigated the triggering of convection over complex terrain (VERTIKATOR (Meißner, 2004; Huckle, 2004), COPS (Behrendt et al., 2007; Corsmeier, 2008)). For numerical meteorological models, convective situations are a great challenge and much research has been invested to achieve a better performance in this field. Therefore, in this work the main objective lies in the modelling of convective clouds over the region described above.

As borders in numerical models are always a problem, the actual model area has to be much larger than the area of interest. Studies have shown, that the nearness to the Alps can result in some unrealistic results. Importantly the increase of precipitation, to amounts near the monthly aggregate, within a few hours showed that the influence of the Alps is too high. Therefore the Alps had to be included into the model area (Meißner, 2008). This then reaches from the Po Valley in the south to Northern Germany in the north. In the West, Belgium is included and in the East the Czech Republic lays within the model area. This way the Alps are completely in the model area and the problems with borders is eliminated for the area of interest.

The area in which the comparison between the cloud masks and the CLM took place is the blue box shown in Fig. 5.1. This area will be referred to as area A1.

# Chapter 6

## Automated cloud mask for MSG

Since the first weather satellite TIROS-1 (Television and InfraRed Observation Satellite) was launched in 1960, the main focus was on the detection and analysis of clouds. At the beginning the work concentrated on extracting features and analysing the cloud type, mostly in a semi automatic process. With the advances in satellite technology the amount of data increased rapidly and the use of satellite data expanded, away from the mere cloud analysis towards atmospheric and surface parameter extraction. With the commissioning of AVHRR (Advanced Very High Resolution Radiometer) first on the polar orbiting TIROS-N satellite in 1978 and later on the NOAA satellite series as AVHRR/2 and 3, the necessity of an automated scheme to detect cloud filled and cloud free pixels became evident. This was the driving force for the development of the APOLLO (AVHRR Processing Over Land cLound and Ocean) scheme (Saunders and Kriebel, 1988). APOLLO uses the data from the visible and infrared AVHRR channels. Different algorithms are applied to day and night conditions.

Although APOLLO was developed for AVHRR, the physical principles behind the scheme (e.g. cloud and surface characteristics at certain wavelengths) are the same for other sensors measuring in a similar spectral range. Optical thick clouds have a high reflectance in the visible spectrum, this feature shows up in METEOSAT data, with a spatial resolution above 3 km as well as in QuickBird images with a spatial resolution of 61cm. But although the spectral characteristics of a cloud do not change, the methods for detecting clouds has to be adjusted for every sensor type. With MSG a high temporal resolution enables the use of diurnal cycles for creating dynamic thresholds. Polar orbiting satellites with a high spatial resolution might not pass over the same area for weeks or even months, within such a time period the vegetation can change considerable and other methods for an automated cloud detection have to be considered.

In the following, the different tests to identify cloud filled pixel in MSG data will be described in detail. Every pixel is treated individually, no references to neighbouring pixels are used, only a time component is used for some tests. The result of each test

is stored in binary counting, enabling the verification of which test detected a cloud. Each test gives a definite result, either a pixel is detected as cloudy by the test or not, there is no 'probability of cloudiness'. For developing the cloud mask data from 2005 was used.

## 6.1 Dynamic threshold in IR 10.8 $\mu\text{m}$ channel

The SEVIRI instrument, onboard METEOSAT Second Generation, has several channels in the infrared part of the atmospheric window (see chapter 3.1 for details). For the use of the prime IR cloud detecting channel IR<sub>108</sub> was chosen, although some clouds have a smaller optical depth than in the IR<sub>120</sub> channel (Olesen and Grassl, 1985), the IR<sub>120</sub> though is affected more strongly by water vapour and aerosols (Reuter, 2005). The IR<sub>087</sub> is similar to IR<sub>108</sub> but clouds with small droplets have a lower emissivity, therefore IR<sub>087</sub> was not chosen. The other two channels (IR<sub>097</sub> and IR<sub>134</sub>) have strong absorption bands of O<sub>3</sub> and CO<sub>2</sub> respectively and can therefore not be used for this purpose.

This test can be used day and night, it is the most important but also a very difficult test to apply. In general, clouds are colder than the underlying sea or land surface (this might not be true in winter, for some cases with inversions and radiative cooling in cloud free areas at night). Therefore a temperature, lower than the surface temperature should indicate a cloudy pixel. The difficulty is how to obtain the expected surface temperature. Some cloud detection algorithms for MSG (e.g. the official EUMETSAT cloud mask, produced by the NoW Casting Satellite Application Facility (SAFNWC)(Lopez Cotin, 2005)) use weather prediction model data. As one part of this project is to compare cloud information, derived from satellite data, with a climate model, the use of data from a numerical weather prediction model seemed inappropriate, as this would result in a (partial) comparison between two models. A second reason not to use external data is, that this is a second data source, which might not always be available or algorithms might be changed (without notice,) which could influence the cloud detection process. Therefore the expected surface temperature has to be extracted solely from MSG data.

The variation of the surface temperature over land is very large during a day and from day to day. The sea surface temperature, on the other hand, is not quite so variable. By looking at the same pixel over a period of time it is very likely to be cloud free at some point. Finding these cloud free temperature values should then enable the calculation of an expected surface temperature for this pixel at a certain time.

The developed MSG cloud mask uses a 30 day gliding window, centred at the day of operation. For each pixel statistical values are then calculated. When calculating the mean, median and standard deviation two possibilities exist. One, using all the data within the 30 day period, the other only using values above a certain threshold.

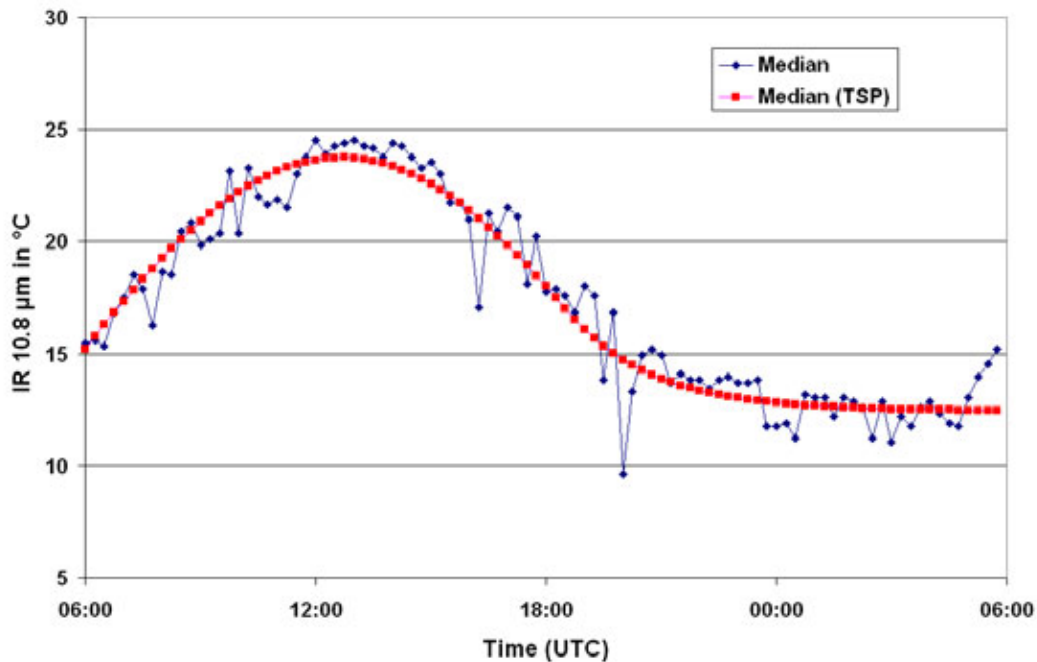


**Figure 6.1:** Blue: 30 day Median for every 15 minutes. Red: Median values after smoothing them with the TSP model.

Using such a threshold clears the data from obvious clouds (gross cloud check). This threshold depends on the time of the year and is lower in winter than in summer.

To obtain the desired clear sky radiance value, the median after the gross cloud check is used. The advantage using the median instead of the mean is that extreme values do not change the result significantly. The median is then calculated for every time slot (i.e. 15 minutes) for one diurnal cycle (Fig. 6.1). The resulting values for one pixel in general follow the assumed diurnal cycle of the land surface temperature (LST), i.e. a sinus form during the day and a decaying exponential form after sunset (Jin and Dickinson, 1999). Very often however the values are not continuous but have rather large jumps from one time slot to the next. Especially in areas with a high amount of cloud cover during the same period of the day, e.g. convective clouds forming over mountain ridges in the afternoon of each day. In order to get a continuous threshold for one diurnal cycle the calculated values of each time slot are used to model a diurnal temperature cycle (DTC) (Göttsche and Olesen, 2001).

The **Thermal Surface Parameter** (TSP) model mathematically represents the physical parameters influencing the surface temperature, most important the irradiance from the sun and the cooling at night. The model calculates seven parameters representing the diurnal cycle of the temperature, with these missing data or cloudy patches can be interpolated. The description of the influence of the sun is based on the solution of the thermal diffusion equation (Carslaw and Jaeger, 1959; Lin, 1980; Price, 1989). The exponential term to model the cooling at night is used as it represents the natural decaying of the temperature very well. This semi empirical approach leads to the

**Table 6.1:** Meaning of parameters of TSP model (see Eq. 6.1 and 6.2 and Fig. 6.2)(Göttsche and Olesen, 2001).

Parameter	Meaning
$T_0$ (°C)	residual temperature ( $\sim$ sunrise)
$T_a$ (°C)	temperature amplitude
$\omega$ (hh:mm)	width over $\pm\pi/2$ (period/2) of cosine term
$t_m$ (solar time)	time of maximum
$t_s$ (solar time)	start of attenuation function
$k$ (hh:mm)	attenuation constant
$\delta T$ (°C)	$T_0 - T(t \rightarrow \infty)$ , where $t$ is the time

following equation:

$$T_1(t) = T_0 + T_a \cos\left(\frac{\pi}{\omega}(t - t_m)\right) \quad \left. \vphantom{T_1(t)} \right\} t < t_s \quad (6.1)$$

$$T_2(t) = (T_0 + \delta T) + \left[ T_a \cos\left(\frac{\pi}{\omega}(t - t_m)\right) - \delta T \right] e^{-\frac{(t-t_s)}{k}} \quad \left. \vphantom{T_2(t)} \right\} t > t_s \quad (6.2)$$

The TSP parameters are explained in Table 6.1, their meaning for the modelling of the diurnal temperature cycle are shown in Figure 6.2. The model assumes:

- clear sky condition (cloud screened pixels) without significant changes in wind speed,
- that only one sunrise takes place, and
- that the temperature decays freely after the 'thermal sunset' defined by  $t_s$ .

The time  $t$  is therefore limited to the time between two successive sunrises. MSG has 96 slot per 24h, but to avoid running into the next sunrise or using data from the previous cooling phase only 88 are used.

As a result we receive smooth and continuous expected clear sky radiances. The threshold to decide whether a pixel is cloudy or not is then set some degrees lower. The modelling of the DTC does not always work, e.g. over water or other places a diurnal cycle does not show up in the data. In these cases the originally retrieved median values will be used. For water bodies this is not a big problem, as the temperature hardly changes over one day.

This process is now done for every pixel individually and every day (Fig. 6.3). Especially in spring and autumn the threshold can change daily.

First tests were made using the same method as described above but using the maximum instead of the median. The idea is that during the 30 day period the cloud

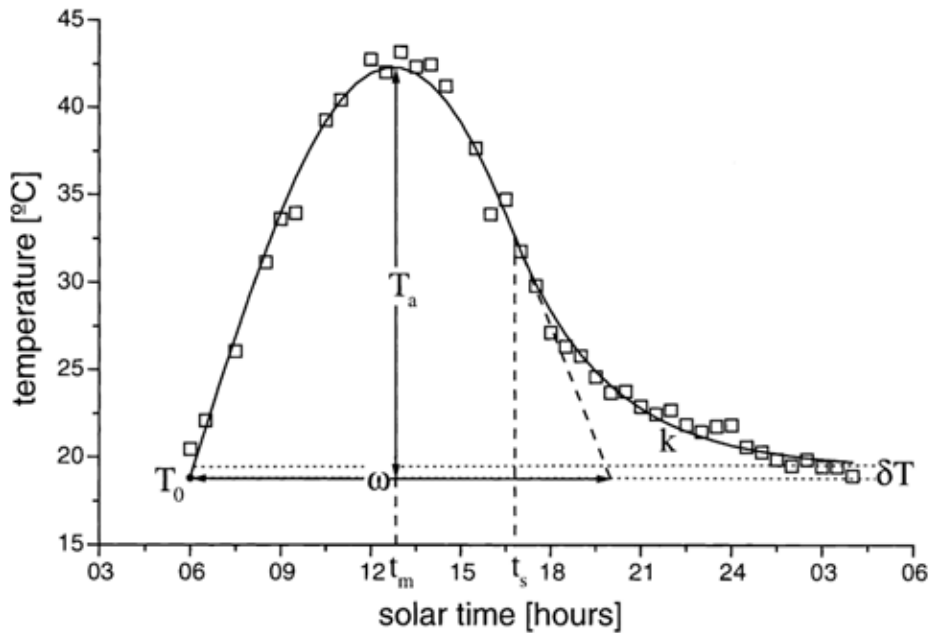


**Figure 6.2:** *BT of METEOSAT (boxes) for August 1996, Algeria. The solid line is the fit to the data using the TSP model described in Eq. 6.1 and 6.2. The parameters are explained in Table 6.1 (Göttsche and Olesen, 2001).*

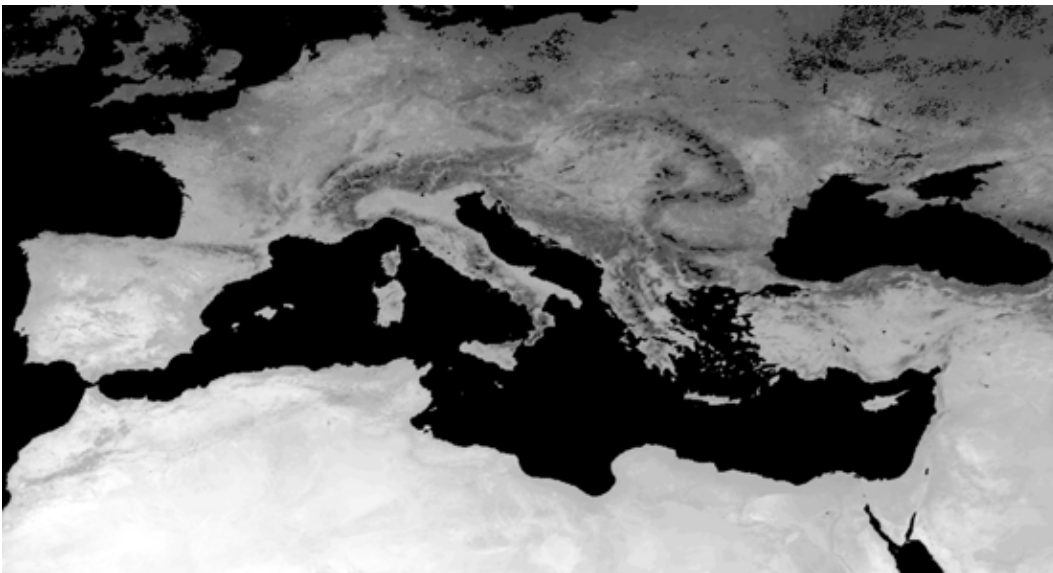


**Figure 6.3:** *10 June 2005, 13:00 UTC. Median for a 30 day window for each pixel, after using the TSP model to smoothen the diurnal cycle. Black areas: no diurnal cycle or not enough data for the TSP model, mostly water bodies but also areas with high cloud cover. Values are used for the IR threshold, if no values from the TSP model available, original median values for each slot are used.*

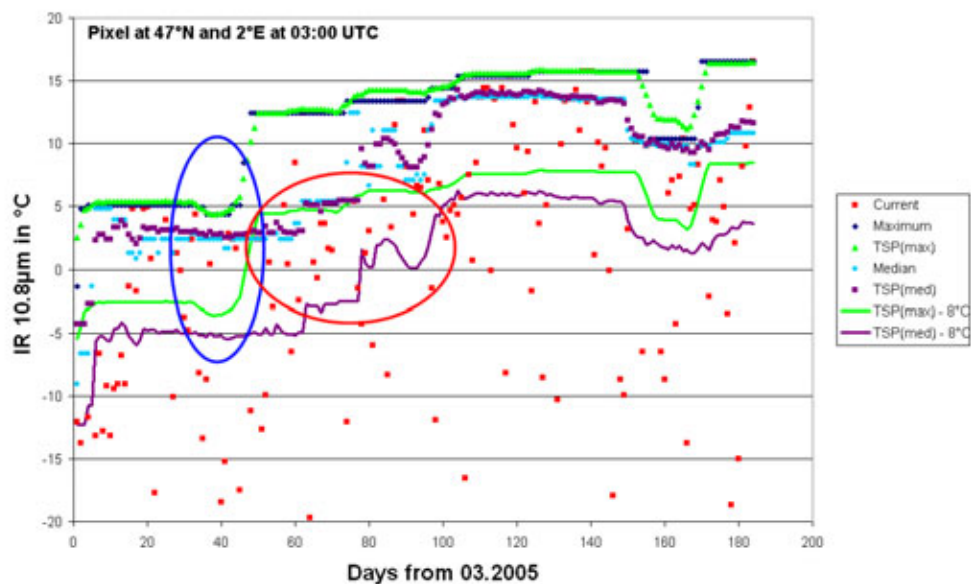


**Figure 6.4:** Comparison between 30 day maximum and median for one pixel at 3:00 UTC over a period of six months, starting in March 2005. Red: current MSG  $IR_{108}$  value, dark blue: 30 day maximum, light blue: 30 day median, green triangles: TSP maximum, purple squares: TSP median, green line: TSP maximum minus 8 K purple line: TSP median minus 8 K. In the Blue circle an abrupt jump in the maximum values is marked, the correspondent median value rises a lot slower. The values in the red circle are not cloudy when using the median value.

free areas have the highest temperature and all lie rather near together, as opposed to clouds which have a wide temperature range. However it proved that this assumption is not true for spring and autumn but only works during the summer months when the surface temperatures do not change so significantly over a period of a few days. Figure 6.4 shows that the 30 day maximum has large, abrupt jumps (blue circle). The 30 day median rises more gradually, the values in the red circle would be classed as cloudy when using the maximum, but not when using the median. Another drawback on using the maximum is that extreme (false) values can be used and will lower the performance of the cloud mask considerably. Since using the median value, the cloud mask has improved significantly, especially in spring and autumn.

A 30 day window centred around the day of operation can only be used when reprocessing data. When using this method with real time data no more than two weeks of previous data should be used, as the changes in spring and autumn would otherwise be too large. Alternatively data from previous years could be used, but no experience has been gained in this case.

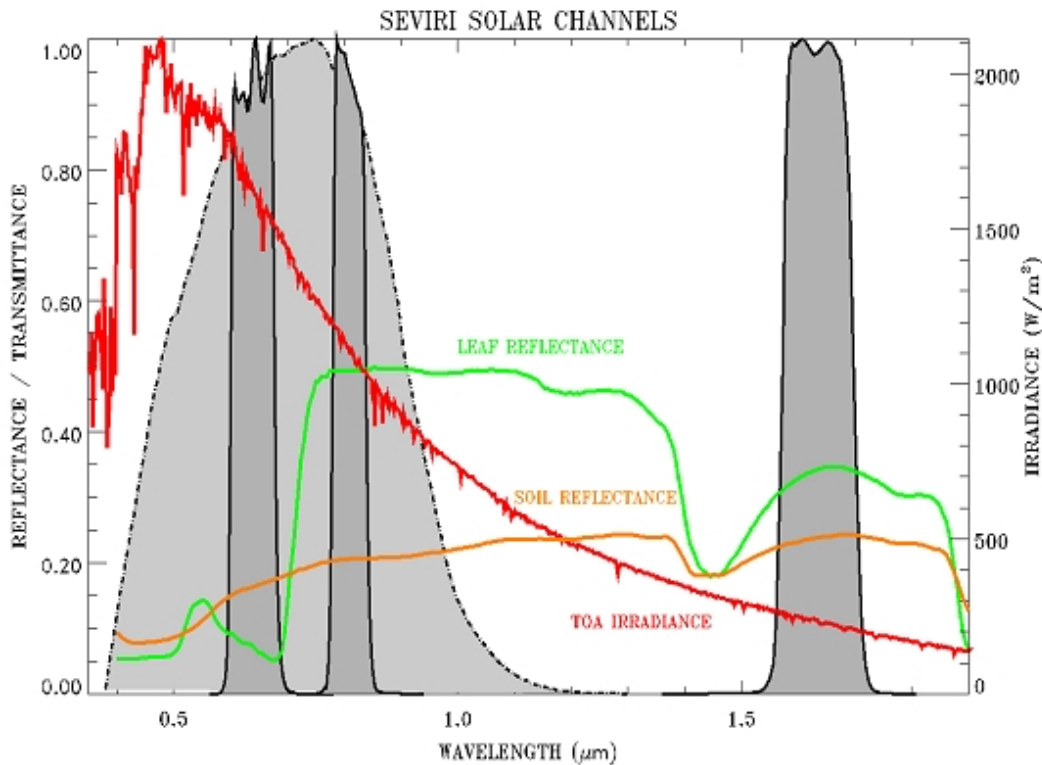


**Figure 6.5:** *The three SEVIRI solar channels (0.6  $\mu\text{m}$ , 0.8  $\mu\text{m}$  and 1.6  $\mu\text{m}$ ) are in dark grey. the atmospheric window is shown in light grey. Red: Top Of Atmosphere (TOA) irradiance, orange: soil reflectance, green: leaf reflectance. A significant jump in the leaf reflectance takes place between the 0.6  $\mu\text{m}$  and 0.8  $\mu\text{m}$  channel, therefore the 0.6  $\mu\text{m}$  is more suitable for cloud detection over vegetated land.*

## 6.2 Dynamic threshold in VIS 0.6 $\mu\text{m}$ channel

In the visible part of the electromagnetic spectrum SEVIRI has two channels one at 0.6  $\mu\text{m}$  and the other at 0.8  $\mu\text{m}$ . For cloud identification the 0.6  $\mu\text{m}$  channel is more favourable as reflection from clouds is high but over water and vegetated land it is low. At 0.8  $\mu\text{m}$  clouds have a similar reflection but the reflection over vegetated land is also high, due to the chlorophyll in the plants which has a maximum reflectance near 0.8  $\mu\text{m}$  (Kasperbauer, 1987)(Fig. 6.5). Over water the effect of sun glint has to be taken into account when using the visible channels.

After the test described above using the 10.8  $\mu\text{m}$  channel the 0.6  $\mu\text{m}$  channel is the most important for detecting clouds during daylight hours. Optical thick clouds show up very distinctly in the 0.6  $\mu\text{m}$  channel, some however are nearly invisible (e.g. thin cirrus) but still alter the radiation coming from the earth's surface substantially. On the other hand some areas with no or dried vegetation (e.g. bare soil, harvested crop land, stone and sand) have a very high reflectance.

Analog to the test described in chapter 6.1 a non cloudy background value has to be found from the MSG data. The same 30 day window as described above is used for the  $0.6 \mu m$  channel, this time retrieving the minimum value. Again this is done for each pixel individually and for every time slot. This is then used as a reference and if the measured value is higher than the reference plus a small threshold the pixel is flagged as cloudy.

The use of the minimum follows the same idea as in chapter 6.1 the use of maximum or median. Within the 30 day period the lowest value is very likely to describe the surface reflectance. The reflectance does not change as rapidly from day to day as the LST. It is more bound to the vegetation cycle and the land use (e.g. ploughing or harvesting). The reflectance is dependant on the elevation of the sun, describing a sinus curve from sunrise to sunset. The use of the minimum is so good and constant that a model like for the IR test is not necessary.

Problems will occur with snow covered ground, which has the same high reflectance in the  $0.6 \mu m$  channel and will often be falsely flagged as a cloud. Chapter 6.6 describes in detail how to differentiate between snow and clouds.

With this test and the  $10.8 \mu m$  channel test approx. 80-90% of the clouds can be detected. The following tests therefore describe ways of identifying these last 10-20%. Although the overall number of clouds detected with the following tests is not very high, the detection of these clouds can be very important (e.g. fog at night, for traffic safety).

### 6.3 Thin cirrus detection

The detection of (optical) thin cirrus in a single channel is very difficult. In the visible channels a thin cirrus cloud is hardly recognisable. In a single infrared channel the transmission of surface radiation can be very high and the measured top of atmosphere (TOA) brightness temperature (BT) may only be a few degrees lower than in the clear atmosphere. The combination of two window channels in the infrared however is very favourable for detecting thin cirrus clouds. The radiance at the top of a thin cloud is dependant on the emissivity/transparency of the cloud at a frequency  $\nu$  (see Eq. 2.5). The transparency at  $10.8 \mu m$  is higher than at  $12.0 \mu m$ . This results in a higher BT in the  $IR_{108}$  channel (Ou et al., 1996; Inoue, 1987). As stated in Eq. 2.5 this channel difference is temperature dependant. The higher the temperature, the higher the difference, also if there is no cirrus, this is then due to aerosols and water vapour which have a higher influence on the  $IR_{120}$  channel.

In very hazy areas, e.g. northern Italy (Po Valley) there can be a difference of more than  $3 K$  even in the absence of thin cirrus clouds. For the region around the Mediterranean and central Europe a static value of  $3.5 K$  was used as a threshold. Cirrus clouds

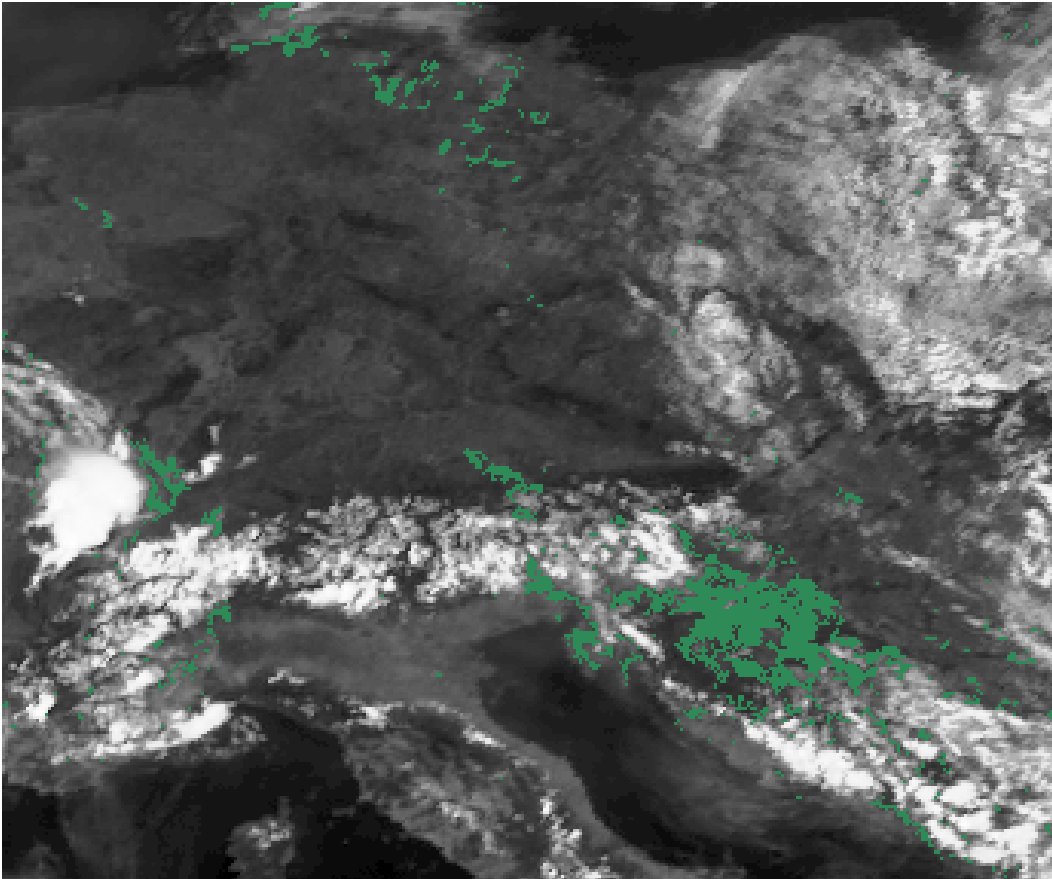


**Figure 6.6:** 23 June 2005, 13:30 UTC,  $VIS_{006}$ , in green the clouds only detected by the thin cirrus algorithm. In the visible channels these clouds do not show up at all. In the IR the temperature is only 5-7 K lower than the cloud free areas nearby.

can have a major impact on the climate change (Liou, 1986; Minnis et al., 2004). Because the clouds are very high i.e. cold, they act as an insulation of the atmosphere. Especially during the night the cooling of the atmosphere is reduced when cirrus clouds are present.

## 6.4 Fog detection during night

The biggest advantage of MSG compared to METEOSAT first generation is the increase of channels and the IR inflight calibration. In addition to the information gained from one single channel, the combinations of two or more channels reveals a lot more about the state of the atmosphere. Identifying fog filled pixels as cloudy during the day is rather easy as the reflectance in the VIS<sub>006</sub> and VIS<sub>008</sub> channels is very high compared to the cloud free surface, an analysis of thickness high above ground etc. requires more calculations (Cermak and Bendix, 2008). At night however the detection is much more difficult. Fog or low stratus have if at all only a marginal lower temperature than the cloud free surface. The temperature difference is much too small for it to be picked up by the IR<sub>108</sub> threshold test (chapter 6.1). Due to the higher emissivity of fog and low stratus at 10.8  $\mu m$  ( $\varepsilon_c = 0.99$ ) than at 3.9  $\mu m$  ( $\varepsilon_c = 0.8 - 0.9$ ) (Hunt, 1973) a temperature difference occurs between these two channels. If  $IR_{108} - IR_{039} > 6.5$  K the pixel will be flagged as cloudy. In Figure 6.7 the channel difference between IR<sub>108</sub> and IR<sub>039</sub> is shown (left) and the corresponding IR<sub>108</sub> (right). The red circles indicate ground fog/low stratus, which only shows up in the channel difference. The introduction of this test increased the amount of clouds detected by 3 percentage-points for October.

## 6.5 Use of the channel difference IR<sub>039</sub> - IR<sub>108</sub>

The same two channels used for the fog detection at night (IR<sub>108</sub> and IR<sub>039</sub>) can be used for further cloud detection. At night the channel difference changes over cirrus clouds compared to low clouds and fog. Here the IR<sub>039</sub> channel has a higher BT than IR<sub>108</sub>. In Figure 6.7 the yellow circle indicates a high cloud, in this case another test picked up this cloud as well, about 1% of the clouds are detected with this algorithm at night.

The IR<sub>039</sub> channel is the only SEVIRI channel in the overlap of terrestrial emitted radiation and reflected solar radiation. During the night IR<sub>039</sub> has the same characteristic as the other IR channels, i.e. the BT is dependant on the emissivity, but during the day this is not the case, as additionally also solar radiation is reflected. The reflected solar radiation can be useful in detecting clouds. Due to the higher reflectance of sun light on clouds compared to the cloud free ground, clouds have a significant higher BT in the IR<sub>039</sub> than in the IR<sub>108</sub> channel. This is especially helpful in detecting low (warm) clouds that do not show up in the IR<sub>108</sub> threshold test or the VIS<sub>006</sub> test.

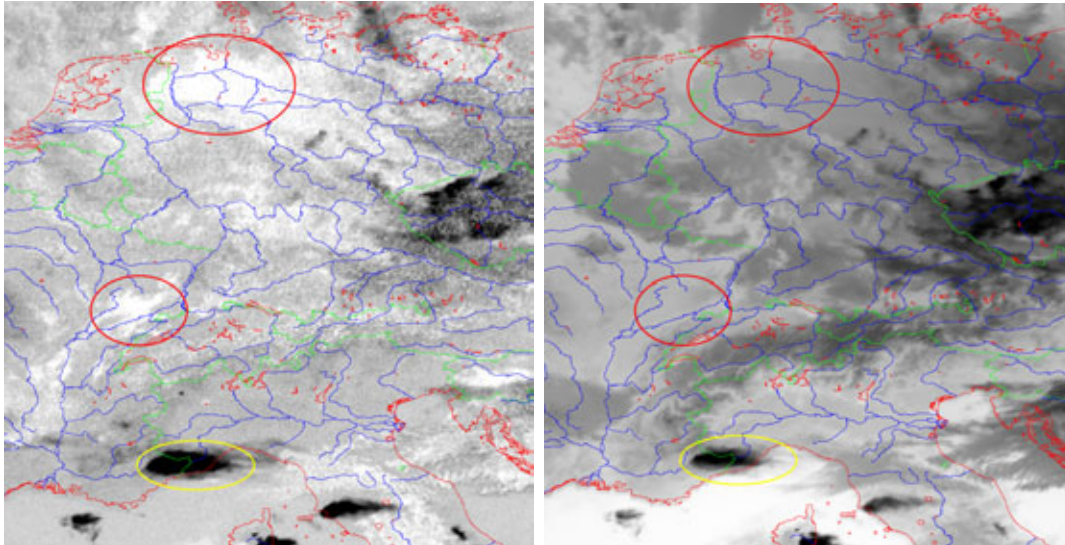


**Figure 6.7:** *Left: channel difference  $IR_{108} - IR_{039}$ , red circles: fog/low stratus, temperature difference  $> 7K$ , yellow circle: high clouds temperature difference  $< 14 K$ . Right:  $IR_{108}$  channel, the fog in the red circles can not be detected, especially in the lower circle.*

## 6.6 Snow detection

All the above tests are used to detect cloud filled pixels. In the following two verification algorithms are described. Discriminating between clouds and ice or snow (on the ground) is not easy, especially in the two visible channels. The spectral signature of clouds and snow in  $VIS_{006}$  or  $VIS_{008}$  is very similar. This is not the case for the  $NIR_{016}$  channel. At a wavelength of  $1.6 \mu m$  the reflection of snow and ice is very low (they appear to be 'black') compared to that in the two visible channels (Hall et al., 1995; de Wildt et al., 2007). While clouds reflect solar radiation, this feature can be used to discriminate between snow and clouds. All pixel flagged as cloudy are checked whether either  $VIS_{006}/NIR_{016} > 1.8$  or  $VIS_{008}/NIR_{016} > 1.5$  is true, if so ice or snow is dominant in the pixel. If the BT in  $IR_{108}$  is above  $-15^\circ C$  the pixel is then flagged as cloud free again (Fig. 6.8). This of course can only be used in day time. This test considerably increases the performance in mountainous regions.

## 6.7 Special meteorological situations

In some situations the  $IR_{108}$  threshold test detects too many clouds, this is the case when the surface temperature does not follow the expected diurnal cycle. One scenario is the convective area behind a cold front. In this case the passage of the cold front has a large influence on the LST. Firstly, the clouds block out the solar radiation, so that no heating of the ground can take place, secondly the rain will cool the ground even



**Figure 6.8:** Red: areas detected as clouds in the first round and then marked as snow due to the  $NIR_{016}$  to  $VIS_{006}$  or  $VIS_{008}$  ratio.

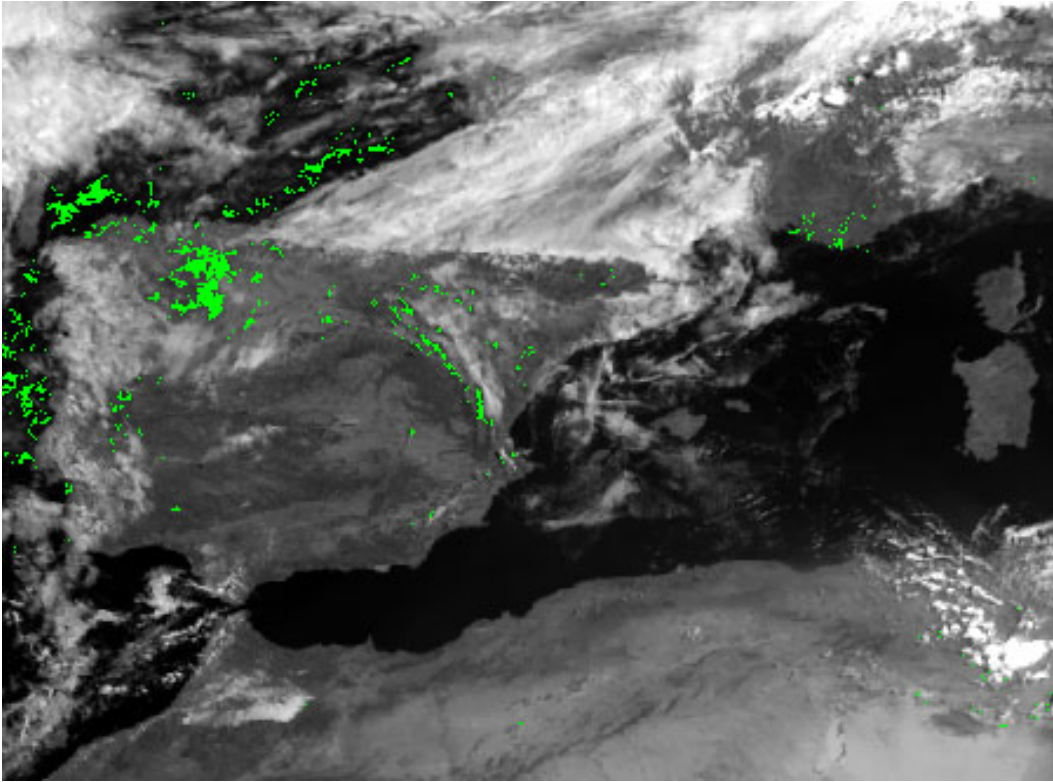


**Figure 6.9:** 25.07.2005 09:00 UTC  $VIS_{008}$ , green: areas where clouds in the clouds mask only detected with the IR threshold test were flagged as not cloudy due to a very low reflectance in the VIS.

further and when the front has passed the evaporation will prevent the ground from heating up quickly. This results in significant lower LST behind a cold front as would be expected for that time of the day. The effect is especially large in the morning and midday. During the night the influence on the LST is not important, in fact clouds and rain can actually lead to a higher LST than would be expected (e.g. no radiative cooling)(Baker et al., 1995).

Behind a cold front shallow convection often takes place, therefore the cloud temperature is not so low as for other convective situations (e.g. thunderstorms). This results in a BT for the cloud free ground very similar to that of the convective clouds. Discriminating between clouds and cloud free areas is then not possible with an IR channel. The differences in the  $VIS_{006}$  channel on the other hand is very significant. The clouds show up very bright and the ground is very dark, enhanced by the wetness following the rain during the cold front pass. The discrimination in the VIS channels is therefore very good.

Every cloud pixel flagged as cloudy is checked for this feature. To be flagged as cloud free the cloud flag has to be solely from the  $IR_{108}$  threshold, if this is the case and the value of the  $VIS_{006}$  is very near the 30 day minimum (only daytime situations), the pixel is then flagged as cloud free (Fig. 6.9). This check has decreased the false cloud

rate behind cold front significantly.

## 6.8 Further possibilities of cloud detection

Some cloud detection algorithms used by other cloud detection schemes are not used in this cloud mask for MSG. Nevertheless they shall be described briefly.

**Ratio  $VIS_{006}/VIS_{008}$ .** The ratio of two visible channels can be used for detecting clouds. The idea behind this is, that clouds in both channels have a similar reflectance but over land or water this is different. As mentioned in chapter 6.2  $VIS_{008}$  has a higher reflectance over vegetated land than  $VIS_{006}$  (the ratio would be  $< 1$ ). Over water  $VIS_{006}$  is more sensitive to aerosols (e.g. salt) than  $VIS_{008}$ , the resulting ration would be  $> 1$ . A ratio near 1 would then detect a cloud. A problem arises when dealing with coastal pixels. A coastal pixel has a mixed spectral characteristic from both land and water, therefore most coastal pixels show up as clouds (Fig. 6.10). The false cloud detection in coastal areas is very high (nearly all the coastlines are permanently registered as cloudy), therefore this test is not used. This test can be useful when detecting clouds in high resolution images (e.g. Quickbird) where time information is not available, the area is small and coast lines well known.

**Difference  $IR_{108}-IR_{087}$ .** The difference between these two IR channels results from a lower emissivity of fog at  $IR_{087}$ . This is helpful at night, especially if the  $IR_{108} - IR_{039}$  difference is not available (see chapter 6.4). As the  $IR_{087}$  channel is not affected by sunlight this fog detection can be used over 24 hours. The problem is that the difference between the two channels is not so large as in the other fog test. Detecting fog over such a large area and during different seasons would be very difficult. During the day the detection of foggy pixels as cloud filled is very easy. The use of this test is useful as a backup.

## 6.9 Detection of dust clouds, sun glint and other special cases

Depending on the purpose of the cloud mask the thresholds and the 'type' of clouds looked for can vary. One 'type' of clouds are dust or sand clouds, including their outbursts from the deserts. Depending on the underlying surface, e.g. desert or water, the detection of these dust events can be different. If the aim of the cloud mask is to mask out all contaminated pixels, e.g. for the study of land or sea surface parameters, then the masking of sand and dust is definitely useful. When looking at

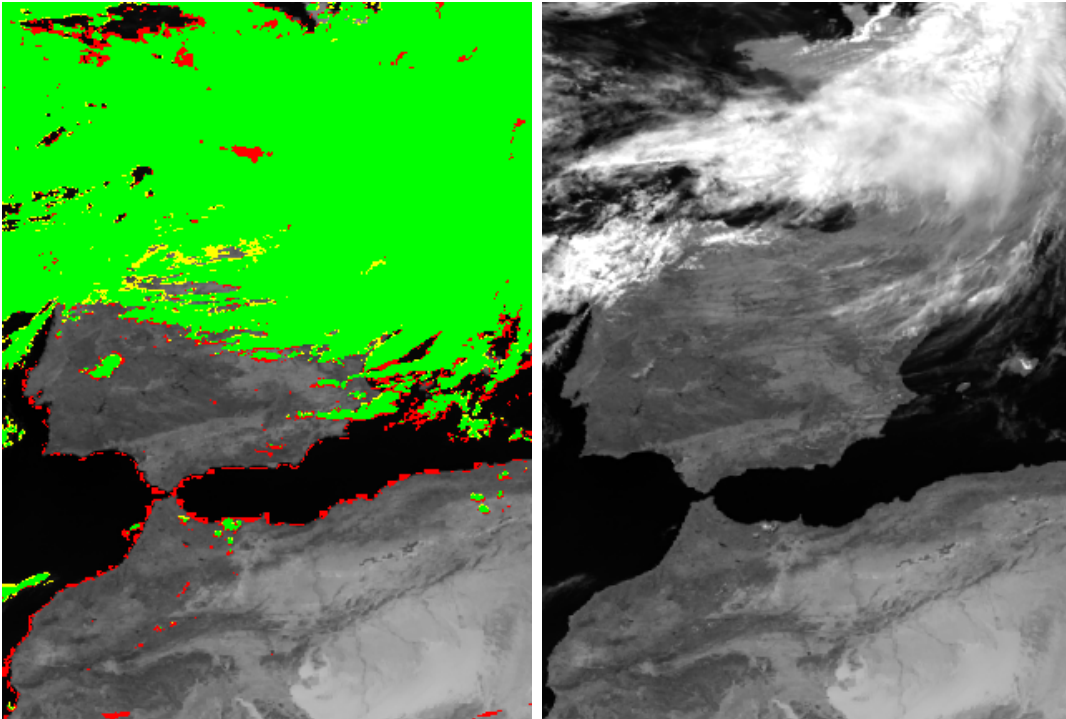


**Figure 6.10:** 15.06.2005 13:00 UTC, Left:  $VIS_{008}$  channel, overlaid with comparison between IMK and EUMETSAT Nowcasting SAF cloud mask. Green: both have clouds, red: clouds only in SAF cloud mask, yellow: clouds only in IMK cloud mask. Along the coast of Northern Africa and the Iberian Peninsula falsely detected clouds in the SAF cloud mask show up, probably due to the use of VIS channel ratio. Right:  $VIS_{008}$  channel, along the coast lines no clouds are visible.

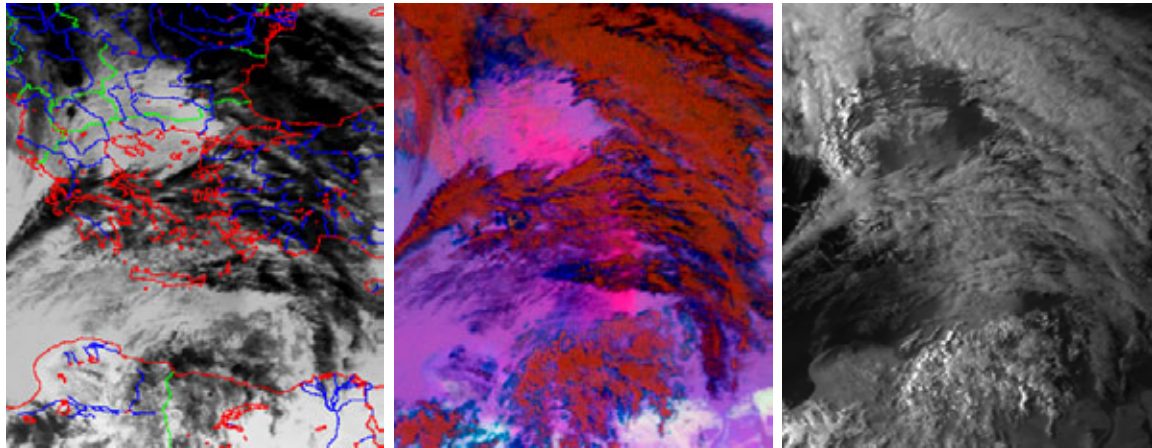


**Figure 6.11:** 17 April 2005, 15:00 UTC. Left:  $IR_{108}$  channel overlaid with coastlines, political borders and rivers. The scene shows the Aegean with the surrounding eastern part of the Mediterranean. Centre: RGB composite of  $IR_{120}-IR_{108}$ ,  $IR_{108}-IR_{087}$  and  $IR_{108}$ . The bright pink area in the centre of the picture shows the dust following a frontal system. Right:  $VIS_{006}$  the sand can only just be recognised underneath the high clouds.

the clouds themselves a discrimination between water or ice clouds and dust events should be made. A possible method is the use of channel differences in the IR. For example the  $IR_{120}$  channel has a higher transmissivity in the case of dust particles than the  $IR_{108}$  channel. Hence the difference between these two can give an indication whether a pixel is dust contaminated. Also the difference between the  $IR_{108}$  and the  $IR_{087}$  channel can reveal dust in the atmosphere (Ackerman, 1997; Schepanski et al., 2007). However these tests have not yet been implemented into the IMK cloud mask.

In Figure 6.11 a dust event on 17 April 2005 is shown. A major dust outbreak from the north African desert followed a cyclone over the Mediterranean and struck the Greek isles in the morning hours, grounding many air crafts in Crete and limiting visibility in Athens to a minimum.

The IMK cloud mask was developed in an area containing most climatic regions and weather phenomena. Permafrost areas and tropical regions with a high amount of clouds every day are not in the area. Any adjustments that might be needed when extending the cloud mask for global use still have to be developed. Another feature appearing near the equator is the so called sun glint. This is an area in which the sun light is reflected from water directly into the sensor. This results in a very bright spot that would normally be interpreted as clouds. The effect of sun glint can also appear near the poles when the sun in summer shines over the poles and the sunlight is reflected by the sea surface. In the current version of the IMK cloud mask no precautions for sun glint are implemented.

# Chapter 7

## Validation of the IMK cloud mask

The development of the MSG cloud mask (chapter 6) was based not only on known and established algorithms but also on new ideas and available information. To validate the newly developed MSG cloud mask the comparison with other cloud masks is a necessity. For this purpose two MSG cloud masks were chosen, one from EUMETSAT's Now Casting SAF (NWC-SAF)(Lopez Cotin, 2005), the other from the FU Berlin (Reuter, 2005). The source in both cases is MSG data, the same as with this newly developed cloud mask, referred to as IMK cloud mask. The advantage of using data from the same source, is that any differences appearing between the cloud masks are entirely due to the algorithms used.

### 7.1 Validation with MSG cloud mask from FU Berlin

The first comparison to an external cloud mask was carried out with the MSG cloud mask, produced by the Institut für Weltraumwissenschaften (Institute for Space Sciences) at the Freie Universität Berlin (Reuter, 2005). The FUB cloud mask uses many of the techniques the IMK cloud mask uses (described in chapter 6). One of the most important tests for detecting clouds day and night is the use of the IR channels. The FUB cloud mask uses the  $10.8\mu\text{m}$  channel for this task. As in the IMK cloud mask a diurnal cycle as described by Göttsche and Olesen (2001) is used for retrieving clear sky radiances. The FUB approach however is different. For example: instead of using mean or median values from a certain time window around the day of interest as in the IMK cloud mask, clear sky radiance values for every time slot are chosen, so that the changes from one slot to the next and from one day to the next are smooth.

The output of the FUB cloud mask is a probability value for cloudiness between 1 and 255. The threshold for comparison with the IMK cloud mask was set to 150, above

**Table 7.1:** Comparison between IMK cloud mask and FUB cloud mask for MSG in percent. All days from March to October 2005, as well as only the convective days. This is the same study area as in the comparison between IMK cloud mask and CLM. In addition, the agreement for the entire European window between the IMK & FUB cloud masks is listed.

	Average over area of interest		Europe
	All days	Convective days	
IMK & FUB cloud free	33.5	69.1	58.3
IMK & FUB cloudy	53.7	21.0	31.2
IMK non cloudy, FUB cloudy	5.0	1.5	4.4
IMK cloudy, FUB non cloudy	7.7	8.4	6.1
<b>Total agreement of IMK &amp; FUB</b>	<b>87.2</b>	<b>90.1</b>	<b>89.5</b>
Total cloud cover in IMK	61.4	29.6	37.4
Total cloud cover in FUB	58.7	22.5	35.7

was treated as cloudy, below as cloud free. A histogram analysis of the FUB data showed that most of the values are near the two ends and that, a moderate change of the threshold will not change the results in any significant way.

The FUB and IMK cloud masks were compared in the same region with the CLM, area A1. The results show that the agreement for convective and non convective situations from March to October is good (87.2% and 90.1% respectively). We also see that the IMK cloud mask is able to identify more clouds than the FUB cloud mask (details see table 7.1). A monthly analysis reveals that, in spring and autumn the FUB cloud mask has more clouds than the IMK cloud mask but in the summer the amount of clouds increases in the IMK cloud mask (Table 7.2).

Over the entire window that the IMK cloud mask is available (see chapter 5.1) the agreement between IMK and FUB cloud mask is 2 percentage-points better than in the A1 area. The agreement for cloud free pixels is higher (58.3% vs. 33.5%) this is because of the Mediterranean and the deserts of North Africa that are included in this window. Hence the total cloud amount is also lower.

During the day the IMK cloud mask seems to be more sensitive towards the edge of the clouds and marks more pixels as cloudy, compared to the FUB cloud mask (Fig. 7.1). This is especially noticeable during the morning hours and during the day, the major portion of the clouds, which are only picked up by the IMK cloud mask, are these additional clouds at the edges. This higher sensitivity leads to a high number of clouds, which are only detected by the IMK cloud mask, especially for the summer months (see Table 7.3). The number of clouds only detected by the FUB cloud mask from 08:00 UTC to 16:00 UTC is nearly zero. The verification of the results in some selected cases leads to the conclusion that the majority of these edge clouds are correctly detected by the IMK cloud mask. This shows, therefore that the IMK cloud mask is able to identify over 10%-points more clouds during summer days than the FUB cloud mask.

**Table 7.2:** Comparison between IMK cloud mask and FUB cloud mask for MSG in percent. All days for every month from March to October 2005 (no data from Berlin for May and September. Same study area as the comparison between IMK cloud mask and CLM).

	March	April	June	July	August	October
IMK & FUB cloud free	23.0	13.9	35.0	25.9	38.5	47.2
IMK & FUB cloudy	61.2	77.4	50.0	61.0	50.2	43.5
IMK non cloudy, FUB cloudy	9.9	5.4	2.1	3.6	3.2	6.1
IMK cloudy, FUB non cloudy	5.9	3.3	12.8	9.5	8.0	3.3
<b>Total agreement of IMK &amp; FUB</b>	<b>84.2</b>	<b>91.3</b>	<b>85.0</b>	<b>86.8</b>	<b>88.7</b>	<b>90.7</b>
Total cloud cover in IMK	67.1	80.7	62.8	70.5	58.3	46.8
Total cloud cover in FUB	71.2	82.8	52.1	64.8	53.4	49.7

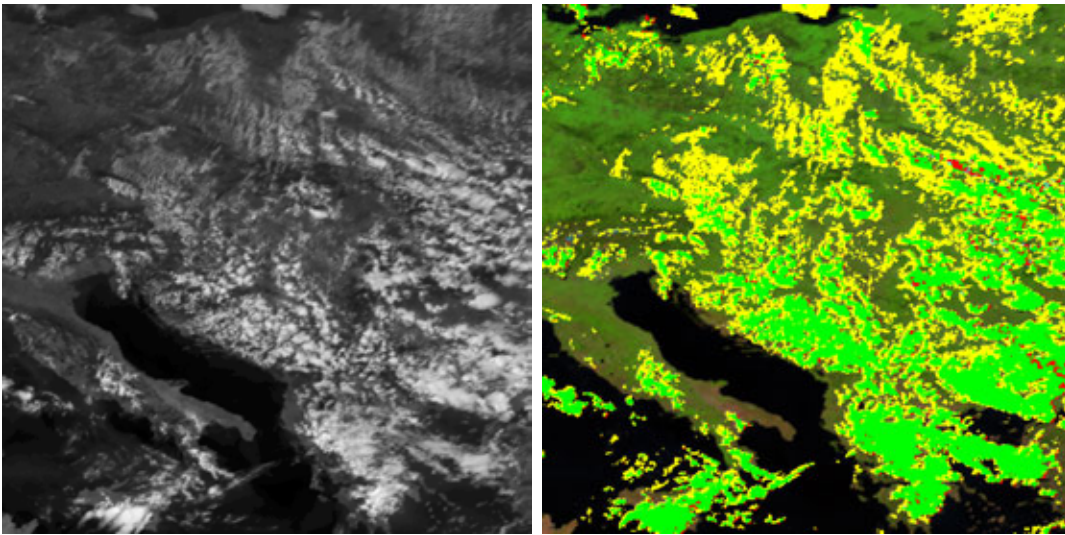


**Figure 7.1:** 20 June 2005, 14:00 UTC. . Left:  $VIS_{006}$ , the clouds show up very clearly. Right: Comparison between IMK and FUB cloud mask. Green: both have clouds, red: clouds only in FUB cloud mask, yellow: clouds only in IMK cloud mask. The FUB cloud mask does not pick up many of the clouds from shallow convection over eastern Europe.

**Table 7.3:** Comparison between IMK cloud mask and FUB cloud mask for MSG in percent. All days from 08 to 16 UTC for every month from March to October 2005 (no data from Berlin for May and September). Same study area as the comparison between IMK cloud mask and CLM.

	March	April	June	July	August	October
IMK & FUB cloud free	19.6	12.4	27.9	17.4	28.0	47.8
IMK & FUB cloudy	60.8	79.5	56.4	67.9	58.5	43.6
IMK non cloudy, FUB cloudy	2.0	0.7	0.1	0.1	0.1	3.9
IMK cloudy, FUB non cloudy	17.5	7.6	15.5	14.5	13.2	4.7
<b>Total agreement of IMK &amp; FUB</b>	<b>80.5</b>	<b>91.9</b>	<b>84.3</b>	<b>85.3</b>	<b>86.6</b>	<b>91.3</b>
Total cloud cover in IMK	78.4	87.0	71.9	82.4	71.8	48.3
Total cloud cover in FUB	62.8	80.0	56.6	68.2	58.8	47.6

**Table 7.4:** Comparison between IMK cloud mask and FUB cloud mask for MSG in percent. All days from 21 to 03 UTC for every month from March to October 2005 (no data from Berlin for May and September). Same study area as the comparison between IMK cloud mask and CLM.

	March	April	June	July	August	October
IMK & FUB cloud free	20.4	15.4	39.4	30.7	46.6	45.1
IMK & FUB cloudy	61.6	73.5	46.4	58.5	43.5	45.4
IMK non cloudy, FUB cloudy	15.3	10.9	5.0	7.8	6.6	5.9
IMK cloudy, FUB non cloudy	2.6	0.3	9.2	3.0	3.3	3.6
<b>Total agreement of IMK &amp; FUB</b>	<b>82.0</b>	<b>88.9</b>	<b>85.8</b>	<b>89.1</b>	<b>90.1</b>	<b>90.5</b>
Total cloud cover in IMK	64.3	73.7	55.7	61.6	46.8	49.0
Total cloud cover in FUB	76.9	84.3	51.4	66.2	50.1	51.3

The FUB cloud mask appears to have difficulties during and before dawn. The agreement between IMK and FUB is good during the early morning hours, but at some time before sunrise the FUB cloud mask appears to switch from a night mode into a twilight mode and the detection of clouds decreases, until the visible channels come into play.

In the evening and at night the IMK cloud mask sometimes picks up clouds that are not found by the FUB cloud mask (Table 7.4). This is because the expected clear sky radiance modelled with the TSP-model for this time of day is relatively high (Fig. 7.2). If the ground cools off quicker, than the model predicts, clear pixels will be flagged as cloudy. The FUB cloud mask works better in these cases. A possible enhancement of the IMK cloud mask could be a new version of the TSP model, which has a different cooling function resulting in a faster decay after thermal sunset (Göttsche and Olesen, 2008). Often cloudy pixels at the edge of clouds are not detected by the IMK cloud mask, the FUB cloud mask seems to work better here (Fig. 7.3).

The comparison for convective days shows a better overall agreement (90.1% vs. 87.2%

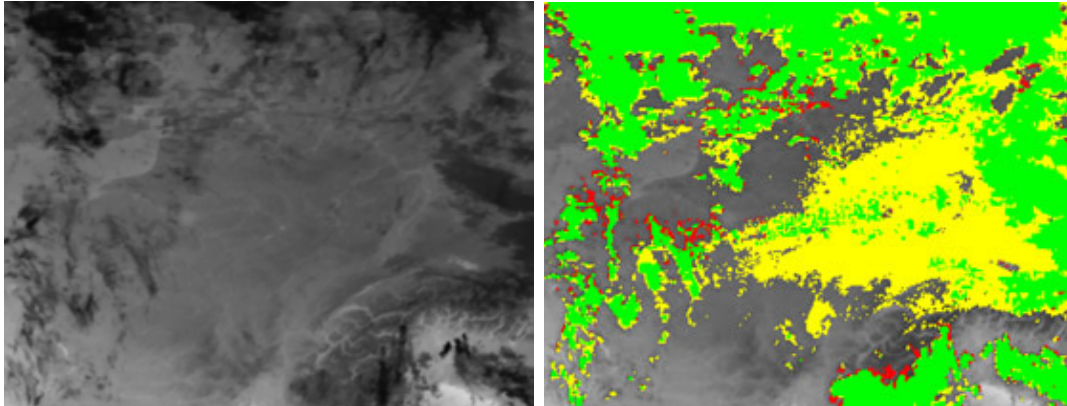


**Figure 7.2:** 07 June 2005, 21:00 UTC. Left:  $IR_{108}$ , clouds around the edges of the picture but the centre is cloud free. Right: comparison between IMK and FUB cloud mask. Green: both have clouds, red: clouds only in FUB cloud mask, yellow: clouds only in IMK cloud mask. The extensive area of 'clouds' only detected by the IMK cloud mask is due to a slow cooling in the TSP model, resulting in a too high expected radiance. The FUB cloud mask has, in this case, a better result.

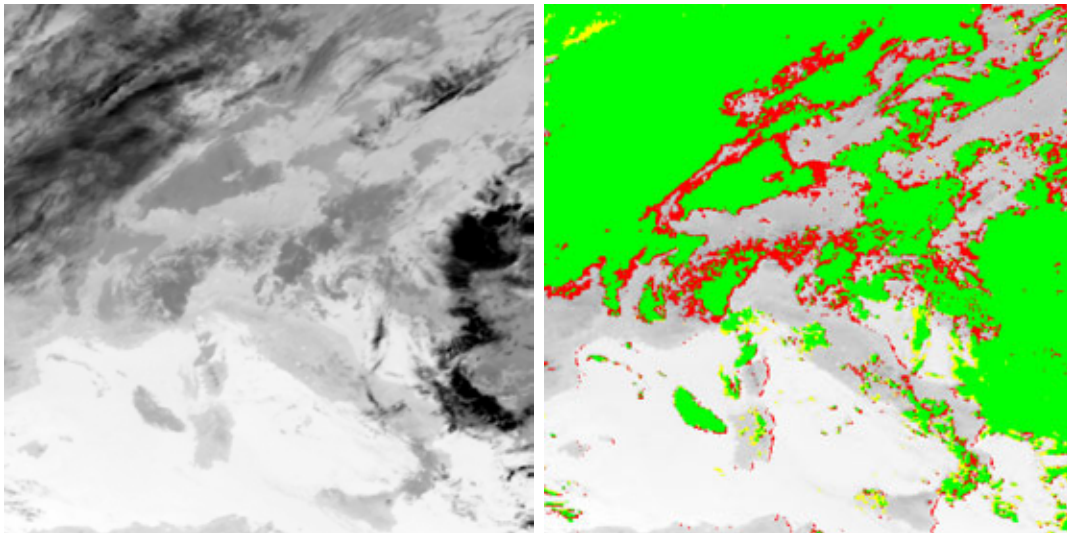


**Figure 7.3:** 14 April 2005, 02:00 UTC. Left:  $IR_{108}$ , solid cloud band to the northwest, very cold clouds in the east, broken up cloud cover in the centre. Right: comparison between IMK and FUB cloud mask. Green: both have clouds, red: clouds only in FUB cloud mask, yellow: clouds only in IMK cloud mask. Along the edges of the clouds the FUB cloud mask picks up more clouds. The FUB cloud mask has a better result in this case, with the exception of the eastern coastlines, the clouds there are incorrect.

**Table 7.5:** Comparison between IMK cloud mask and FUB cloud mask for MSG in percent. For convective days only for every month for June, July and August 2005. Same study area as the comparison between IMK cloud mask and CLM.

	June	July	August
IMK & FUB cloud free	65.0	50.1	80.4
IMK & FUB cloudy	24.5	37.8	11.4
IMK non cloudy, FUB cloudy	1.2	3.1	1.4
IMK cloudy, FUB non cloudy	9.4	9.0	6.8
<b>Total agreement of IMK &amp; FUB</b>	<b>89.4</b>	<b>87.9</b>	<b>91.8</b>
Total cloud cover in IMK	33.8	46.9	18.2
Total cloud cover in FUB	25.7	40.8	12.8

for all days) for the complete period (in this case June to August)(Fig. 7.1). For convective days the agreement on cloud free pixels is higher than for the complete period (69.1% vs. 33.5%), the opposite is the case for cloud filled pixels (21.0% vs. 53.7%). This is not surprising as on convective days the amount of clouds is much lower compared to times when frontal systems pass through an area.

The three months compared individually show some variance in the amount of clouds ranging from 46.9% (IMK, June) to 12.8% (FUB, August) and hence the portion of the cloudy and cloud free part in the overall agreement (Table 7.5). But the disagreement remains generally constant, with a high amount of the clouds only detected by the IMK cloud mask (up to 9.4%) and only a very low amount only detected by the FUB cloud mask (1.2% in June). This shows that the cloud masks have a similar performance for convective and non convective situations.

The confidence in the performance of the IMK cloud mask is strengthened by the comparison with the FUB cloud mask. The majority of clouds are detected by both algorithms. Most of the differences can be explained by the higher sensitivity of the IMK cloud mask during the day and some other known issues with the slow cooling of the expected clear sky radiance during the night. The comparison confirms that the IMK cloud mask works better and picks up more clouds during the day (especially in summer) and that the FUB cloud mask has its strength under certain conditions during the night.

Comparing the cloud mask from Berlin with the CLM shows us that the agreement is a little lower than between the CLM and the IMK cloud mask (74.6% vs. 77.5%). The amount of clouds only in the CLM is with 20.4% nearly 4%-points higher (Table 7.6). The difference in the total cloud cover in the CLM between the IMK and the FUB cloud mask comparisons is due to some missing data in the IMK and FUB files. The comparison between the FUB cloud mask and CLM again shows that the IMK cloud mask works very well.

**Table 7.6:** Comparison between IMK cloud mask and FUB cloud mask for MSG, IMK and CLM, FUB and CLM in percent. For all days March to October 2005.

	IMK (1) FUB (2)	IMK (1) CLM (2)	FUB (1) CLM (2)
(1) and (2) cloud free	33.5	21.8	20.8
(1) and (2) cloudy	53.7	55.7	53.8
(1) non cloudy, (2) cloudy	5.0	16.8	20.4
(1) cloudy, (2) non cloudy	7.7	5.8	5.0
<b>Total agreement of (1) &amp; (2)</b>	<b>87.2</b>	<b>77.5</b>	<b>74.6</b>
Total cloud cover in (1)	61.4	61.3	58.8
Total cloud cover in (2)	58.7	72.4	74.2

## 7.2 Validation with Now Casting SAF cloud mask

The second external MSG cloud mask the IMK cloud mask was validated against is the cloud mask produced by the Now Casting SAF. In November 1992 EUMETSAT decided to introduce a network of so called Satellite Application Facilities (SAFs), as specialised development and processing centres. Each SAF is led by the National Meteorological Service of a EUMETSAT Member State and to each SAF a consortium of EUMETSAT Member States and Cooperating States, government bodies and research institutes contribute a part of the work.

The six original SAFs still in operation include:

- SAF on Support to Nowcasting and Very Short Range Forecasting (NWC SAF)
- Ocean and Sea Ice SAF (OSI SAF)
- Climate Monitoring SAF (CLM SAF)
- Numerical Weather Prediction SAF (NWP SAF)
- Land Surface Analysis SAF (LAND SAF)
- Ozone and Atmospheric Chemistry Monitoring SAF (O3M SAF)

In 2008 a seventh SAF took up operational service:

- GRAS Meteorology SAF (GRAS SAF)

An eighth SAF is still under development:

- Support to Operational Hydrology and Water Management (H SAF)

The overall objective of a SAF is the provision of operational services, ensuring a cost-effective and synergetic balance between the central and distributed services. The SAF services are an integral part of the overall EUMETSAT operational services. The SAFs provide data, products, software and research in their specialised field.

The cloud mask used for this validation is produced by the NWC SAF. The aim of this SAF is to provide a weather forecast for the next few hours based on current information. These short range forecasts are important for short-lived but severe weather situations such as thunderstorms, tornadoes, hail, surface ice, flash floods or dust storms. Operational weather forecast can normally not deliver exact forecast for these events with the necessary temporal and spatial resolution.

The NWC SAF has several products concerning clouds, precipitation, clear air, wind and thunderstorms. The cloud mask is produced within this framework. The main aim of all the products is to enable forecasters to generate short range weather forecasts. Therefore, the cloud mask is robust and made to detect the important clouds for these applications. This on the other hand leads to an insensitivity to some not so easily detected clouds (Kabsch et al. 2008).

The NWC SAF cloud mask uses similar tests to detect clouds in MSG data as the IMK and the FUB. The biggest difference is in the use of the IR cloud test. The IMK and FUB cloud mask use MSG data to extract expected clear sky radiances in the IR. The SAF cloud mask, on the other hand, uses computed surface temperatures from a numerical weather prediction model as a threshold. The advantage of this method is clearly that it is independent from any clouds in the area which could affect the threshold. On the other hand it is dependent on the performance of the model. Changes in the model can have significant influence on the performance of the cloud mask.

Other tests mainly include channel differences in the IR (thin cirrus , fog, etc.), the use of the VIS channels, including areas of sun glint and the detection of snow or ice. Also tests for the detection of dust and volcanic ashes are used. If one test identifies a pixel definitely as cloudy the remaining tests are then not performed. A detailed description of the NWC SAF cloud mask is given by the SAF consortium (Lopez Cotin 2005).

In Table 7.7 the IMK cloud mask (IMK) and the EUMETSAT NWC-SAF cloud mask (SAF) are compared for all months from March to October 2005. The total agreement for all slots is at 89.9%. For convective days the agreement increases to 92.4%. The agreement is equally high for all days during sunshine hours from 8 to 16 UTC. At night the agreement is 4%-points lower at only 88.2%. For the entire Europe window in the IMK data set (see chapter 5.1) the agreement is at 88.4%. Compared with the FUB cloud mask the agreement between IMK and SAF is slightly better (89.9% compared to 87.2% (Table 7.1)). Also for convective days the agreement is slightly better and also the differences in the cloud amount is small.

The clouds only picked up by one of the algorithms is very similar for the comparison using all slots (5.2% only in the SAF data and 4.9% only in the IMK data). For

**Table 7.7:** Comparison between IMK cloud mask and EUMETSAT cloud mask (SAF). Analysis from March to October 2005. Comparison for the CLM area, for all days, for convective days only, for all days from 8 - 16 UTC, for all days from 21 - 3 UTC. Last Comparison for entire Europe window of IMK cloud mask.

	March to October 2005				
	all days	convective days	8 - 16 UTC	21 - 3 UTC	Europe
IMK & SAF cloud free	33.8	72.7	27.9	38.0	54.0
IMK & SAF cloudy	56.1	19.7	64.4	50.2	34.4
IMK non cloudy, SAF cloudy	5.2	5.0	3.2	6.3	8.4
IMK cloudy, SAF non cloudy	4.9	2.6	4.5	5.5	3.2
<b>Total agreement of IMK &amp; SAF</b>	<b>89.9</b>	<b>92.4</b>	<b>92.3</b>	<b>88.2</b>	<b>88.4</b>
Total cloud cover in IMK	61.0	22.3	68.9	55.8	37.6
Total cloud cover in SAF	61.3	24.7	67.6	56.5	42.8

convective days the difference is a little bigger with 5.0% of the clouds only picked up by the SAF and only 2.6% for the IMK. During the day the IMK cloud mask is a little more sensitive (4.5%) compared to 3.2% only picked up by the SAF. At night the ratio changes (6.3% SAF and 5.5% IMK). Over the entire Europe window the SAF has 8.4% clouds not found by the IMK cloud mask, but only 3.2% only present in the IMK data.

The results for the comparison between the different months are shown in Table 7.8. The best agreement is in April with 94.3% and the worst agreement is in March with only 86.1%. May, June and September are also below the average. For July, August and October the agreement is above 90%. The total cloud cover decreases from March to October in both data sets, which is in compliance with the FUB cloud mask and also the CLM data (see chapter 8). The amount of clouds only detected by one algorithm varies considerably from month to month, with a high of 8.5% for the SAF cloud mask in March and a low of 2.0% for the IMK cloud mask in April.

Comparing day and nighttime separately we see a better agreement during the day than in the night (Table 7.7), which is not surprising as the cloud detection during the day is obviously easier than during the night due to additionally available solar channels, for effects during dawn see further down in this chapter. The best agreement in the individual months is in April (day 95.4% and night 93.4%), the worst agreement during the day is in September (89.8%) and for the night in May (81.1%) (Table 7.9 and 7.10). The biggest difference between day and night is found in May with 93.2% agreement during the day and only 81.1% during the night. The smallest difference is in September, where the agreement during the day is also not so good.

With the exception of October (6.5%) the SAF cloud mask only has very few clouds not detected by the IMK cloud mask during the day (between 1.3% in June and 3.7%

**Table 7.8:** Comparison between IMK cloud mask and EUMETSAT cloud mask (SAF) in percent. Monthly analysis from March to October 2005. Analysis for all days of every month.

	March	April	May	June	July	August	September	October
IMK & SAF cloud free	22.2	30.2	27.4	33.0	32.2	34.3	42.0	47.3
IMK & SAF cloudy	63.9	64.1	60.1	55.4	59.3	58.5	46.2	43.1
IMK non cloudy, SAF cloudy	8.5	3.7	6.6	3.9	4.7	3.9	4.1	6.0
IMK cloudy, SAF non cloudy	5.4	2.0	5.9	7.7	3.8	3.2	7.7	3.6
<b>Total agreement of IMK &amp; SAF</b>	<b>86.1</b>	<b>94.3</b>	<b>87.5</b>	<b>88.4</b>	<b>91.5</b>	<b>92.8</b>	<b>88.2</b>	<b>90.4</b>
Total cloud cover in IMK	69.3	66.1	66.0	63.1	63.1	61.8	53.9	46.8
Total cloud cover in SAF	72.3	67.8	66.7	59.3	64.0	62.5	50.3	49.1

in September). But also the clouds only detected by the IMK cloud mask are lower than in other comparisons, with a maximum of 7.5% in June and a minimum of 1.6% in October. This leads to a very good agreement between the two cloud masks ranging from 89.8% in September to 95.4% in April. Most of the clouds only detected by the IMK cloud mask are found by the VIS<sub>006</sub> channel. The IMK algorithm seems to be more sensitive, picking up more clouds, most of them correctly.

During the night we have a completely different picture. The amount of clouds only detected by one of the algorithms is relatively high with a maximum for the SAF data of 10.5% in May and for the IMK with 9.2% in June. Some of the clouds only detected by the SAF and not by the IMK algorithms seem to result from a problem with the TSP model during the night. Too many clouds during the night lead to low median values, resulting in a very (too) low TSP result. This seems to be a particular problem for May and has to be improved in the IMK algorithm. The high value of clouds only detected by the IMK in June seems to have the same source as in the comparison between IMK and FUB cloud mask (chapter 7.1). The TSP algorithm smoothing the median values models the cooling too slow, therefore the threshold is too high and clear sky values are actually classed as cloudy. In July the picture is somehow different, the number of clouds only detected by the IMK algorithms is relative low (2.6%) but the SAF detects 6.1% clouds which are not found by the IMK. Most of these clouds seem to be detected incorrectly.

Concentrating on the convective situations in the year 2005 we have more possibilities of comparison as the months April and May have enough data in both data sets. The data set available from the FUB is missing these two months. The agreement on days with convective days is in general a little bit better, only in July the agreement is not quite as good (Table 7.11). Compared with the agreement between the IMK and FUB cloud mask the agreement between IMK and SAF cloud mask is higher, the biggest difference is in August with 3.3%-points. When comparing the IMK with the FUB

**Table 7.9:** Comparison between IMK cloud mask and EUMETSAT cloud mask (SAF) in percent. Monthly analysis from March to October 2005. Analysis for all days from 8:00 to 16:00 UTC of every month.

	March	April	May	June	July	August	September	October
IMK & SAF cloud free	16.1	25.0	24.0	26.5	22.2	25.9	37.0	43.8
IMK & SAF cloudy	76.5	70.4	69.3	64.7	70.9	68.8	52.8	46.8
IMK non cloudy, SAF cloudy	3.1	1.6	1.5	1.3	2.4	2.0	3.7	6.5
IMK cloudy, SAF non cloudy	4.3	3.0	5.2	7.5	4.5	3.3	6.5	2.9
<b>Total agreement of IMK &amp; SAF</b>	<b>92.6</b>	<b>95.4</b>	<b>93.2</b>	<b>91.2</b>	<b>93.1</b>	<b>94.7</b>	<b>89.8</b>	<b>90.6</b>
Total cloud cover in IMK	80.8	73.4	74.5	72.2	75.4	72.1	59.3	49.7
Total cloud cover in SAF	79.6	72.0	70.8	66.0	73.3	70.8	56.5	53.4

**Table 7.10:** Comparison between IMK cloud mask and EUMETSAT cloud mask (SAF) in percent. Monthly analysis from March to October 2005. Analysis for all days from 21:00 to 03:00 UTC of every month.

	March	April	May	June	July	August	September	October
IMK & SAF cloud free	25.3	34.0	28.8	38.8	40.9	40.7	45.6	48.4
IMK & SAF cloudy	59.6	59.4	52.3	46.5	50.4	51.6	41.9	41.4
IMK non cloudy, SAF cloudy	9.0	5.5	10.5	5.5	6.1	5.0	3.8	4.9
IMK cloudy, SAF non cloudy	6.1	1.1	8.4	9.2	2.6	2.7	8.7	5.3
<b>Total agreement of IMK &amp; SAF</b>	<b>84.9</b>	<b>93.4</b>	<b>81.1</b>	<b>85.3</b>	<b>91.3</b>	<b>92.3</b>	<b>87.5</b>	<b>89.8</b>
Total cloud cover in IMK	65.6	60.5	60.6	55.7	53.0	54.3	50.6	46.7
Total cloud cover in SAF	68.5	64.9	62.8	52.0	56.5	56.6	45.7	46.3

**Table 7.11:** Comparison between IMK cloud mask and EUMETSAT cloud mask (SAF) in percent. Monthly analysis from April to September 2005. Analysis for convective days of every month only, from 08:00 to 16:00 UTC.

	April	May	June	July	August	September
IMK & SAF cloud free	81.7	79.7	64.9	44.1	77.2	66.4
IMK & SAF cloudy	12.7	12.5	26.0	44.4	17.6	21.9
IMK non cloudy, SAF cloudy	2.8	3.2	3.0	4.9	2.6	10.2
IMK cloudy, SAF non cloudy	2.8	4.6	6.1	6.6	2.6	1.5
<b>Total agreement of IMK &amp; SAF</b>	<b>94.4</b>	<b>92.2</b>	<b>90.9</b>	<b>88.5</b>	<b>94.8</b>	<b>88.3</b>
Total cloud cover in IMK	15.5	17.1	32.1	51.0	20.2	23.4
Total cloud cover in SAF	15.5	15.7	29.0	49.3	20.2	32.1

cloud mask the IMK had upto 9.4%-points more clouds than the FUB cloud mask. The comparison between IMK and SAF cloud mask reveals a different picture. The SAF cloud mask has more clouds, but the difference is not so significant.

In Figure 7.4 the convective situation over central Europe is shown. The left picture shows the VIS<sub>008</sub> channel. In the middle picture clouds detected only by the VIS<sub>006</sub> channel test in the IMK cloud mask algorithms are marked in yellow. These make up approx. 20% of the scene. Clouds marked as snow due to the IR<sub>016</sub> test are coloured in red. This is definitely not correct for these places in July. Approximately 2% of the scene are marked as snow. This contributes about 50% to the clouds that are only detected by the SAF cloud mask. The other clouds are mainly at the northeastern edge of the cloud fields. Correspondingly at the southwestern edges of the clouds more cloud only detected by the IMK cloud mask appear (right picture in Fig. 7.4). This might be due to some small differences in the reprojection of the data, as different programs for the IMK and the SAF data had to be used. General the sensitivity of the IMK solar channel seems to be higher than in the SAF algorithms. Although the detection of convective clouds during the day is generally better in the cloud masks we see a slight decrease of agreement between all days and those with convection only (Table 7.9 and 7.11). This is probably due to small convective clouds that are only picked up by one algorithm.

In the following some scenes will be compared, not necessarily in the area of the CLM comparison. The detection of clouds during the day is obviously easier due to the availability of the VIS channels. The time around sunrise and sunset however adds another difficulty, as some night algorithms (e.g. fog detection using channel differences between IR<sub>108</sub> and IR<sub>039</sub>) can not be used anymore but the solar channels have not yet come into play. An example of this is shown in Figure 7.5. The IR<sub>108</sub> channel is overlayed with the comparison between the IMK and the SAF cloud mask (green: both have clouds, red: clouds only in SAF cloud mask, yellow: clouds only in IMK

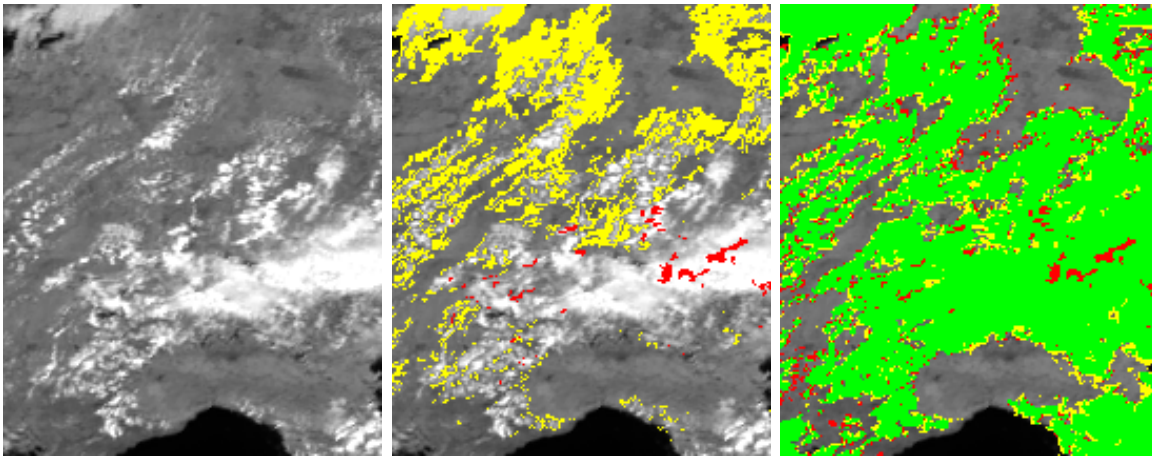


**Figure 7.4:** 11 June 2005, 12:00 UTC. Shallow convection over central and western Europe. Left:  $VIS_{008}$  channel. Middle: in yellow clouds detected only by the  $VIS_{006}$  channel test in the IMK cloud mask algorithms, approx. 20% scene, in red clouds marked as snow, definitely not correct for these places in July (2% of initially detected clouds). Right: comparison between IMK and SAF cloud mask. Green: both have clouds, red: clouds only in SAF cloud mask, yellow: clouds only in IMK cloud mask. The agreement is quite good (with the exception of the incorrectly classed snow in the IMK data), but the edges of the convective clouds tend to be difficult. The IMK picks up more clouds than the SAF cloud mask does.

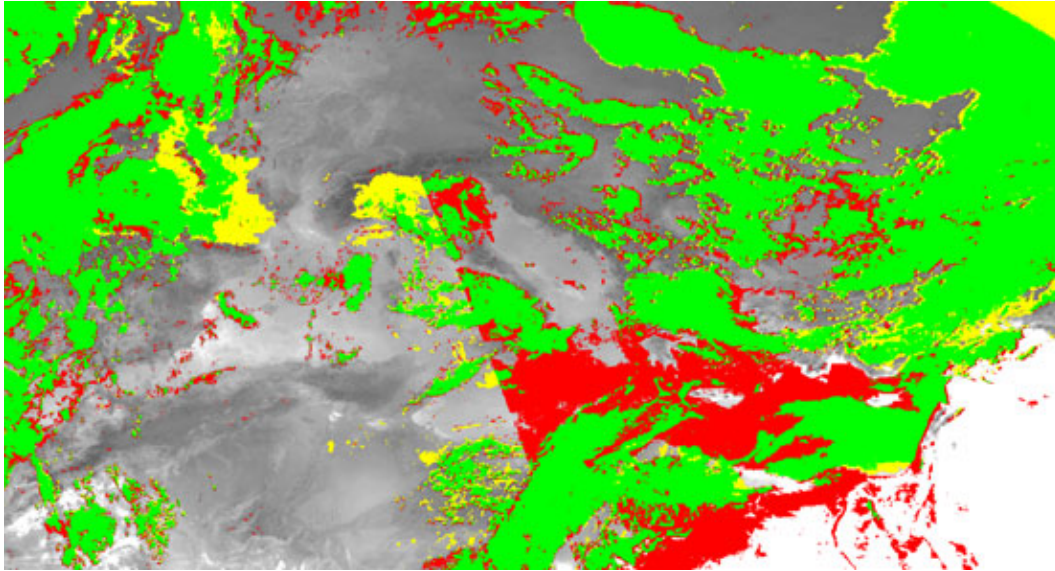


**Figure 7.5:** 20 June 2005, 05:15 UTC,  $IR_{108}$  channel, overlaid with comparison between IMK and SAF cloud mask. Green: both have clouds, red: clouds only in SAF cloud mask, yellow: clouds only in IMK cloud mask. In the centre a sharp line in the SAF clouds is visible, to the right visible information is used in the SAF cloud mask, to the left this is not the case. The result is that fog in the Po valley is not picked up by the SAF cloud mask, but on the other hand sand over the eastern Mediterranean is classed as cloudy. The IMK cloud mask also picks up some sand outbursts from the desert as clouds, only the FUB cloud mask is better and does not classify this as clouds.

cloud mask). In the centre a sharp line in the SAF cloud mask is visible, to the right visible information is used in the SAF cloud mask, to the left this is not the case, this is due to the sunrise, the algorithm only uses the solar channels when a certain elevation of the sun is reached. The result is that fog in the Po valley is not picked up by the SAF cloud mask, but on the other hand sand over the eastern Mediterranean is classed as cloudy. The IMK cloud mask also picks up some sand outbursts from the desert as clouds, only the FUB cloud mask is better and does not classify this as clouds. The detection of sand and dust in the atmosphere by the cloud mask is not generally bad. Depending on the use of the cloud mask, e.g. for extracting land or sea surface parameters the masking out of disturbing aerosols is of a benefit. A discrimination whether the masked areas contain water or ice clouds or other material would however be important.

In general the SAF cloud mask has great difficulties with deserts. In the area around the eastern end of the Mediterranean the SAF cloud mask classifies vast areas as cloudy, especially in the early hours of the day. None of these clouds are picked up by the IMK nor the FUB cloud mask, also the single satellite channels show now clouds. These clouds seem not to be picked up by the visible tests, but this can not be said for sure as the SAF cloud mask has no information on which test detected the cloud. In Figure

7.6 this is illustrated for July 11, 2005 at 03:00 UTC. The sunrise has just begun at the very edge of the scene. In red clouds are coloured that are only detected by the SAF cloud mask. In the corresponding  $IR_{108}$  picture no clouds are visible. Here the SAF cloud mask seems to have difficulties with the cooling of the surface in the night in deserts and areas with probably low moisture content in the air.

Another big issue in cloud detection is the correct discrimination between snow on the ground and clouds. Snow has an equally high reflectivity in the solar channels as clouds have. This will result in a classification of snow as clouds, especially in alpine regions this can be an issue all year round. On the other hand with the NIR channel centred at  $1.6 \mu\text{m}$  snow and ice can easily be identified as snow and ice do not reflect light at this wavelength (see chapter 6.6 for details). However the SAF cloud mask seems not to use this feature all the time. In Figure 7.7 the  $VIS_{006}$  channel is shown and the snow covered Alps can be clearly seen. The IMK cloud mask identifies the snow correctly, but the SAF cloud mask still classes the Alps as cloudy, this does not change over the day.

The overall agreement between IMK and SAF cloud mask is very high, for some periods more than 95%. This as such does not necessarily mean that either of the cloud masks works exceptionally well. But the probability, that both cloud masks are wrong is also very small. The comparison between IMK and FUB also shows a high agreement, although not quite as high. The fact that all three cloud masks have similar results is promising and strengthens the confidence in the IMK cloud mask.

However good the agreement is, the comparison has revealed some significant differences between the cloud masks, showing up the strengths and weaknesses at different times and for different situations. The IMK cloud mask has some major problems at night related with the cooling of the surface modeled by the TSP model. This leads to a higher threshold resulting in quite a few falsely detected clouds. The FUB cloud mask works better at this time of the day. A solution for the IMK cloud mask can be the new version of the TSP (Göttsche and Olesen, 2008), this includes a faster cooling after sunset. In the early morning hours however the IMK cloud mask picks up in performance especially compared to the SAF cloud mask, which starts to use the visible channels a lot later in the day. During the day the IMK cloud mask picks up more clouds compared to FUB and SAF cloud mask, most of these clouds are detected using the solar channels.

In special situations the performance of the cloud masks are also different. The SAF cloud mask seems not to have a very good snow detection, most of the Alps are always marked as cloudy, the FUB and IMK cloud mask work here better. On the other hand the IMK snow detection has to be improved as especially in summer for convective situations, iced but not very cold cloud tops are sometimes marked as snow and not clouds. In hazy conditions, especially from sand and dust (Kaskaoutis et al., 2008) the SAF cloud mask picks up many clouds, the IMK also identifies some clouds but the FUB does not mark these events as clouds. In terms of finding undisturbed pixels, whether by moist or dry particles, the marking of dust as cloud is not totally wrong,

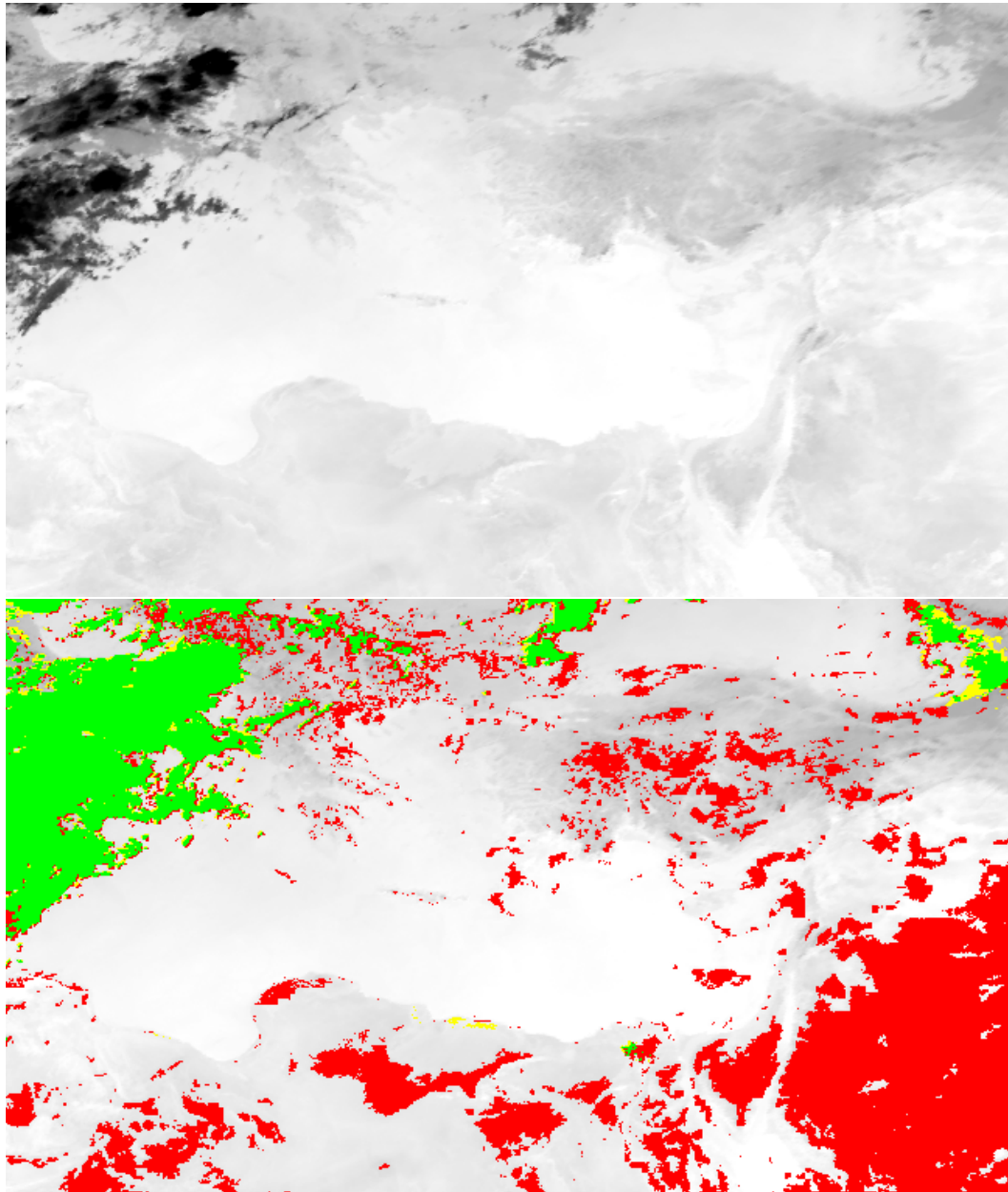


**Figure 7.6:** 11 July 2005, 03:00 UTC,  $IR_{108}$  channel (top), and  $IR_{108}$  channel, overlaid with comparison between IMK and SAF cloud mask (bottom). Green: both have clouds, red: clouds only in SAF cloud mask, yellow: clouds only in IMK cloud mask. Many clouds in the SAF cloud mask (red) probably due to problems with the cooling of the ground in the early morning hours.

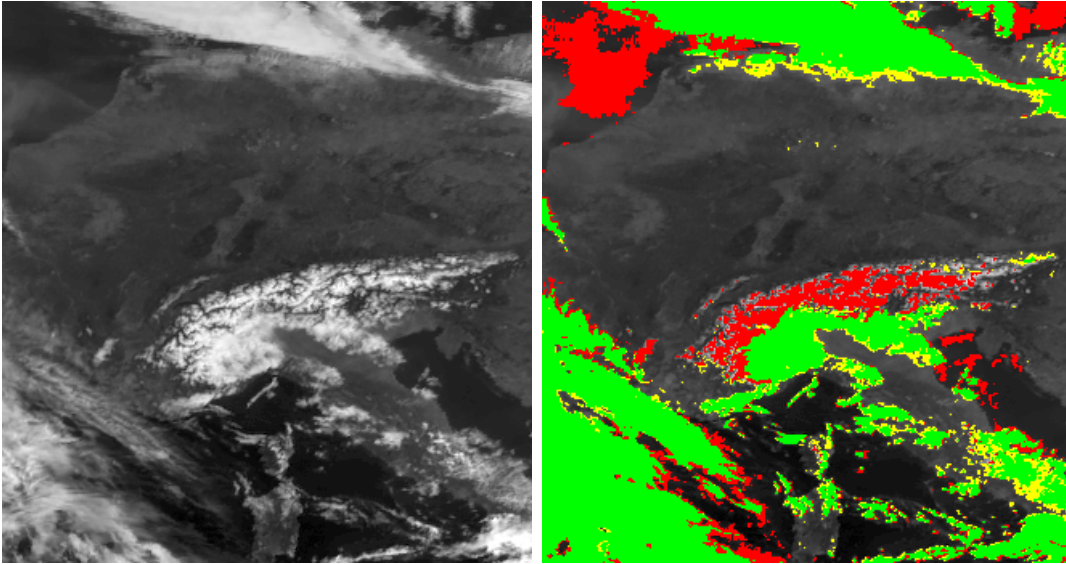


**Figure 7.7:** 22 April 2005, 08:15 UTC,  $VIS_{006}$  (left), and  $VIS_{006}$  channel, overlaid with comparison between IMK and SAF cloud mask (right). Green: both have clouds, red: clouds only in SAF cloud mask, yellow: clouds only in IMK cloud mask. The Alps are snow covered and the IMK cloud mask classifies the snow correctly. The SAF cloud mask apparently does not use the snow detection and classifies the Alps as cloudy.

but it should be flagged appropriately. The SAF also has problems over desert areas, especially in the morning, often wide stretches are masked as cloudy. A difficulty the SAF and FUB cloud mask have is that both very often mask coastlines as cloudy. This is probably due to a ratio test between  $VIS_{006}$  and  $VIS_{008}$ , over clouds this ratio is near one, but this is also true for coastal pixels (see chapter 6.8 for details). The IMK cloud mask does not use this test, as the number of additionally found clouds is low, but the problems that arise along coastlines are huge.

Over all the IMK cloud mask seems to have a solid performance, than can withhold the comparison with other MSG cloud masks. Therefore the use of the IMK cloud mask as a validation data set for the CLM is possible. The results will be described in the next chapter.

# Chapter 8

## Comparison between MSG and CLM data

The comparison between cloud information derived from Meteosat and cloud data from the regional climate model CLM is one of the main aspects of this work. With the help of satellite data, the model cloud data will be evaluated and some model and detection algorithm deficits can be identified. The correct modelling of clouds in weather and climate models is not trivial, but essential for many processes. In the atmospheric water cycle, clouds are a very prominent part, easily viewed and detected from the ground and from space. The every day weather conditions like sunshine, rain, snow, cold or warm nights depend on clouds. But also in the long term clouds play an important role in the earth's climate. Due to their influence on the solar (reflectance) and terrestrial (absorption) radiation, changes in the earth's cloud distribution can have a significant impact on the climate.

A first comparison between CLM and Meteosat data was performed with CLM data for the year 2001 (Haller, 2005). This was compared to the cloud mask of Meteosat 7 (Schmidt, 2008). The overall agreement was reasonably good, but in convective situations the performance of the CLM was only mediocre (Huckle and Olesen, 2007).

With the commissioning of the first MSG satellite, as Meteosat 8 the available spectral information for cloud detection was strengthened (chapter 6) and a more advanced CLM version became available in 2007 (chapter 4).

As mentioned before convective situations belong to the more problematic issues for numerical weather and climate prediction models. On the other hand, detecting convective clouds in satellite data is comparatively easy and robust. Convective clouds in general have a great vertical extension and therefore show up distinctively in the infrared. During the day they also have high reflectivity in the visible due to their large optical depth.

**Table 8.1:** Comparison between MSG cloud mask (IMK) and CLM data. From March to October 2005, all days, convective days, non convective days.

	Average over area of interest		
	All days	Convective days	Non convective days
IMK & CLM cloud free	21.8	56.1	12.2
IMK & CLM cloudy	55.7	15.9	66.3
IMK non cloudy, CLM cloudy	16.8	21.2	15.5
IMK cloudy, CLM non cloudy	5.8	6.8	5.8
<b>Total agreement of IMK &amp; CLM</b>	<b>77.5</b>	<b>72.0</b>	<b>78.6</b>
Total cloud cover in IMK	61.3	22.7	72.1
Total cloud cover in CLM	72.4	37.1	81.9

The comparison of the data took place in the region of interest described in chapter 5.2, which is smaller than the actual model area. If not stated otherwise all comparisons in this chapter are on a pixel basis. This means every pixel in the two data sets is compared individually.

The first comparison in the region of interest is done for all days from March to October 2005. For every pixel an agreement in percent is calculated, also the number of clouds in only one of the data sets is given in percent. The total agreement for this period is 77.5 %. The total amount of cloudiness is more than 10 percent-points higher in the CLM data (72.4 %) than in the satellite data (61.3 %)(Table 8.1).

Looking at different areas in the region of interest no large spatial variations in the total agreement show up. The highest total agreement is over the Black Forest (80 %), the lowest is along the Rhine (approx. 75 %). In this area the clouds only modelled in the CLM, but not verified by the cloud mask increase to over 15 %, above the Black Forest the difference is as low as only 5% (Fig. 8.1). For convective days only, the numbers change quite significantly in some cases, a detailed description is found in chapter 8.1.

The results of comparing the data sets for each month individually are shown in Table 8.2. The total agreement in each month varies from 74.2% to 84.6%. The agreement on cloud free and cloudy pixels changes drastically between March and October. The amount of clouds only modelled in the CLM and not found in the MSG data is relatively high and with the exception of April (11.6%) and July (21.9%) also relative constant. The clouds only detected in the MSG data and not modelled in the CLM is low, as is the variation, with the exception of June (10.3%). The total amount of clouds in the two data sets changes from more than 70% (MSG) and 85% (CLM) in March to just 41% (MSG) and 54% (CLM). The difference in the total cloud amount has its maximum in July (18%) and its minimum in June (4.6%). The decrease of clouds is continuous from March to October, with the exception of July in the CLM data.

Interesting is the fact that in the CLM data, as well as in the clouds detected in the MSG data, the total number of clouds decreases enormously in September and

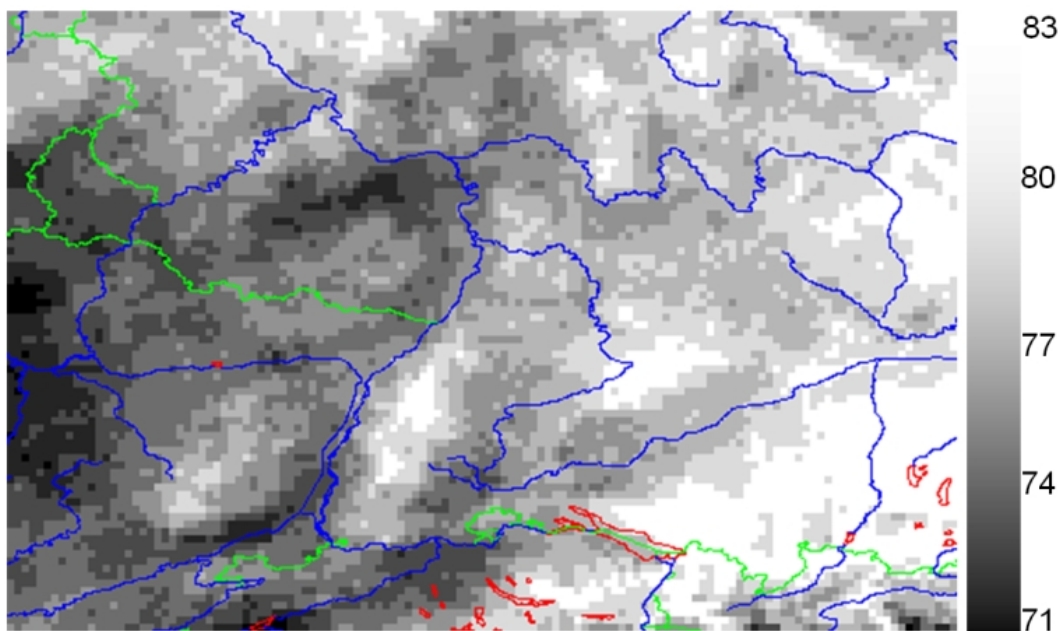


**Figure 8.1:** Comparison between MSG cloud mask and CLM cloud cover on pixel basis for March to October 2005. Total agreement (cloudy and non cloudy) in percent.

**Table 8.2:** Comparison between MSG cloud mask (IMK) and CLM data. Monthly analysis from March to October 2005, all days of every month.

	March	April	May	June	July	August	September	October
IMK & CLM cloud free	9.2	21.4	17.3	20.9	14.3	20.5	27.8	41.6
IMK & CLM cloudy	66.9	63.2	58.9	53.6	59.9	58.9	48.6	37.1
IMK non cloudy, CLM cloudy	18.3	11.6	16.0	15.2	21.9	16.9	17.0	17.4
IMK cloudy, CLM non cloudy	5.5	3.8	7.8	10.3	3.9	3.7	6.6	3.9
<b>Total agreement of IMK &amp; CLM</b>	<b>76.1</b>	<b>84.6</b>	<b>76.2</b>	<b>74.5</b>	<b>74.2</b>	<b>79.4</b>	<b>76.5</b>	<b>78.7</b>
Total cloud cover in IMK	72.4	67.0	66.7	63.9	63.8	62.6	55.2	41.0
Total cloud cover in CLM	85.2	74.8	74.9	68.8	81.8	75.8	65.6	54.5

**Table 8.3:** *Convective days in the study area*

Months	Days
March	–
April	2, 3, 4, 21, 22
May	1, 27, 28, 29
June	18, 19, 23, 24, 27, 28
July	11, 12, 13, 14, 15
August	10, 17, 18, 29, 30, 31
September	1, 2, 7, 8
October	–

October. This indicates that the cloud mask as well as the CLM represent the 'reality' in their own way. If the distinct cloud decrease in the last two months would to occur in only one data set, questions on how good both algorithms work would arise. It is a fact, that trying to model such complex events as convection and cloud development, can not represent the reality perfectly, but in a general way this is possible. Also the automatic detection of clouds in the satellite data has its obvious drawbacks, so that not every pixel will be analysed correctly. But the similar behaviour of two so different data sets shows that the algorithms behind both programs work and produce (more or less) reliable results. Nevertheless improvements in both algorithms are possible and necessary.

The extreme changes in the total cloud cover in the CLM from June (68.8%) to July (81.8%) with a constant cloud cover in the satellite data makes a closer investigation into these two months interesting. The changes also occur when only looking at the convective days in these months (table 8.4). A detailed analysis will be done in chapter 8.4.

## 8.1 Convective situations

For the eight months from March to October convective days in the region of interest were selected by visual inspection in the MSG data. The main selection criterion was the forming of clouds independently from large meteorological systems, such as fronts and low pressure systems. The development of clouds mainly started over the Black Forest and the Vosges Mountains. The exact days chosen can be found in Table 8.3.

Looking at the pixel by pixel comparison in the study area, for convective days only, we see a decrease of agreement between cloud mask and model output, from an average above 77% to only 72%. This is mainly due to a nearly 5% increase of clouds only modelled by the CLM, but not detected in the MSG data. Over all in convective days the amount of clouds is significantly lower than for days without convection, for exact figures see table 8.1. The slight variation of the total agreement in the study area for

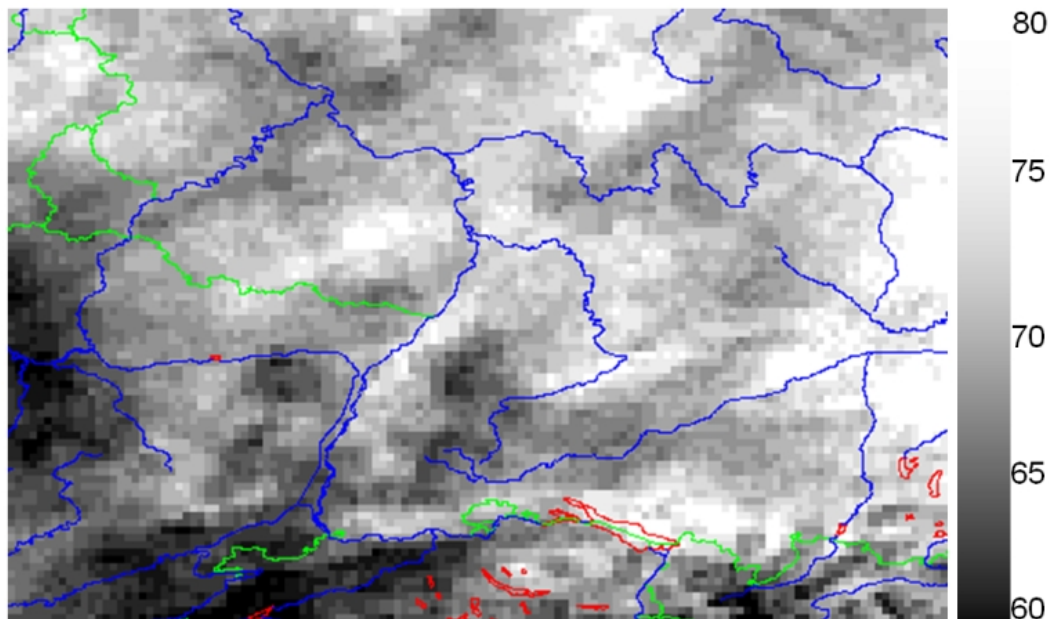


**Figure 8.2:** Comparison between MSG cloud mask and CLM cloud cover on pixel basis for 30 convective days between March and October 2005. See table 8.3 for details on convective days. Total agreement (cloudy and non cloudy) in percent.

all days increases on convective days. In some areas the agreement remains stable (to the east of Lake Constance), others have only a slight decrease (e.g. Black Forest) and in some areas the agreement goes down significantly. The difference within the study area is now nearly 20% (Fig. 8.2).

### 8.1.1 Monthly analysis

In this chapter we will take a closer look at the convective days in the individual months. In March and October no convective days were found that match the criteria of developing primarily due to solar heating of the ground or due to the overflow from low and medium range mountain ridges. The numeric results of the comparison for the individual months can be seen in table 8.4.

- **April:** The agreement for cloud free pixels is very high, resulting in an overall agreement for April that is even better than that for non convective days. Taking a closer look we see, that range of total agreement is between 52 and 100% (Fig. 8.3). The lowest agreement is at the western border of the study area. In the Rhine Valley the agreement is also higher than normal with values between 80 and 90%. Over the Black Forest however the agreement is lower, only between 70 and 80%. This is due to the fact that the most of the (shallow) convection

**Table 8.4:** Comparison between MSG cloud mask (IMK) and CLM data. For convective days from April to September 2005, the results are listed for each month individually.

	April	May	June	July	August	September
IMK & CLM cloud free	80.9	58.4	46.2	37.6	65.3	46.7
IMK & CLM cloudy	6.0	8.2	23.8	26.2	11.2	18.3
IMK non cloudy, CLM cloudy	6.2	23.9	19.2	29.2	20.0	31.7
IMK cloudy, CLM non cloudy	6.9	9.5	10.7	7.0	3.5	3.4
<b>Total agreement of IMK &amp; CLM</b>	<b>86.9</b>	<b>66.6</b>	<b>70.0</b>	<b>63.8</b>	<b>76.5</b>	<b>65.0</b>
Total cloud cover in IMK	12.9	17.7	34.5	33.1	14.7	21.6
Total cloud cover in CLM	12.2	32.1	43.1	55.4	31.2	50.0

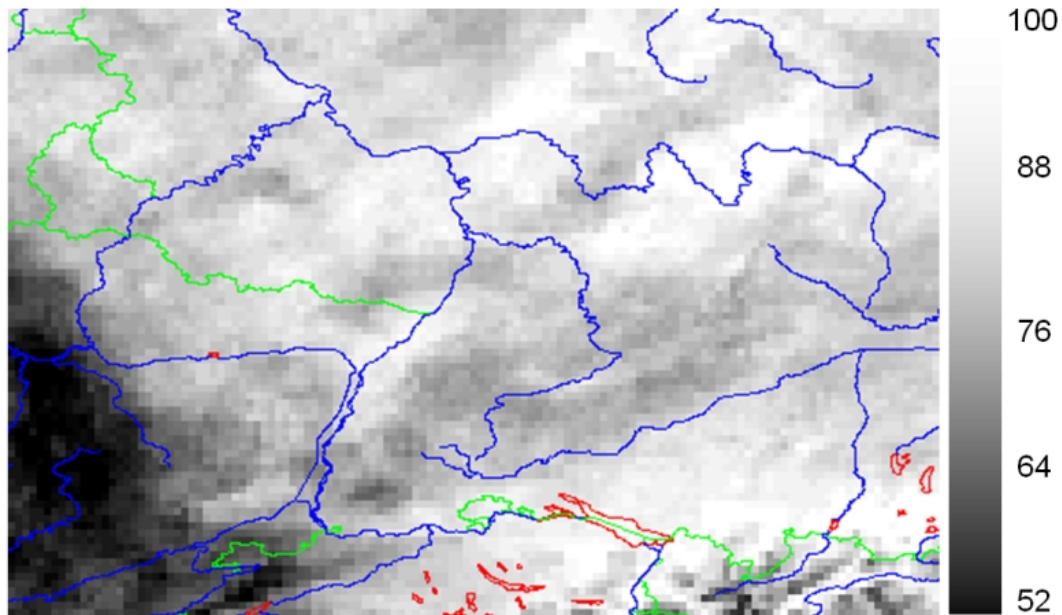


**Figure 8.3:** Total agreement between CLM and MSG cloud mask data for convective days in April 2005.

taking place over the Black Forest is not modelled by the CLM. This means that although the comparison is generally good in the whole study area, the performance of the CLM concerning the modelling of convective clouds is poor.

- **May:** The total agreement in May is 20%-points lower than in April. Mainly due to clouds modelled by the CLM not being present in the MSG data. The agreement on clouds is still low with only 8.2%. Looking at the locally induced convection especially on May 28 we see again, that the CLM does not model the convection over the Black Forest. Consequently, the agreement here is very low (below 50%). On May 29 the agreement is better, but the clouds modelled by the CLM are not due to convection but come in from the north, so the agreement is more accidental.
- **June:** The convective days in June are not so favourable for validating the CLM with regard to its ability to model locally induced convection. The days in June have a large amount of deep convection taking place, although it is not very often that these initiated in the Black Forest or Vosges Mountains, but originated further to the west. The agreement for the movement of these large thunderstorms is good although the extent is often smaller in the CLM data than in the cloud mask. Thus the amount of clouds only detected in the MSG data and not modelled by the CLM is relatively high with more than 19% (Tab. 8.4).
- **July:** A detailed description of the comparison for July can be found in chapter 8.1.2 where the agreement for individual points is discussed. The agreement on cloudy pixels is higher than in the other months and the modelling of convection seems to work better as well.
- **August:** The agreement in August is the second highest for convection in one month. The convection over the Black Forest is modelled better than in other months leading to an agreement of over 90% for the southern part of the Black Forest. On some occasions the agreement is lower but when looking at the region of Black Forest and Swabian Alb the amount of clouds in the two data sets seems to be similar. Further comparisons in this direction can be found in chapter 10. Although the agreement concerning the convection is better than for other months during some mornings the CLM models great patches of fog along the Danube and to the south of the Black Forest, resulting into over 40% of clouds only modelled in the CLM but not verified by the satellite data.
- **September:** Not many convective days were observed in September, all of them were in the first week. The overall agreement is not so good, with the CLM modelling many clouds not validated by the cloud mask. Again a large amount of fog is modelled without it showing up in the satellite data. For the first convective days the agreement is very poor with the CLM producing wide spread clouds in contrast to the more structured and smaller clouds picked up by the cloud mask. During the second two days of convection the pixel by pixel agreement is not very good, but the CLM produces a similar kind of cloud pattern compared to the MSG data, with convection initiating over the study area.

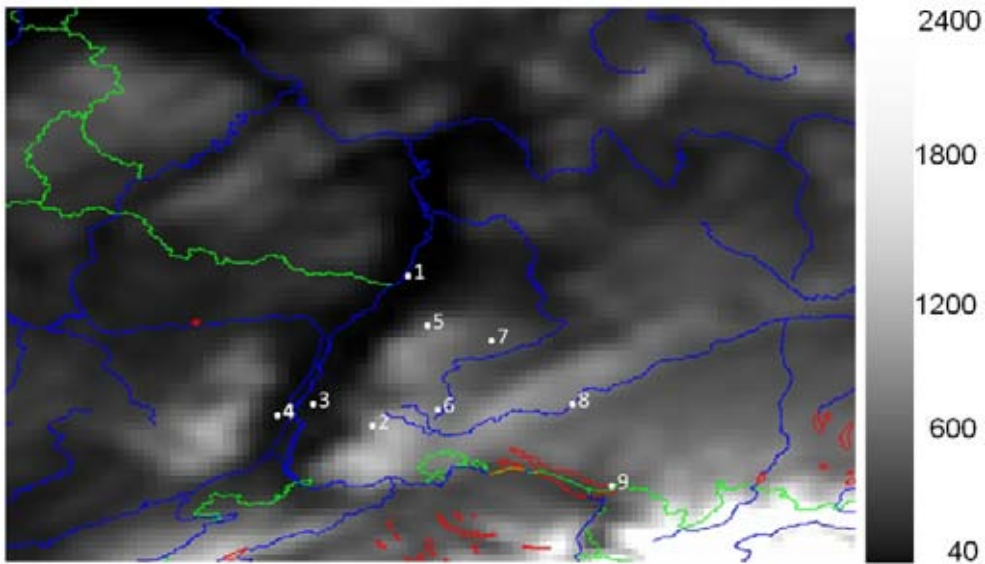


**Figure 8.4:** Grey scale topography of study area in meters above sea level. Numbers according to points described in Table 8.5

### 8.1.2 Point comparison

To analyse some areas in more detail a total of nine points were chosen representing areas with good and bad agreement between the MSG cloud mask and the CLM output cloud data. Four pixels have an agreement above 73% and five pixels have an agreement below 66%. The location of these pixels is described in table 8.5 and shown in Figure 8.4. The period these points will be analysed in more detail is from July 11 to 15 in 2005.

During these days in July central Europe is under the influence of a high pressure system, which changes only moderately during the time (Fig. 8.5). During this period the area of South West Germany has an Easterly airflow. No fronts or low pressure systems pass through in this time so the clouds are mainly due to local convection, mostly triggered over the mid range mountains of the Black Forest and the Swabian Alb (Fig. 8.6).

On the first two days convective clouds develop over the mountains in the afternoon. On July 13 and 14 only very few clouds occur, followed by some more convection on July 15.

Turning to the analysis of the single pixels for each day we see that for July 11 the agreement between MSG cloud mask and CLM cloud output data is very good for most of the pixels. Especially for the points 2, 6, 7, 8 and 9, at certain times the cloud mask has some cloud free slots whereas the CLM is constantly cloudy. At the points 1, 3, 4 and 5 the cloud mask has more cloud free patches, but the CLM remains constantly cloudy. Overall for this day we can recognise, that the good agreement is due to

**Table 8.5:** List of pixels analysed in detail. The agreement refers to all convective days from March through October 2005. Numbers according to Figure 8.4.

Number	Location	Coordinates	Height above msl	Agreement for convective days	
				March - October	July
1	Karlsruhe	49° 4' N 8° 23' E	110 m	73%	63%
2	Southern Black Forest (East of Freiburg)	48° 0' N 8° 2' E	798 m	75%	76%
3	Kaiserstuhl (Baden) (Northern end)	48° 6' N 7° 43' E	225 m	67%	62%
4	Colmar (France)	48° 3' N 7° 24' E	180 m	66%	58%
5	Forbach (Murgtal) (Northern Black Forest)	48° 39' N 8° 23' E	723 m	64%	62%
6	Villingen-Schwenningen (East of Black Forest)	48° 9' N 8° 28' E	708 m	65%	64%
7	Tübingen (Swabian Alb)	48° 33' N 8° 55' E	436 m	75%	73%
8	Riedlingen (Swabian Alb)	48° 11' N 9° 28' E	582 m	66%	76 %
9	Lindau (Bodensee)	47° 35' N 9° 138 E	390 m	82%	82%

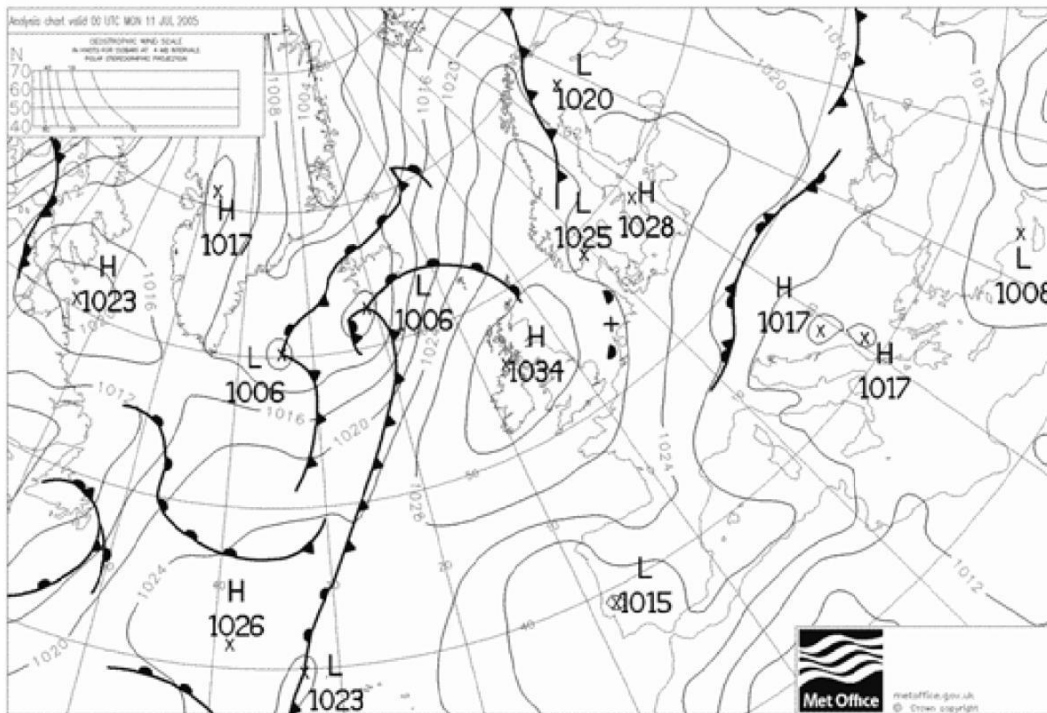


**Figure 8.5:** Surface Pressure for 11 July 2005, 00:00 UTC (UK Met Office, 2005)

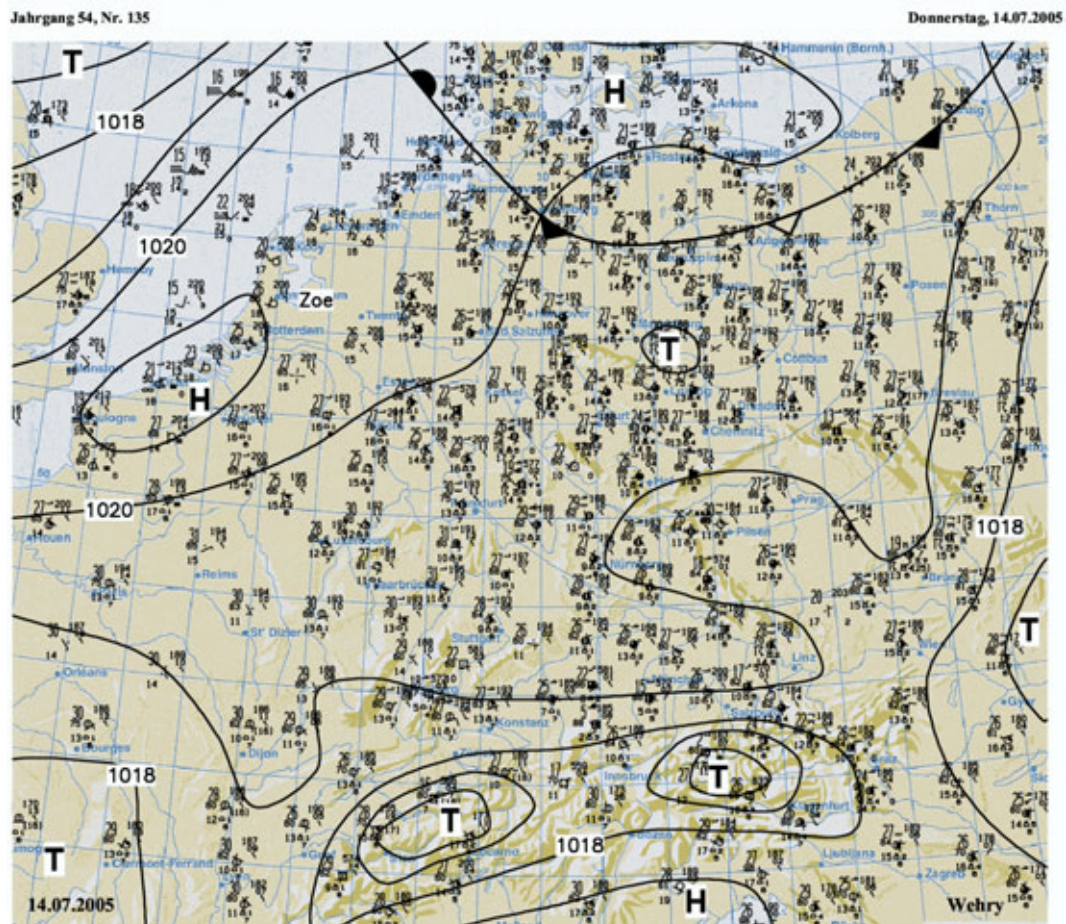


**Figure 8.6:** Surface Pressure for 14 July 2005, 12:00 UTC (DWD, 2005)

the fact, that the CLM has a constant cloud cover over the whole area. Looking at the comparison over the entire region of interest we see that the agreement is generally good, however the CLM has more clouds especially to the west of an area with compact cloud cover seen in the MSG data. This area of relative compact clouds is over and to the east of the Swabian Alb, thus the additional clouds that the CLM models are situated were most of the points of comparison are located.

On the following day July 12, the amount of clouds is still high but more cloud free patches occur at all points. The agreement between the two data sets reduces considerably, only at points 8 and 9 it is still high. Again the day starts with a high reaching cloud mass to the eastern part of the area of interest. And again the CLM has too many clouds to the west of this, thus the agreement at points 8 and 9 is high and at the more westerly points it is lower, with a large number of clouds not validated by the cloud mask in the morning. Around 11:00 UTC convection starts producing some low clouds and the agreement increases for the points 2 - 7. Later in the afternoon some deep convection develops, but the agreement does not increase, there are too many clouds in the CLM data. The broken up cloud distribution in the MSG data is not represented in the CLM. There are also areas with broken up clouds in the CLM but these do not match with the MSG data and are far less than in the satellite data.

The night from July 12 to 13 is mostly cloud free in the MSG data, but in the CLM many clouds remain. Around 8:00 UTC these clouds have shrunk to a minimum but still occupy significantly more space towards the Rhine Valley than can be detected by the cloud mask. Approximately two hours later convective clouds start to form over the mountain ridges. But convection is only shallow on this day. The convective cell structure is represented well by the CLM. In the area the mixture of cloudy and non cloudy patches is modelled, but also looking at the selected points the cloudy character of the noon hours is clearly designated, with just at points 3 and 4 showing too many clouds in the CLM. According to the MSG data the clouds dissolve around 17:00 UTC in the CLM however, clouds are modelled for a further two hours. The night is cloud free in both data sets.

On July 14 not much happens in terms of convection. At all selected points the morning is cloud free in both CLM and MSG data. In the late morning hours some clouds start to develop in the north of the region of interest. None of the selected points are that far north. The temporal agreement between CLM and MSG seems to be quite good, but the spatial agreement is lower, however the convective character is represented well in the model. In the afternoon some clouds form over the Black Forest (points 2, 5 and 6). These clouds are shown mainly in the cloud mask, but looking at the entire region clouds are modelled by the CLM as well just not at the exact same place. Again the dissolving of the clouds in the CLM is registered about 2 hours later than in the MSG data. On this day points 4, 7 and 9 are completely cloud free in both data sets.

The last day of this point evaluation is July 15. The night is cloud free (CLM and MSG agree). At 5:00 UTC clouds come into the region from the west, these are connected with a cold front that will pass by north of the region during that day. The CLM

however, models too many clouds coming in from the west. During the rest of the day broken up clouds pass over the region, these are mainly connected with the cold front, but also there is some local convection taking place. The agreement at the points 2, 3 and 4 is reasonably good over most of the day, there are just some differences due to broken up clouds around noon. At the other points the CLM data shows too many clouds coming in from the west, during the morning. Around noon this is better, showing the usual differences in such a patchy environment. The late afternoon and early evening are mostly cloud free, but again the CLM models more clouds at this time of the day than the cloud mask can pick up, especially at the points 1 - 4.

Concluding this point analysis we see a reduction of agreement at the points 1 and 4 compared to all convective days. Also evident is that the CLM produces a high amount of clouds which are not shown by the MSG cloud mask (up to 38%-points at point 4). Generally the MSG only detects more clouds compared to the CLM by max. 5%-points, that is with the exception of point 5, here the figure is 12%-points. After convection dies down, clouds remain longer in the CLM model, than are picked up by the satellite. Most of these 'cloudy pixels' are however only given a low cloud amount (approx. 20%). In addition the cloud detection in the satellite data is very difficult during the hours around sun set. So the amount of clouds modelled by the CLM that appears too high. Even so, the over all amount of CLM clouds remains too high compared with the MSG cloud mask.

## 8.2 Spatial averaging

The pixel by pixel comparison between MSG data and CLM output has obvious drawbacks. Only a minimal spatial shift between the data sets can lead to a poor result. To try and correct this problem the comparison between CLM and cloud mask was repeated with a spatial averaging over 3x3 pixels, centred around the current pixel. Each pixel was now compared by adding the number of cloudy and non cloudy pixels in the 3x3 pixel box for each data set and then comparing the numbers.

The agreement did not increase significantly in any region. The changes in the differences was less than 1%-point in any category (for details see table 8.6). The spatial shift between the two data sets is obviously not as simple or systematic that it could be detected and accounted for with such a method. As this proved not do be very promising and the additional time needed for computing is significantly higher, this type of spatial averaging was abandoned. The idea of accounting for a spatial dislocation is however, taken up again in chapter 10.

**Table 8.6:** Comparison between MSG cloud mask (IMK) and CLM data, for a 3x3 pixel average around a single pixel. All days from March to October 2005, as well as only the convective days.

	Average over area of interest	
	All days	Convective days
IMK & CLM cloud free	22.6	56.8
IMK & CLM cloudy	54.9	15.9
IMK non cloudy, CLM cloudy	17.2	20.6
IMK cloudy, CLM non cloudy	5.4	6.7
<b>Total agreement of IMK &amp; CLM</b>	<b>77.5</b>	<b>72.8</b>
Total cloud cover in IMK	60.2	22.6
Total cloud cover in CLM	72.0	36.5

**Table 8.7:** Comparison between MSG cloud mask (IMK) and CLM data. Monthly analysis from March to October 2005. Daytime (8 - 16 UTC) analysis for all days of every month.

	March	April	May	June	July	August	September	October
IMK & CLM cloud free	7.9	19.0	16.9	17.8	9.1	17.6	27.8	40.9
IMK & CLM cloudy	74.9	69.3	66.7	62.8	70.3	68.0	53.0	41.9
IMK non cloudy, CLM cloudy	11.1	7.1	9.0	10.2	15.6	10.3	14.4	12.2
IMK cloudy, CLM non cloudy	6.1	4.6	7.3	9.2	5.0	4.1	4.8	5.0
<b>Total agreement of IMK &amp; CLM</b>	<b>82.8</b>	<b>88.3</b>	<b>83.6</b>	<b>80.6</b>	<b>79.4</b>	<b>85.6</b>	<b>80.8</b>	<b>82.8</b>
Total cloud cover in IMK	81.0	73.9	74.1	72.0	75.3	72.1	57.8	46.9
Total cloud cover in CLM	86.0	76.4	75.8	72.9	85.9	78.4	67.4	54.1

### 8.3 Day and Night comparisons

The comparison between the IMK cloud mask and the cloud mask from the Freie Universität Berlin (FUB) shows that the performance of the IMK cloud mask is very good during the day but has some difficulties during the night. Sometimes not detecting all cloudy pixels at the edge of cloud bands or declaring cloud free land pixels cloudy because the expected clear sky radiance is calculated to high (see chapter 7.1). This raises the question whether there are any day and night differences between CLM and the cloud masks.

In Table 8.7 the comparison between the cloud mask and the CLM for the daytime (08 to 16 UTC) is shown for every month from March to October. The time from 8 to 16 UTC was chosen because during this time of the day for all eight months the sun is high enough above the horizon in the study area, so that the heating of the ground can take place, the solar channels on SEVIRI can then contribute to the cloud

**Table 8.8:** Comparison between MSG cloud mask (IMK) and CLM data. Monthly analysis from March to October 2005. Nighttime (21 - 3 UTC) analysis for all days of every month.

	March	April	May	June	July	August	September	October
IMK & CLM cloud free	10.4	23.5	16.5	22.4	19.3	23.5	29.5	42.5
IMK & CLM cloudy	60.4	57.4	51.3	44.4	50.0	51.3	43.7	33.1
IMK non cloudy, CLM cloudy	24.0	15.3	23.6	21.7	27.7	22.1	20.3	21.1
IMK cloudy, CLM non cloudy	5.2	3.8	8.6	11.5	3.1	3.1	6.5	3.3
<b>Total agreement of IMK &amp; CLM</b>	<b>70.8</b>	<b>80.9</b>	<b>67.8</b>	<b>66.8</b>	<b>69.2</b>	<b>74.8</b>	<b>73.2</b>	<b>75.6</b>
Total cloud cover in IMK	65.6	61.2	60.0	55.9	53.1	54.4	50.3	36.4
Total cloud cover in CLM	84.2	72.7	74.8	66.1	77.7	73.4	64.0	54.2

detection and, most importantly the cooling of the ground has not yet taken place, or has just begun. So any problems in the MSG cloud mask relating to the modelling of the diurnal temperature cycle are avoided.

For every month the total agreement is higher than for the 24 hour comparison. The cloud free agreement is lower and the agreement in cloudy pixels is much higher. We also see that the number of pixels only marked as cloudy in the CLM drops by a couple of percent points in every month for the daytime analysis. In comparison the number of pixels only marked as cloudy in the MSG cloud mask remains stable. The amount of clouds in the cloud mask data for the daytime increases significantly, in some months more than 10%-points. The number of clouds in the CLM data does not change significantly during the day time.

For the nighttime comparison the time from 21 to 03 UTC was chosen. During this time there is no sun and hence no solar channels available. Here the ground cooling comes fully into play. Also no dawn algorithms should be active in the area of interest during this time. The comparison during the night (Tab. 8.8) give opposite results. The total agreement drops compared to the 24 hour cycle and of course even more compared with the daytime. The amount of clouds only present in the CLM data rises dramatically and reaches a high of 27.7% in July and only in April (15.3%) it is lower than 20%. Again the clouds only present in the MSG cloud mask remain stable. The total amount of clouds in the CLM is slightly lower during the night than during the day. For the amount of clouds in the cloud mask data the difference from day to night is much higher, in July the amount of clouds is up to 22.2%-points lower in the night compared with the day.

The results for the individual months are representative for the entire eight months period from March to October 2005 (Table 8.9). The agreement is much better during the day than during the night (83.0% vs. 72.5%), the amount of clouds in the MSG

**Table 8.9:** Comparison between MSG cloud mask (IMK) and CLM data. From March to October 2005, all days, daytime and nighttime analysis.

	0 - 24 UTC	8 - 16 UTC	21 - 3 UTC
IMK & CLM cloud free	21.8	19.9	23.7
IMK & CLM cloudy	55.7	63.1	48.8
IMK non cloudy, CLM cloudy	16.8	11.2	21.9
IMK cloudy, CLM non cloudy	5.8	5.8	5.7
<b>Total agreement of IMK &amp; CLM</b>	<b>77.5</b>	<b>83.0</b>	<b>72.5</b>
Total cloud cover in IMK	61.3	68.9	54.4
Total cloud cover in CLM	72.4	74.4	70.6

data is 14.5%-points higher during the day, while the clouds in the CLM data are only 3.8%-points higher.

When looking at the day and night comparison with the FUB cloud mask (chapter 7.1) we see that the IMK cloud mask has slightly less clouds during the night than the FUB cloud mask. For the entire period this is 3.7%-points. But although the total amount of clouds during the night might be a little too low in the IMK cloud mask data, the amount of clouds in the CLM data is definitely much too high, by about 20%-points.

## 8.4 Special case: June and July 2005

In the CLM the amount of clouds change significantly in these two months, from 68.8% in June to 81.8% in July. The changes as such are not surprising, as the weather can change over a couple of weeks. Astonishing is however that in the MSG data the cloudiness remains unchanged in these two months (Table 8.2). For the convective days the amount of clouds is very similar in the MSG data but changes from 43.1% to 58.1% in the CLM data (Table 8.4).

Looking at the region in more detail we see that the clouds in the CLM increase from June to July significantly in France to the west of the Vosges Mountains and slightly decrease to the east of Lake Constance (Fig. 8.7). Over the Vosges Mountains the number of clouds increases by 12%-points from June to July. Along the Rhine Valley the increase is between 16 and 20%-points. The clouds over the Black Forest increase between 15 and 22%-points. To the east of the Black Forest and along the Danube the increase is only small, around 5%-points. Near Lake Constance there is no change, with only a slight decrease even further to the east.

These changes are not necessarily wrong. However, when comparing these to the MSG cloud mask data we see an increase of clouds between 4 and 9%-points along the Rhine Valley and the Black Forest and a slight decrease along the Danube. Comparing the total agreement for June and July in the area of interest we see no changes. This is

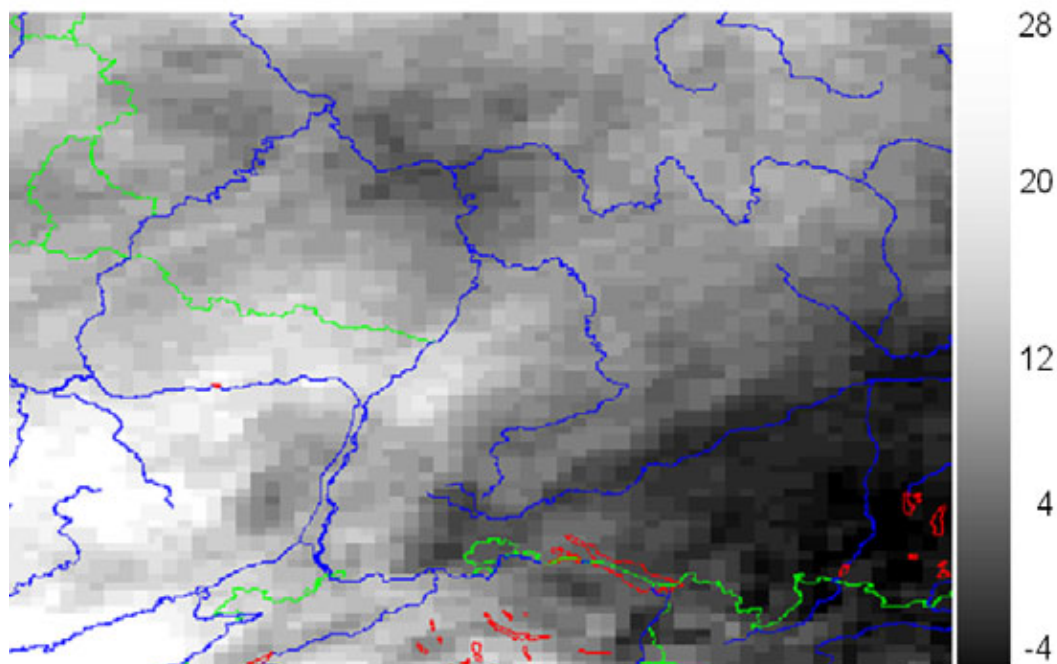


**Figure 8.7:** Differences in the CLM cloud cover between July and June 2005 in percentage points. The biggest differences appear to the west of the Vosges Mountains. In June higher values are recorded to the east of Lake Constance, than in July.

mainly due to the increase of clouds only detected by the cloud mask to 10.3% in June and a decrease to only 3.9% in July. Not only are too many clouds modelled in July (clouds only in the model and not detected in the MSG data rise to 21.9%) but also many clouds are not modelled in June. This implies that the CLM seems to work better in the other months.

Although there is no change of the over all agreement between CLM and MSG data from June to July in the area of interest in some parts there are however quite large changes. In Figure 8.8 the differences between the overall agreement in July and June are displayed. To the north and the north east the agreement is better in June but over the medium range mountains of the Vosges and the Black Forest the agreement increases in July by up to 9%-points. In the Rhine Valley the increase is around 4%-points and near Lake Constance 5%-points. Whereas along the Danube the agreement decreases slightly.

For the convective days in these two months the picture is somewhat different. The increase in clouds in the CLM is still apparent but with 11.7% not quite as high. The amount of clouds in the MSG data even goes down a little in July. While the over all agreement for all days in June and July is the same, the value for convective days drops from 70.0% in June to 63.8% in July, the value for convective days for July is the lowest for all six month.

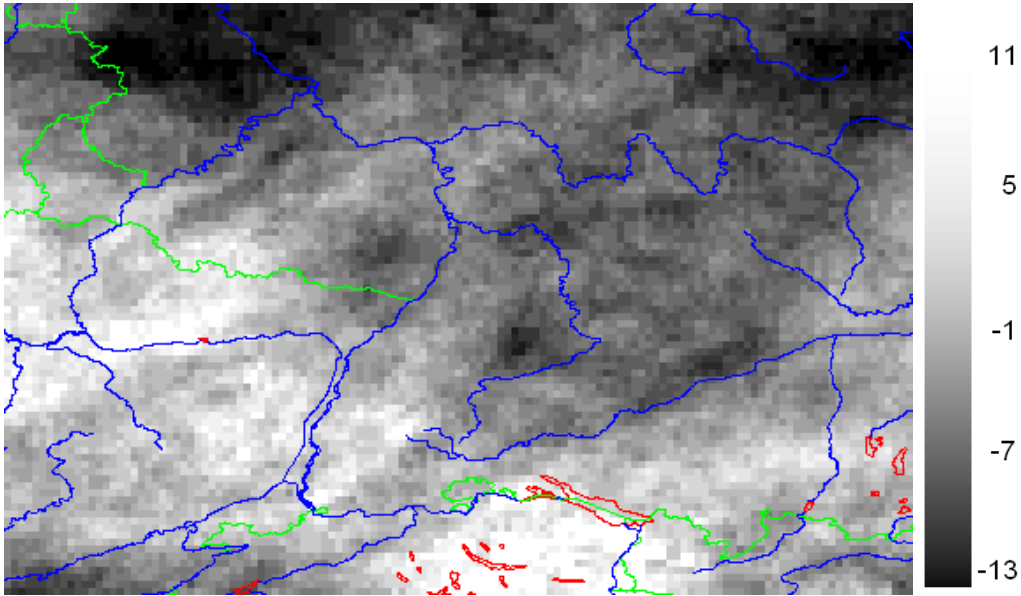


**Figure 8.8:** Differences between the total agreement between CLM and MSG cloud mask July vs. June 2005.

It is noticeable that in France and to the north of the area of interest the agreement drops considerably, in some places more than 30%-points (Fig. 8.9). Over the Vosges Mountains and the Rhine Valley the agreement is down approx. 10%-points. Over the Black Forest the agreement is around 6%-points better. The best values are along the Danube and towards the east, with an improvement of up to 20%-points.

We can summarise that the CLM has quite a lot of difficulties in these two months. The overall amount of clouds is very low in June compared to the other months, but number of clouds not modelled by the CLM is exceptionally high. On the other hand, the amount of clouds shown in the CLM increases drastically in July, but is not confirmed in the MSG data, resulting in every 5th CLM cloud not being contained in the satellite data. The overall agreement between CLM and MSG increases over the middle range mountains. But when looking at the convective days the performance worsens. Only a slight increase over the Black Forest but a dramatic decrease to the north and the west implies that the quality of the modelling of clouds for the convective days in July is not very good. However only a comparatively short time period has been compared. Further steps should include multi year analysis, to see if changes in the detection algorithm occur and how the model reacts in different years. Also the influence of the horizontal resolution of the model on the modelled clouds should be analysed.

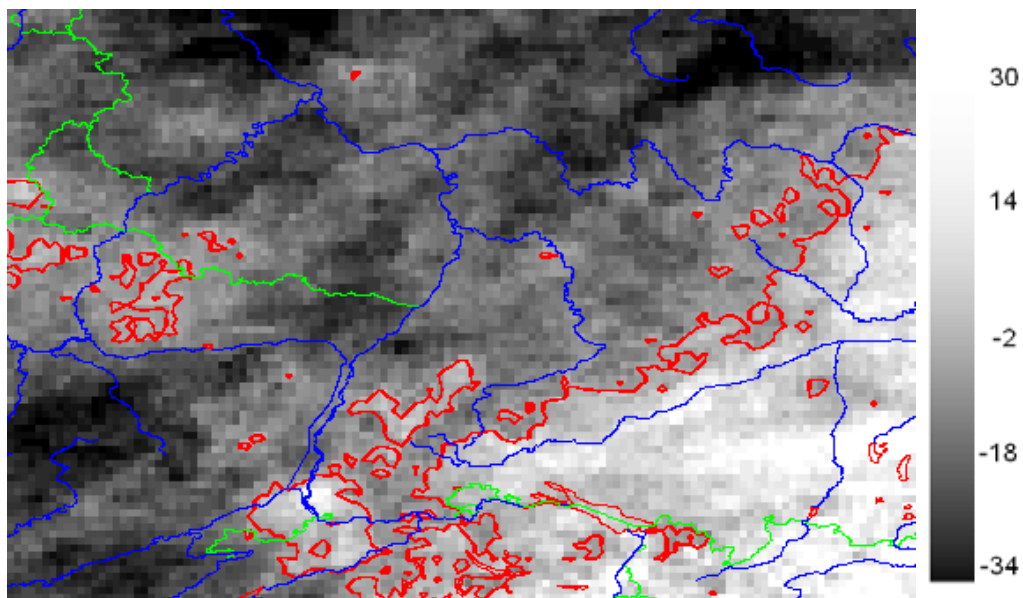


**Figure 8.9:** Differences between the overall agreement between CLM and MSG cloud mask July vs. June 2005 for convective days only. Solid red: line of 0%-points change.

# Chapter 9

## Cloud types

In this chapter the standard cloud types and classifications are introduced. In chapter 10 the clouds in the MSG data will be classified into the groups as described here.

The description of clouds in most (meteorological) literature is based on observations from the ground. The characteristics of the clouds are described as a human observer on the surface would see them. The view from space can be quite different. Where the observer on the ground can see the height of the cloud base above the ground, he can sometimes also see the full vertical extend (e.g. thunderstorm) but at other times he can not. From space, on the other hand, with a normal passive sensor in the VIS and IR only the top of the clouds can be observed. In some cases with (semi) transparent clouds (e.g. thin cirrus) the view through the top most layer onto a lower layer or the ground is possible, the determination of the height above ground for the base of a cloud is in generally not possible. Although the two points of view could not be more different it does make sense to use similar classes for the cloud classification from satellites as from the ground .

The classical definition or classing of clouds from the ground uses two main criteria:

- The height of the cloud base.
- The appearance of the cloud.

Three height ranges for the cloud base are used, in Table 9.1 these levels are listed according to the region.

In the following the main classes, as defined by the WMO (WMO, 1956) are listed according to their height, Figure 9.1 shows these ten main cloud types in the relevant height and vertical extent.

**Table 9.1:** *Standard classification of clouds, height assignment appertaining to the region (DWD, 1990).*

Cloud level	Polar region	Mid latitudes	Tropics
upper	3 - 8 km	5 - 13 km	6 - 18 km
middle	2 - 4 km	2 - 7 km	2 - 8 km
low	from ground to 2 km	from ground to 2 km	from ground to 2 km

### High clouds

- Cirrus (Ci) - composed of detached cirriform elements in the form of white, delicate filaments, of white (or mostly white) patches, or of narrow bands.
- Cirrocumulus (Cc) - appearing as a thin, white patch of cloud without shadows, composed of very small elements in the form of grains, ripples, etc. The elements may be merged or separated and more or less regularly arranged; they subtend an angle of less than  $1^\circ$ .
- Cirrostratus (Cs) - appearing as a whitish veil, usually fibrous but sometimes smooth, that may totally cover the sky, and that often produces halo phenomena, either partial or complete.

### Medium high clouds

- Altopcumulus (Ac) - white and/or gray in color, that occurs as a layer or patch with a waved aspect, the elements of which appear as laminae, rounded masses, rolls, etc.
- Altostratus (As) - in the form of a gray or bluish (never white) sheet or layer of striated, fibrous, or uniform appearance. Altostratus very often totally covers the sky and may, in fact, cover an area of several thousand square miles. The layer has parts thin enough to reveal the position of the sun, and if gaps and rifts appear, they are irregularly shaped and spaced.

### Low clouds

- Stratocumulus (Sc) - predominantly stratiform, in the form of a gray and/or whitish layer or patch, which nearly always has dark parts. Its elements are tessellated, rounded, roll-shaped, etc.; they may or may not be merged, and usually are arranged in orderly groups, lines, or undulations, giving the appearance of a simple (or occasionally a cross-pattern) wave system.
- Stratus (St) - in the form of a grey layer with a rather uniform base. Stratus does not usually produce precipitation, but when it does occur it is in the form

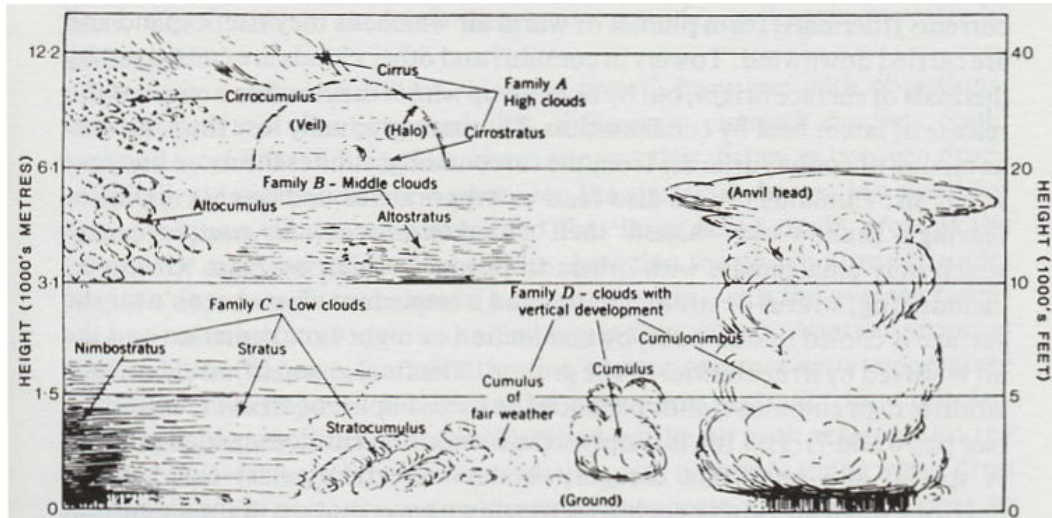


**Figure 9.1:** *The ten basic cloud types classified according to height and form (Strahler, 1965).*

of minute particles, such as drizzle, ice crystals, or snow grains. Stratus often occurs in the form of ragged patches, or cloud fragments (stratus fractus), in this case rapid transformation is a common characteristic.

### Clouds with large vertical extend

- Nimbostratus (Ns) - grey coloured and often dark, rendered diffuse by more or less continuously falling rain, snow, sleet, etc., of the ordinary varieties and not accompanied by lightning, thunder, or hail. In most cases the precipitation reaches the ground, but not necessarily.
- Cumulus (Cu) - in the form of individual, detached elements that are generally dense and possess sharp non fibrous outlines. These elements develop vertically, appearing as rising mounds, domes, or towers, the upper parts of which often resemble a cauliflower. The sunlit parts of these clouds are mostly brilliant white; their bases are relatively dark and nearly horizontal.
- Cumulonimbus (Cb) - exceptionally dense and vertically developed, occurring either as isolated clouds or as a line or wall of clouds with separated upper portions. These clouds appear as mountains or huge towers, at least a part of the upper portions of which is usually smooth, fibrous, or striated, and almost flattened as it approaches the tropopause. This part often spreads out in the form of an anvil (incus) or vast plume.

Several of these clouds will be analysed and classified in chapter 10. Although when viewed from space clouds have a different appearance, the basic use of this classification makes sense. Most meteorologists and people interested in the subject will have

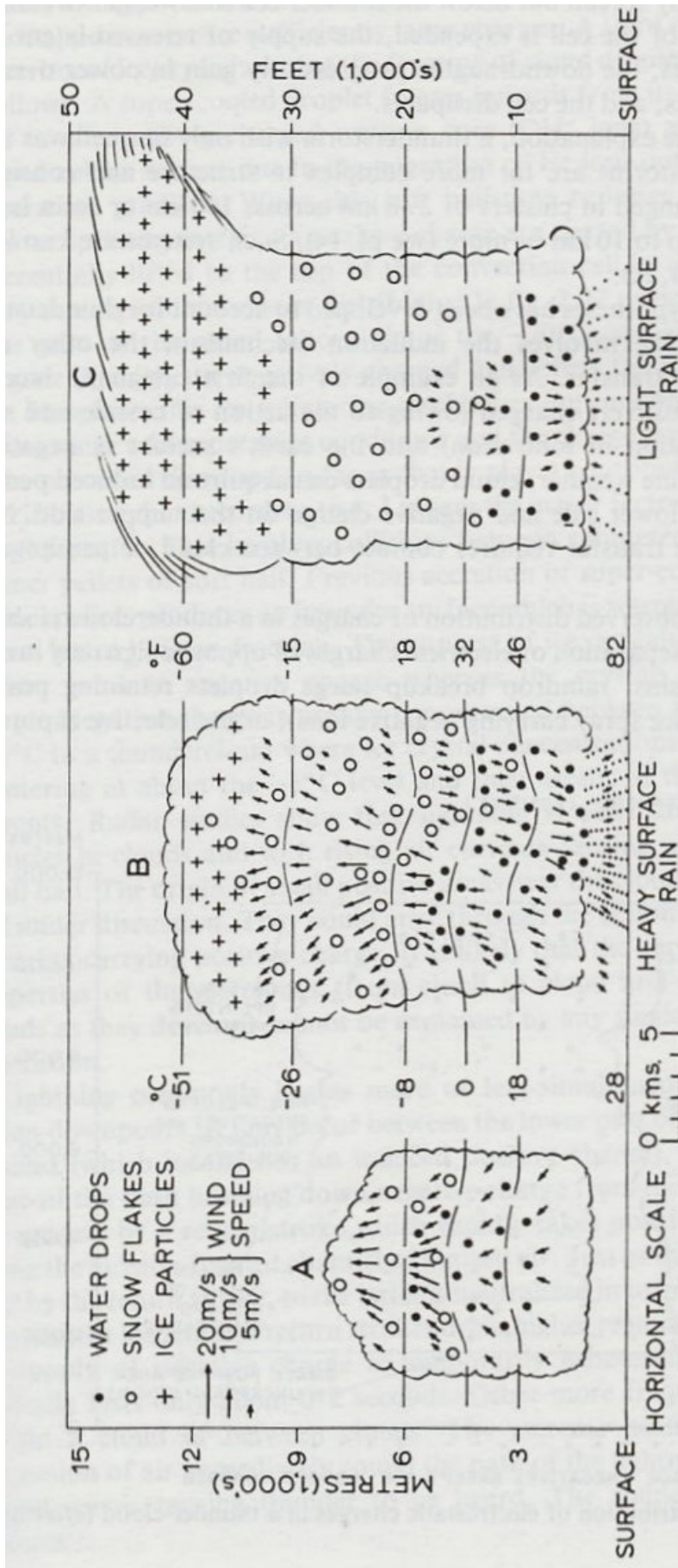


**Figure 9.2:** The cycle of a local thunderstorm. The arrows indicate the direction and speed of air currents. **A** The developing stage of the initial updraught. **B** The mature stage with updraught and downdraught. **C** The dissipating stage dominated by cool downdraughts. (Barry and Chorley 1987)

a general idea what these different classes represent. Also several clouds defined in this way have very distinctive characteristics when viewed from space, although not necessarily identical as when viewed from the ground.

An emphasis in this thesis is on the detection and comparison of convective clouds especially thunderstorms (cumulonimbus). In Fig. 9.2 the development of a local thunderstorm, from a small cumulus cloud to a fully developed cumulonimbus is shown. The development of convection normally takes place when the radiation from the sun heats the ground and the lowest air layer heats up above a certain triggering temperature. This is the temperature, at which an air parcel will continue rising, if it is drawn out of its surroundings. This initiation of convection very often starts where the surface is not homogeneous. Mountain slopes also enhance the possibilities of initiating convection (Meißner et al. 2007; Barthlott et al. 2006). The area of interest contains the Black Forest, Swabian Alb and the Vosges Mountains. Convection will very often be triggered over the leading edges of these mountain ridges.

# Chapter 10

## Object Based Image Analysis

*The Past: Pixels - The Present: Objects - The Future: Intelligence*

During the past decades automated image analysis with computers was mainly based on pixels (Blaschke and Hay, 2001, Asner et al., 2003). Pixels can hold various information, e.g. measured values from sensors, land use/cover etc. With a single pixel point information is available, but the connection to the surrounding area is limited.

A trained human expert can move beyond the pixel level and use semantic information in identifying objects and structures in satellite images. The obvious drawback in using this expert approach is time and consistency. The same image can be analysed differently by different people or even by the same person some time later. Using rule sets for a computer based analysis will deliver the same results every time. For this the classical approach of dealing with pixels has to be abandoned and the step to the use of objects in images has to be taken (Hay et al., 2001).

In the past 15 years the advances in automated image analysis based on objects have been significant, developing the software from 'laboratory use', to commercially available and usable products (Hay et al., 2005). We are now able to use this procedure in a standardised way. This technique can be used for any data based on pixel or gridded data (Castilla et al., 2008). It can be used for the analysis of raster electronic microscope images, as well as radio images from far away stars and galaxies.

Going from pixels to objects is the combination of similar pixels in a meaningful way. Neighbouring pixels, with for example similar spectral values, are grouped together to form an image segment (Fig. 10.1). Depending on the feature one wants to extract these segments can be small (e.g. a single tree) or larger (e.g. an entire forest). When creating these segments the spatial and spectral inhomogeneity is minimised.

The segmentation of an image on different levels brings a parent-child connection between smaller and larger objects. The process of '**region merging**' combines smaller

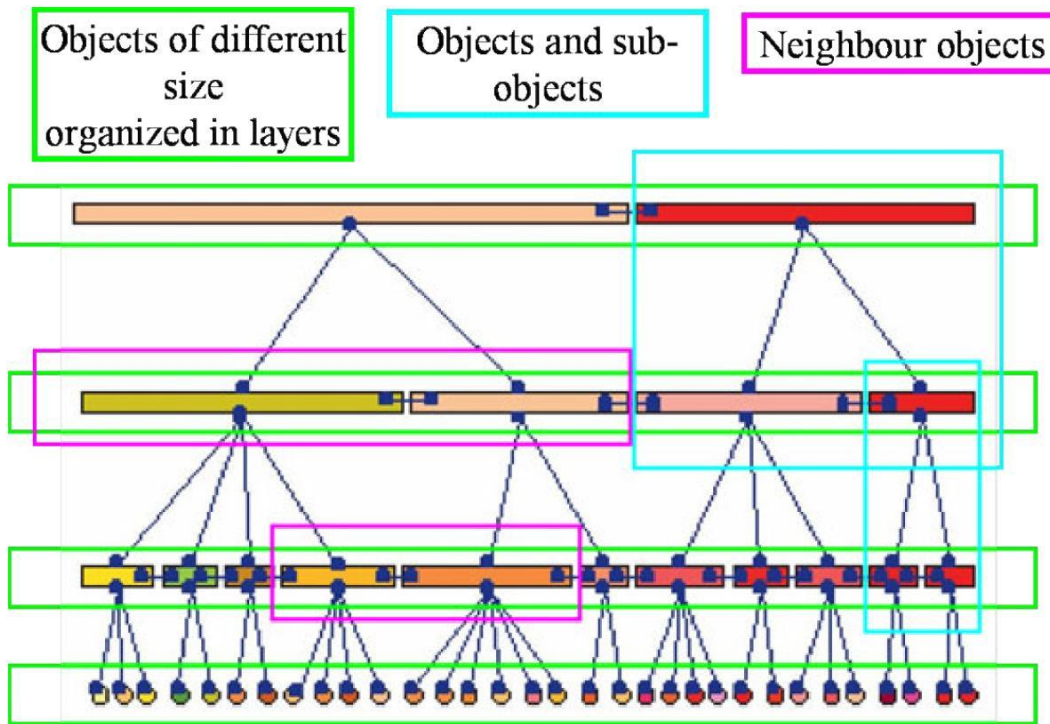


**Figure 10.1:** Segmentation of an image into meaningful objects. Neighbouring pixels with similar characteristics are grouped into segments. Several object layers can be created, adding hierarchical information to the objects and sub-objects. See text for more information.

objects to larger ones, thereby borders are deleted but no new ones are created. The merging of segments follows the same method as creating the first segments, keeping homogeneity as high as possible. In order to avoid the non proportionate growth of very homogeneous regions (e.g. oceans), a function is included keeping a relationship between the smallest and biggest segment.

These segments are dependant on the sub-scale, i.e. the pixels used for creating the segments. A segment now not only has a single value, but also statistical values such as mean, standard deviation, minimum, maximum and median. In addition to these spectral values, segments have geometrical attributes like size (area), length/width, curvature, compactness and - very importantly - a relation to neighbouring segments.

The analysis of the segment's properties lets the segment become an object. It can bring further discrimination of objects with a similar spectral characteristic (e.g. cirrus clouds belonging to a thunderstorm or cirrus not connected with a thunderstorm). The 'region merging' of the segments implies that every smaller object belongs exactly to one bigger object. In this way a small object containing a tree is merged into a bigger object containing a forest (made up of single trees, clearings, tracks etc.). Once the properties of the objects are known, classes can be formed. Classes contain objects with similar properties. The similarity is defined with fuzzy logic algorithms that are fed with expert knowledge.

The method of classification is similar to that used in the classical pixel basis. Classification rules are created and then objects fulfilling these criteria are assigned to this class. The definition of classification rules can be done using fixed thresholds (step function) or using fuzzy logic allowing a certain transition zone (e.g. linear, exponential). When defining more classes some objects may fulfil criteria for more than just one class. An object is then assigned to the class which it fulfils best.

## 10.1 Cloud analysis

Applying the technique of segmentation and object creation on MSG data will be described in this chapter. A rule set for identifying several clouds was developed. The software used was eCognition 4.0 from Definiens. The software allows the creation of rules with fuzzy logic. Operational workflows can be saved enabling a faster and more convenient use.

For the cloud analysis 7 SEVIRI channels were used and in addition the output from the pixel based cloud mask. As the automated detection of clouds is not trivial the results from the pixel based MSG cloud mask were used for identifying cloudy segments. So no further cloud detection was needed for the analysis.

Some first trials showed promising results (Huckle, 2008). On the other hand numerical weather prediction models (including climate models) have always had problems in modelling convective clouds correctly. The results can then be used to validate the CLM results. In the past, tests with object based cloud analysis have been performed at the IMK using AVHRR data from NOAA (Göttsche and Olesen, 2002 and Koch, 2004). The results were very promising and indicated that the use on MSG data should also be possible.

### 10.1.1 Cumulonimbus (Cb)

The most prominent convective systems are cumulonimbus or thunderstorm systems. They mostly form over hot surfaces or mountainous terrain. The characteristic feature of these high reaching clouds when viewed from space is the high reflectance (only during day) and the very cold cloud top (often below  $-50^{\circ}\text{C}$ ).

The temperature does not change between day and night, but the reflectance is dependant on the elevation of the sun. In order to avoid having to define thresholds for every time of the day a maximum of possible reflectance was calculated for every slot. If the measured reflectance was near this value the segment was classed as a Cb.

These two physical parameters, however, apply to all high and optically thick clouds. In Figure 10.2 a daytime image with convection in the Alpine region, southern Germany

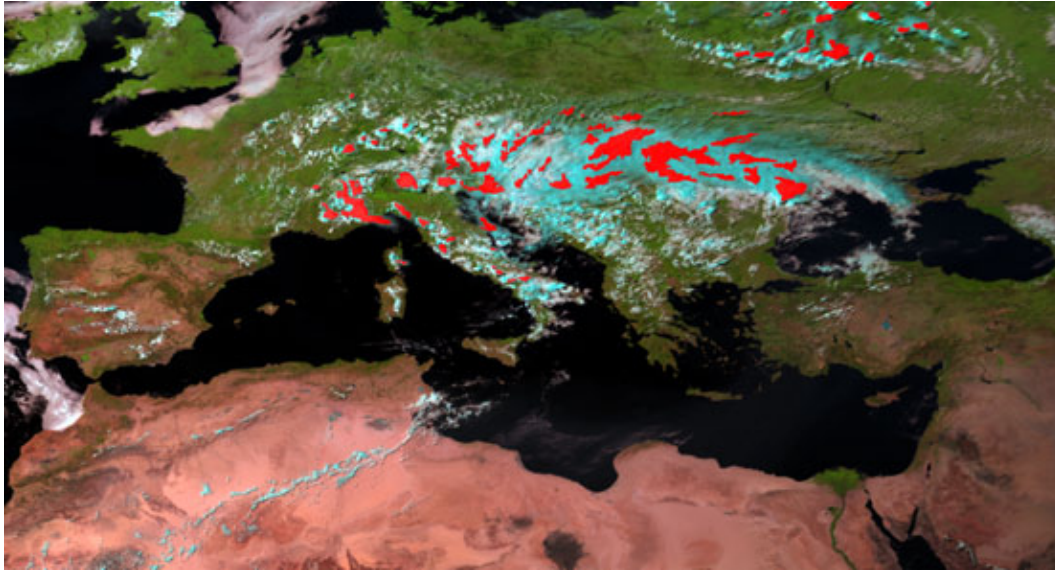


**Figure 10.2:** 12 July 2005, 14:00 UTC. Convection in south Germany, Alpine region and Italy. A cold front is over central/eastern Europe. Red: Objects fulfilling the first two criteria to detect cumulonimbus clouds (cold and bright). Objects in cold front are not Cb forming over heated land surfaces, therefore more criteria have to be defined to exclude these objects.

and Italy is shown. Also a cold front over central and Eastern Europe can be seen in the MSG data. Many segments in this cold front fulfil the two criteria of cold and bright. Therefore, more criteria are needed to discriminate cumulonimbus clouds from clouds in a cold front.

The creation of segments results in geometric features. These can be used for identifying Cb clouds. A Cb in general is compact and round or if the anvil has developed, fans out in one direction, with an elliptical form. Using the form parameters border to area and length to width ratios many objects in the cold front over Central and Eastern Europe are eliminated. To reduce the available objects down to just those representing a single Cb, the difference to the surrounding area is used. In a cold front all the clouds have a similar temperature. A Cb however, develops over a warm ground, therefore the difference between the top of a Cb and the surrounding land is very high. With these criteria most of the objects in the cold front are eliminated and only convective systems over the Alpine region southern Germany and Italy remain (Figure 10.3).

The selection criteria above detect the centre of a thunderstorm. Depending on the segmentation level one thunderstorm can be in several segments that form objects, such as the centre of the Cb, the surrounding of the Cb center and the outer limit of the thunderstorm with very thin cirrus clouds. Moving away from the centre of a Cb the temperatures will rise slowly, as these parts of the cloud are slightly lower and when moving out even further the anvil will become thinner and more radiation from the surface will propagate through the cloud, thus raising the measured Brightness Temperature. To detect the entire thunderstorm more classes are introduced.

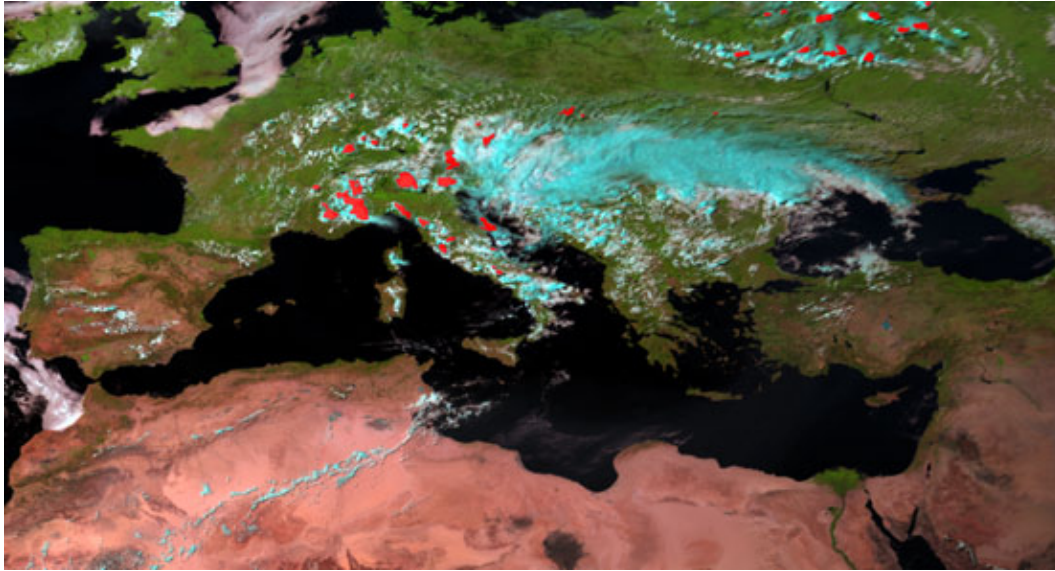


**Figure 10.3:** 12 July 2005, 14:00 UTC. Convection in Southern Germany, Alpine region and Italy. A cold front is over Central/Eastern Europe. Red: Objects fulfilling the all the criteria to detect cumulonimbus clouds (details see text). Objects in cold front are no longer being detected as Cb. Remaining objects in alpine region where convection is active.

One class is used for thunderstorms that are no longer compact but have fanned out into one direction, here the length to width ratio is allowed to be higher. Segments surrounding the centre of a thunderstorm have other geometrical features, so that most of the features used for detecting the centre are not used to identify the adjacent objects. The two main criteria are the temperature and the border to the centre of the Cb. Further away from the centre the clouds become thinner and the temperature increases due to more radiation from the ground propagating through the cloud. The most important factor then is the actual border to the centre element. Without the core of a thunderstorm the other classes surrounding it will not be activated (Fig. 10.4).

### 10.1.2 Thin Cirrus (Ci)

As described in chapter 6.3 thin cirrus clouds are not easily detected, as their optical thickness is low and terrestrial radiation propagates through these clouds. With the combination of the two window channels  $IR_{108}$  and  $IR_{120}$  thin cirrus clouds can be detected. The outer edges of a thunderstorm are mostly made up out of thin cirrus clouds. Objects which have a difference of more than 2K between  $IR_{108}$  and  $IR_{120}$  are classed as thin cirrus. Depending on their neighbourhood, thin cirrus clouds are divided into two different classes. When bordering one of the Cb classes mentioned in chapter 10.1.1 the cirrus will be classed as cirrus near a Cb belonging to the thunderstorm system. With no border it will be classed just as a thin cirrus (Fig. 10.5).

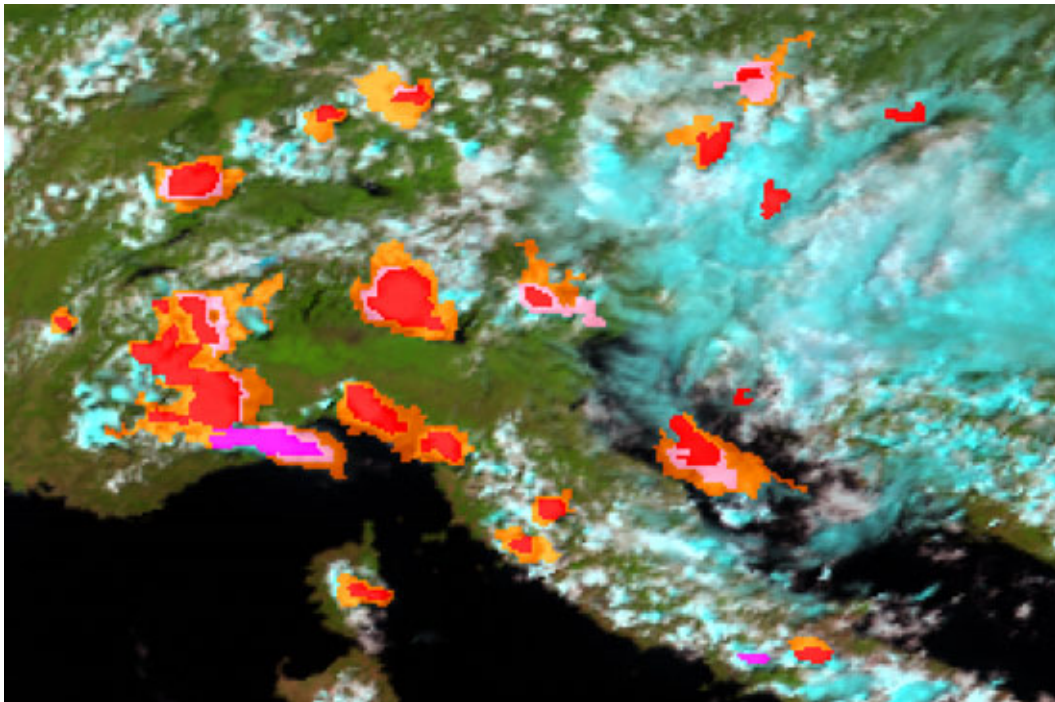


**Figure 10.4:** 12 July 2005, 14:00 UTC. Convection in Southern Germany, Alpine region and Italy. Object based cloud analysis, red: centre of Cb, dark pink: Cb fanning out, light pink: thick clouds next to centre of Cb, orange: clouds belonging to thunderstorm and border to centre of the Cb. The last two classes are only activated if the centre of a Cb is detected.

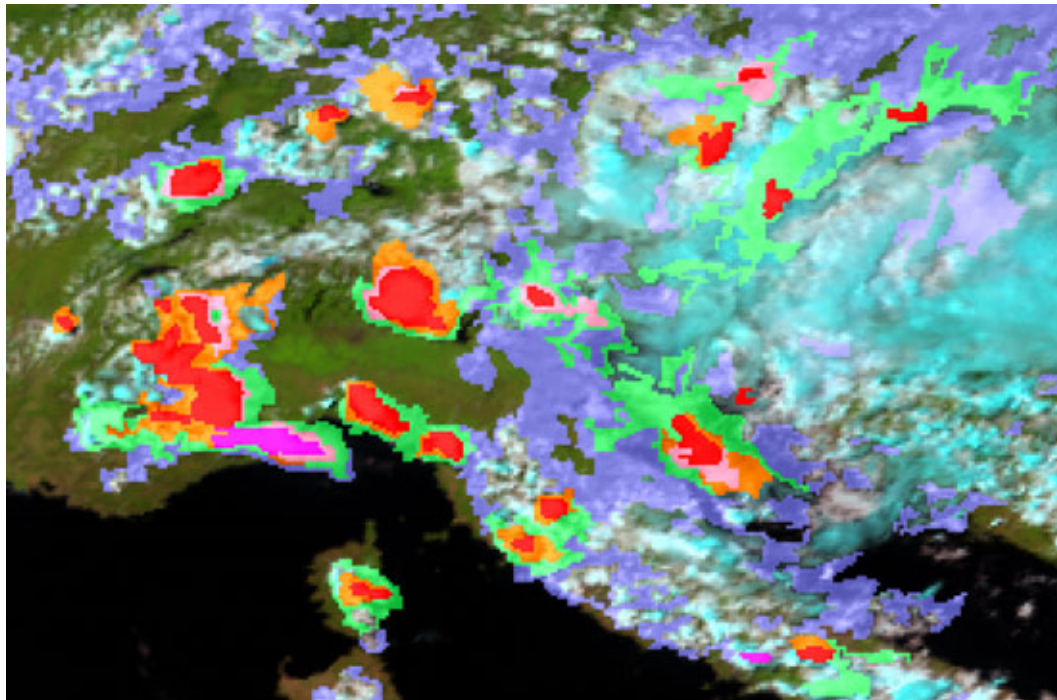


**Figure 10.5:** 12 July 2005, 14:00 UTC. Convection in Southern Germany, Alpine region and Italy. Object based cloud analysis, in addition to the classes described in Figure 10.4 light green: cirrus clouds forming the edge of a Cb (the *ambos*), violet: cirrus clouds not connected to a Cb. Both classes have the same physical principles but the neighbourhood to a Cb puts them in different classes.

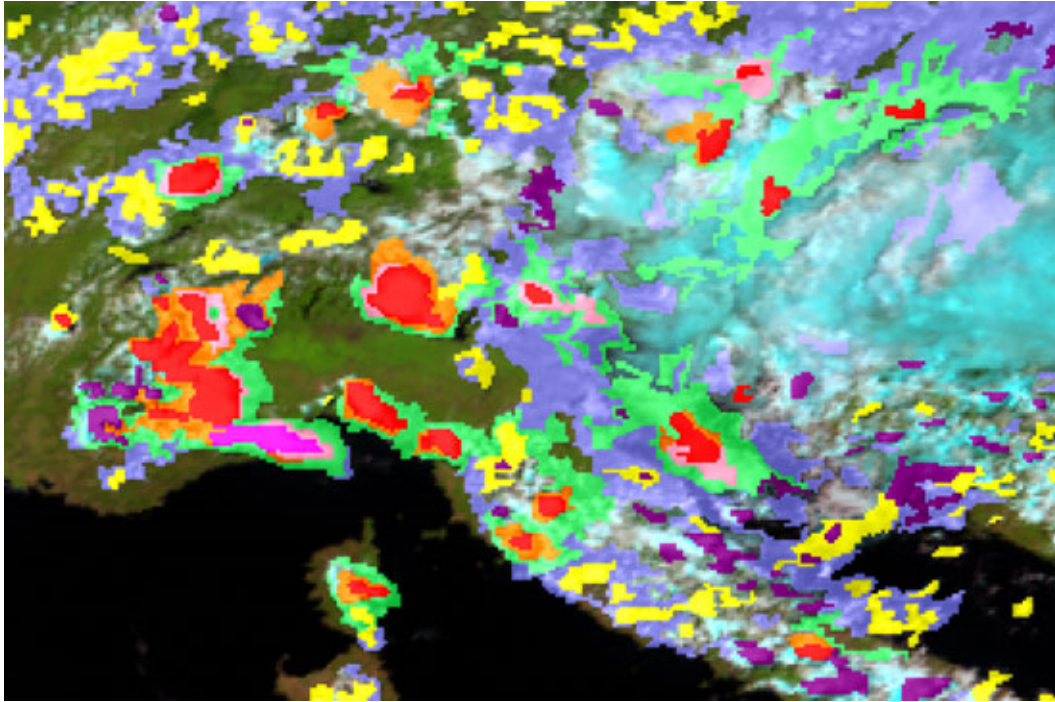


**Figure 10.6:** 12 July 2005, 14:00 UTC. Convection in Southern Germany, Alpine region and Italy. Object based cloud analysis, in addition to the classes described in Figure 10.4 and 10.5 purple: high cumuli, not yet an individual thunderstorm, yellow: low cumuli. With these classes, most convective clouds are detected.

### 10.1.3 High and low Cumulus (Cu)

Convective clouds can have different vertical extents, depending on their stage and the atmospheric conditions. The detection of these cumuli clouds follows similar rules to the identification of the Cb clouds. The cloud top temperature is dependant on the height of the cloud top. The most distinctive criterion for non convective clouds in the temperature range of high or low cumulus clouds is the difference to the neighbouring (cloud free) areas. The size of the objects is also relatively small, in comparison, for example, to low stratus cloud cover. Two classes of cumulus clouds are used. One class containing low clouds with a cloud top temperature above  $-22^{\circ}\text{C}$  and a lower temperature than neighbouring objects of at least 5K. Clouds with a cloud top temperature between  $-20$  and  $-41^{\circ}\text{C}$  and temperatures more than 14K lower than the surrounding are classed as high cumuli. These high cumuli are often not yet fully developed thunderstorms but can be a good indication in a now casting environment of possible developing thunderstorms (fig. 10.6).

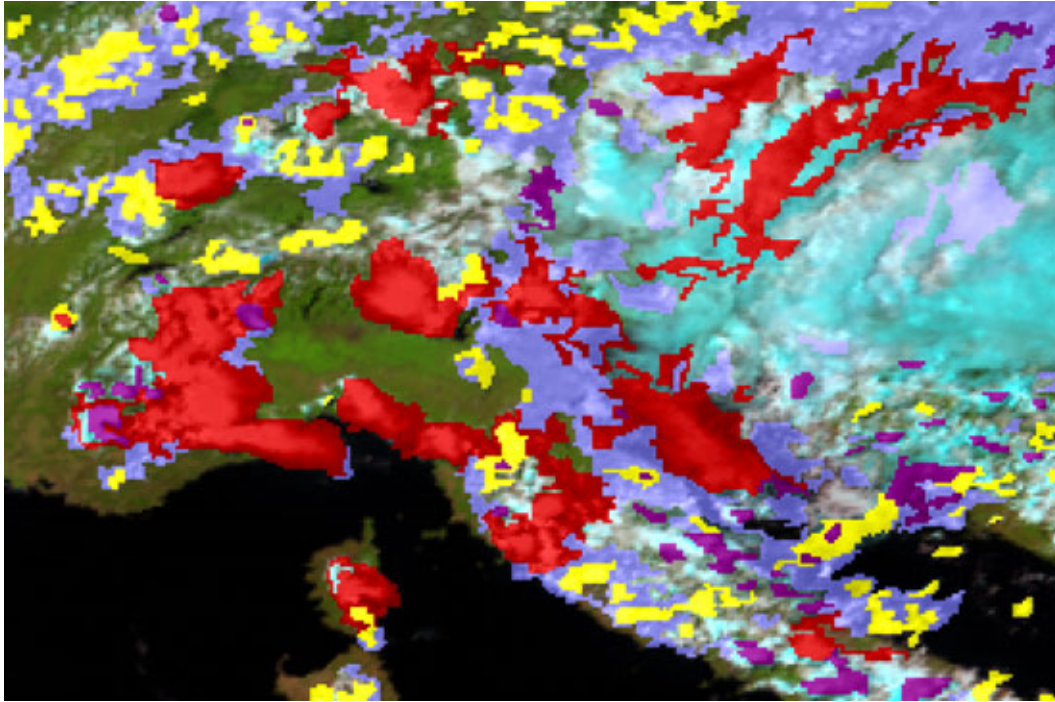


**Figure 10.7:** 12 July 2005, 14:00 UTC. Convection in Southern Germany, Alpine region and Italy. Object based cloud analysis, after analysing the convective clouds (including cirrus connected to thunderstorms) on a bigger segmentation level all classes belonging to a thunderstorm are combined to one class, dark red: thunderstorm, made up out of smaller objects.

#### 10.1.4 Thunderstorms and fields of Cumuli

The level of segmentation is important for the above described classes. The classification is based on a level that is small enough to detect single cumuli and structures in thunderstorms, but is also big enough that geometrical features and neighbourhood information are usable. When choosing a bigger level of segmentation hierarchical information is available. In this case this can be used for two further classes, depending on the rule sets developed earlier.

**Thunderstorm:** After classifying the cumulonimbus clouds as well as the adjacent clouds and connected cirrus on a smaller segmentation level, they can be combined to a thunderstorm system on a bigger segmentation level. Doing this, we can see what extend a thunderstorm has already reached (Fig. 10.7).

**Field of Cumuli:** The classification of low cumuli on a smaller segmentation level, allows the classification of bigger areas including many small (in this case low) cumuli on a bigger segmentation level. The hierarchical structure enables further analysis of clouds (Fig. 10.8).

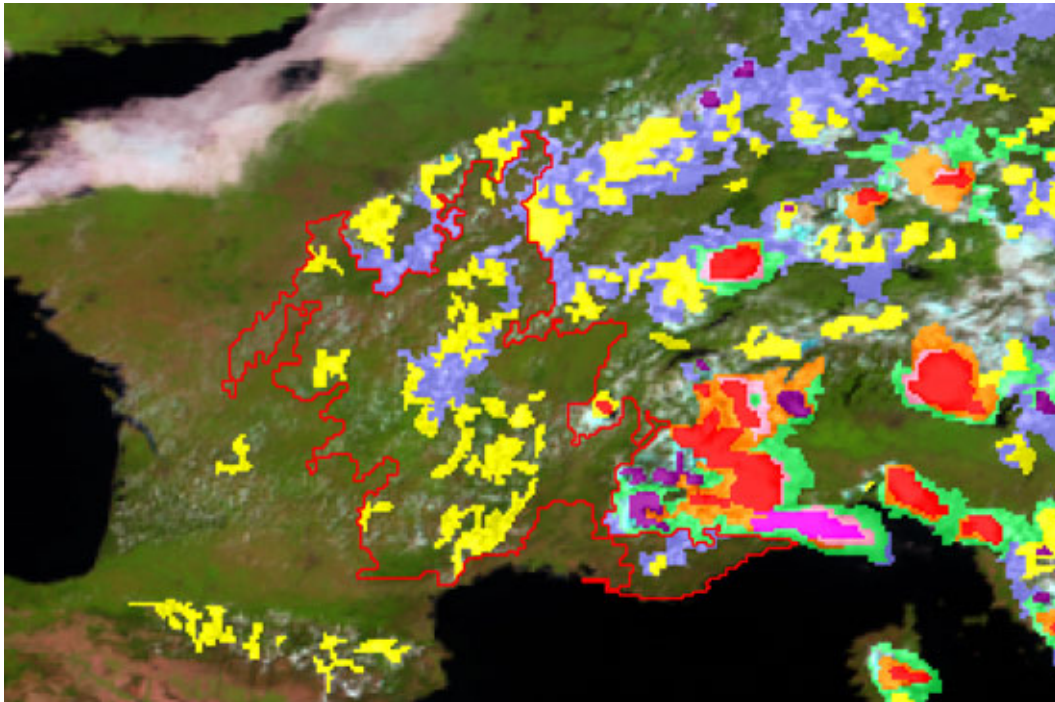


**Figure 10.8:** 12 July 2005, 14:00 UTC. Over France small convection takes place. On a low level single small cumuli are analysed. On a higher level an area (red line) is identified containing small cumuli, thus using hierarchical information for additional analysis.

**Table 10.1:** Object based cloud analysis of MSG data. Percentage of each class in scene from July 12, 2005, 14:00 UTC.

Class	Objects	Objects (%)
Cb I	40	3.56
Cb II	3	0.27
Cb III	15	1.33
Cumulus-Cb	50	4.45
Cirrus-Cb	79	7.02
Cirrus	435	38.66
Cumulus-low	402	35.73
Cumulus-high	101	8.98

### 10.1.5 Non convective clouds

With the classifications described above most convective clouds and thin cirrus are described. Convective clouds are mostly compact and the spatial extend is normally limited. Between convective clouds gaps occur and the cloud free ground is visible. As described above the detection and classification of these clouds is good and the comparison to the CLM data, can supply more information than a pixel based comparison (see chapter 10.2). The remaining non convective clouds could of course also be analysed and classified. These classifications were, however, only done for some general classes, identifying the clouds according to their height (cloud top) and some structures within the objects. A high standard deviation (STD) pointing towards an *Alto*cumulus or *Strato*cumulus. A lower STD is more likely to represent a *Stratus*. A preliminary result is shown in figure 10.9. More research has to be done on this field however.

Another very prominent type of cloud structures, are frontal systems connected to low pressure systems. These systems can very often be easily identified by a human interpreter. The automatic detection, however, has proven to be more difficult. When running the segmentation algorithms on a scene segments are created which have a high homogeneity. But the algorithms do not 'know' what to look for. The fronts and the low pressure system are therefore not segmented into easily identifiable objects. The main feature, the curving and a long band of clouds is lost during the segmentation. Further development in the algorithms is therefore needed to perform this task reliably. This will be the next step in image analysis bringing the expert knowledge from the classification a step nearer to the segmentation. This way more features can be extracted from images.

The results for the convective cloud analysis are displayed in table 10.1. The number of objects classified into each class and the percentage of this class in all clouds analysed. Cloud free area and non convective clouds are not shown in this table.

## 10.2 Object based comparison of MSG and CLM

In chapter 8 the MSG cloud mask and the CLM cloud data were compared. This was done on a pixel basis. The disadvantage of this comparison technique is that just a small spatial shift between the two data sets leads to a huge increase in the nonagreement. Using an object based comparison this effect can be compensated for and a better comparison is possible.

To evaluate the quality of the cloud modelling in the CLM the exact position is not so important. More important is that the amount of clouds in a certain area is modelled correctly. This means, that on a convective day, for example in the region of southwest Germany the amount of clouds in the satellite data and the amount modelled in the

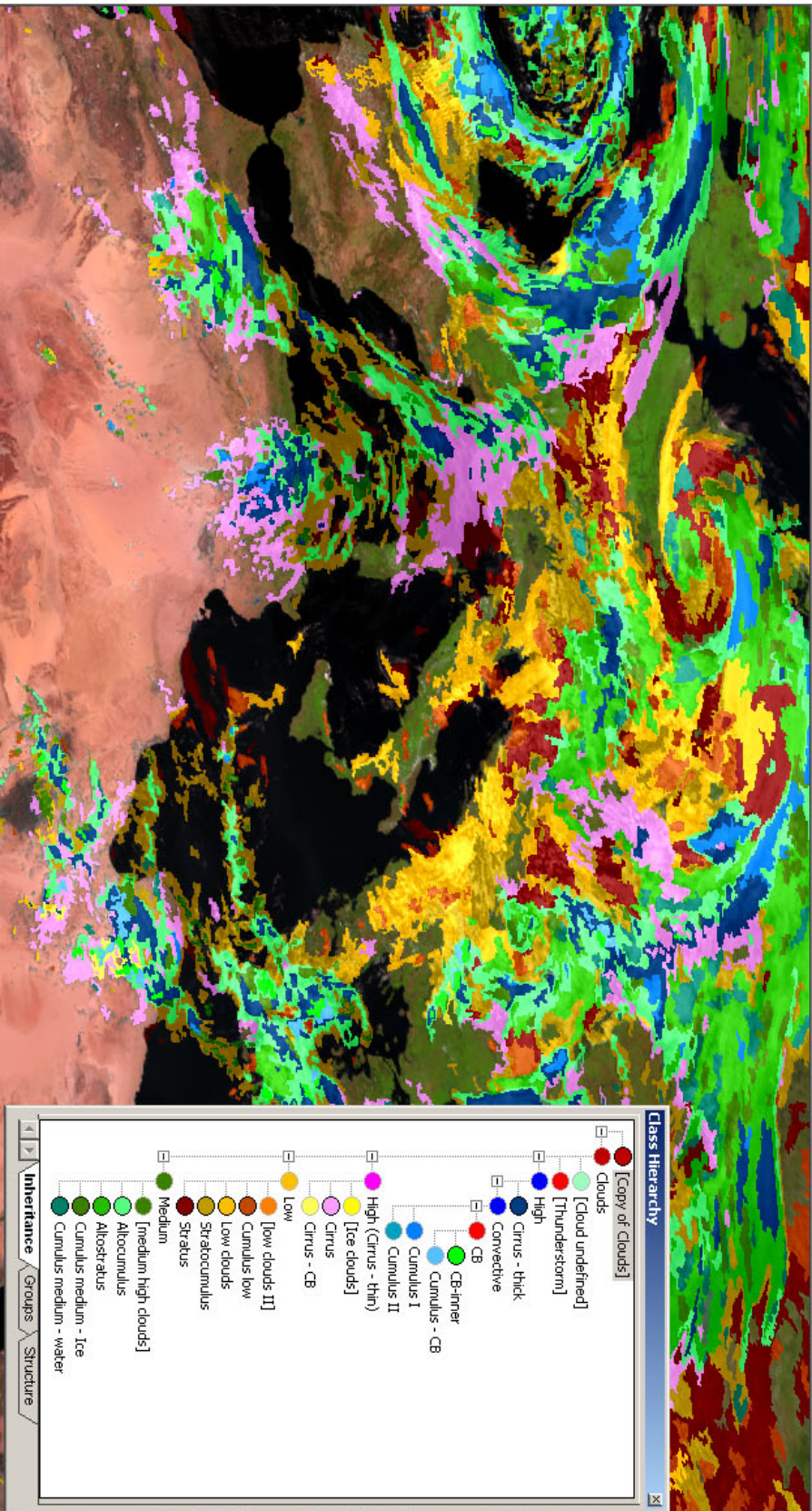


**Figure 10.9:** 12 May 2005, 12:00 UTC. Object based cloud analysis, including low, middle, high and thin clouds. For colour code refer to legend within figure. Preliminary results only.

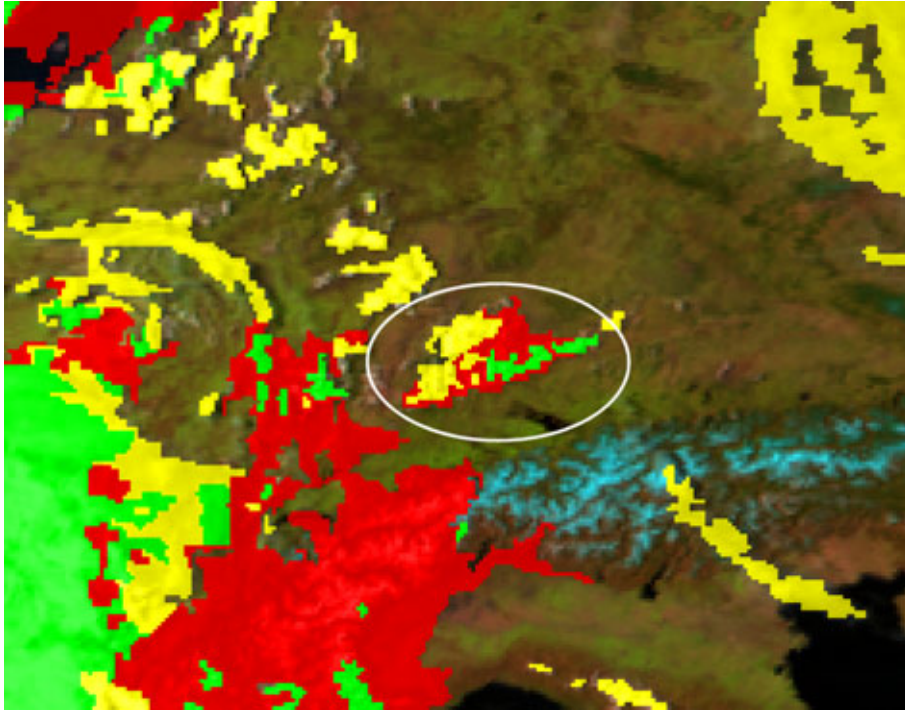


**Figure 10.10:** Comparison MSG cloud mask and CLM total cloud cover on pixel basis, for 03 April 2005, 15:00 UTC. Green: both have clouds, yellow: only clouds in MSG data, red: clouds only in CLM data.

CLM over the Black Forest and the Swabian Alb should be similar. The amount of clouds and also the type of clouds can be analysed. A pixel based comparison can have good values for some areas, but when looking at the cloud types, we see that in the MSG data there are convective clouds and in the CLM there is a great area covered with stratiform clouds. This means that a comparison based on objects enables a better validation of CLM clouds, but not necessarily a better result.

In the following some case studies for individual scenes are presented. An automated analysis has not been developed and is not easily established. The main problem is that the objects change from scene to scene, as they are created from the present data. A static segmentation could be used but that would be contrary to the idea of using image objects. A predefined area (e.g. Black Forest and Swabian Alb) in which the amount of clouds is analysed would then be preferable. Another idea is the tracking of segments from one time slot to the next (Linke et al., 2008). In this approach a starting point in time is set and this scene is analysed. From there the changes in the segmentation are recorded. Using this technique an automated and statistical analysis can perhaps be performed. However, this still has to be implemented. In the following some case studies will be presented.

**03 April 2005** The first case study is of a day with shallow convection over the Black Forest and Swabian Alb. A high pressure system with the centre over Eastern

**Table 10.2:** Comparison on object basis between MSG cloud mask and CLM clouds. Number of clouds from both data sets in one Segment. First case April 3, 2005, 15:00 UTC, containing Black Forest and Swabian Alb. Second case May 29, 2005, 11:30 UTC, for three objects (Black Forest, Vosges Mountains and the surrounding).

Data set	Area of clouds (in sub-pixel)			
	April 3	May 29		
		Black Forest	Vosges	Surrounding
MSG and CLM	106	202	85	80
Only MSG	248	89	118	31
Only CLM	202	96	23	3062

Europe is dominating the weather in Southwestern Germany, with only low winds occurring. After a cloud free night first convective clouds appear at around 10 UTC. The development of shallow convective clouds is continuous until 16 UTC. The convection in the CLM starts and ends approx. one hour later. Analysing the data from 15:00 UTC for the region of the Black forest and the Swabian Alb (Fig. 10.10) we see that the pixel by pixel agreement is not very good. But when analysing the whole area using the segmentation result (object in white circle) the number of clouds in the two data sets is not so different at all (see Table 10.2). For other times of the day there is a similar picture that the pixel based agreement is not very good, especially the agreement on clouds, but for the object based comparison the numbers are similar.

**29 May 2005** The second case analysed shows that the good agreement on first sight is not so good after all. The first object analysed contains the Black Forest and parts of the Swabian Alb. Three convective cells can be distinguished over the Black Forest and some shallow convective clouds over the Swabian Alb. The comparison with the CLM data on pixel basis for this object is rather good, the amount of clouds is nearly identically in both data sets (see Table 10.2 for details). However, the cloud types are not identically. The clouds in the MSG data are clearly convective, but the modelled clouds are more stratiform covering a huge area surrounding the middle range mountains (Fig. 10.11). This can be seen in the cloud amount in the surrounding object, with a hundred times more clouds in the CLM than in the MSG data. The agreement over the mountains is good but this is more coincidental because the modelled clouds do not come from convection triggered in the model but from advection corresponding with an advancing cold front.

**31 August 2005** The third example is an early morning fog near the Alps in south Germany (10.12). The region is under the influence of a high pressure system over the Baltic Sea, with a general northwesterly flow. In the satellite data the fog shows up very distinctively in the VIS<sub>006</sub> and in the IR<sub>039</sub> channel. The fog reaches from the Swabian Alb to the foothills of the Alps in Bavaria. The CLM has some fog corresponding with the MSG data over the Swabian Alps (although

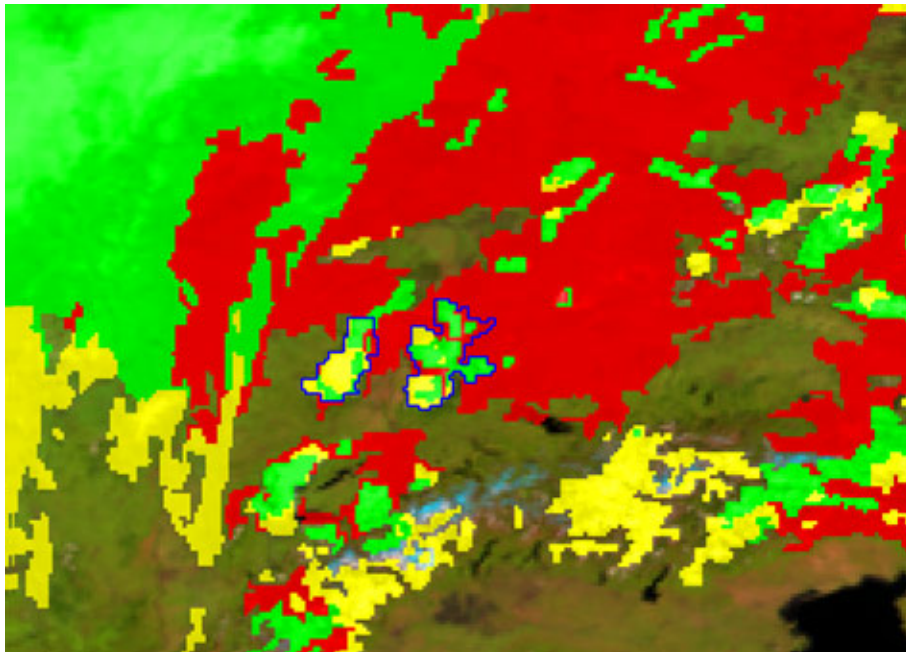


**Figure 10.11:** Comparison MSG cloud mask and CLM total cloud cover on pixel basis, for 29 May 2005, 11:30 UTC. Convective clouds in the MSG data over the Vosges Mountains (blue object on the left) and Black Forest (blue object in the right). Stratiform clouds in CLM data surrounding middle range mountains (vast red areas), with no correspondence in the MSG data.

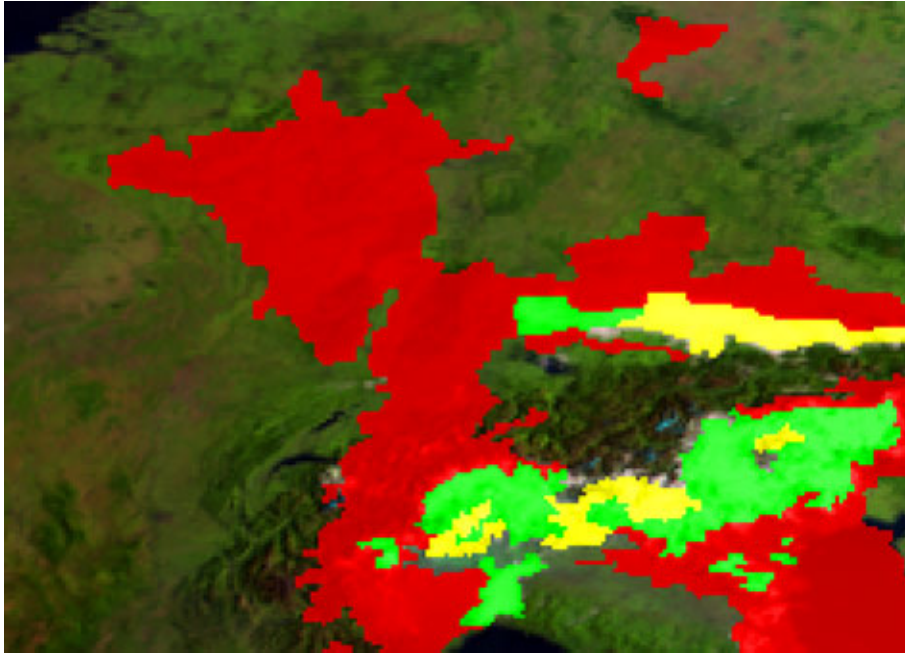


**Figure 10.12:** *Comparison MSG cloud mask and CLM total cloud cover on pixel basis, for 31 August 2005, 06:30 UTC. Fog is detected over the Swabian Alb and near the Bavarian Alps in the MSG data. The CLM models the fog along the Danube, too far north of the actual appearance.*

a bit more) but then models the fog more along the Danube. So the appearance of fog is validated by the MSG data and the general form is similar, but there is a shift in location.

These three cases illustrate the possibilities when using an object based approach. But also show the difficulties when trying to do the comparison in an automated fashion. The cloud analysis can be done automatically as shown in chapter 10.1, but when comparing with the model data automation is not yet accomplished. The biggest problems are that in the segmentation process homogeneity of one channel or data set respectively is kept high. In a convective environment, where clouds and cloud free areas are interweaved segments on a bigger scale often encompass both, clouds and cloud free areas. Here a small local displacement between the two data sets will lead to good results. In a situation, as described in the third case study, the objects with modelled clouds and clouds from satellite data will be separated even on a bigger scale, as the clouds are very solid and there is hardly any overlap. The next step in using object based image analysis would require more possibilities influencing the process of segmentation, thus being able to put more a priori information into the segmentation process.

# Chapter 11

## Conclusions

The man made influence on the world's climate can have numerous effects. One is a modification of the atmospheric water cycle. Clouds play an important role in the radiation budget of the earth's surface and atmosphere and are, due to the distribution of water through precipitation, vital for all life on earth. The climate version of the 'Lokal Modell' (LM) from the DWD is tailor made for the estimation of local climate. The validation of the clouds modelled by the CLM using data from the MSG satellite is the main aspect of this thesis.

The validation of the modelled clouds for convective days is of a special interest. The correct modelling of convection is very difficult. There are numerous reasons. Not all processes of convection and the triggering of convection are fully understood and it is even more difficult to describe them correctly in a numerical model. Another problem arises from the scale of the processes triggering convection that is smaller than the spatial resolution in current models. This means the processes have to be parameterised.

In order to compare the modelled clouds with the satellite data, an automated cloud detection in MSG IR, NIR and VIS channels (SEVIRI) was developed. The aim was to extract cloud information solely from MSG data without the use of external data sets.

The two main tests for detecting clouds use the IR<sub>108</sub> and VIS<sub>006</sub> channels. Individual thresholds for every pixel at every time slot are calculated with a 30 day sliding window centred at the day of operation was used and out of this data the thresholds were calculated. For the IR<sub>108</sub> channel a thermal surface parameter (TSP) model was used to smoothen the values for a diurnal cycle. These two tests detect between 80 and 90% of the clouds. Although most clouds are detected the remaining clouds are still important (e.g. fog at night for traffic).

Other tests include channel differences to detect thin cirrus clouds (IR<sub>108</sub> - IR<sub>120</sub>), fog at night (IR<sub>108</sub> - IR<sub>039</sub>) or low clouds during the day (IR<sub>039</sub> - IR<sub>108</sub>). A channel ratio

between  $VIS_{006}$  and  $NIR_{016}$  to detect snow and ice. And also a check for cloud free areas behind cold fronts.

The results from the IMK cloud mask were compared with two external cloud masks for MSG. One was the cloud mask from the Institut für Weltraumwissenschaften (Institute for Space Sciences) at the Freie Universität Berlin (FUB). As the IMK cloud mask the FUB cloud mask only uses data from the SEVIRI channels. The agreement between the two cloud masks is good. However, some differences do show up. One major difference is the higher sensitivity of the IMK cloud mask detecting cloudy pixels at the edges of clouds during the day. At night the IMK cloud mask at the moment has problems with a too slow cooling in the TSP model, resulting in a higher threshold and thus some falsely detected clouds, the over all number however is relative small. On the other hand the FUB cloud mask picks up more clouds at the edges of clouds, therefore the total amount of clouds at night is higher in the FUB cloud mask. The FUB cloud mask seems to have a better performance during the night.

The second external cloud mask was from EUMETSAT's Now Casting SAF. This cloud mask again uses similar algorithms and tests to detect cloud filled pixels. The biggest difference, however, is the use of data from a weather prediction model as an expected clear sky radiance in the  $IR_{108}$  and  $IR_{120}$  channels. If the measured radiance drops below a certain threshold the pixel is classed as cloudy. The agreement between the IMK and the SAF cloud mask is good. The IMK cloud mask has the same problem at night as in the comparison with the FUB cloud mask. In the early morning hours the performance of the IMK cloud mask increases significantly, due to the much earlier use of the solar channels. During the day the IMK cloud mask picks up more clouds, most of them using the solar channels.

In special situations the performances of the cloud masks are also different. The SAF cloud mask seems not to have a very good snow detection, most of the Alps are always marked as cloudy, the FUB and IMK cloud mask work here better. In hazy conditions, especially sand and dust, the SAF cloud mask picks up a lot of clouds, the IMK also identifies some clouds but the FUB does not mark these events as clouds. In terms of finding undisturbed pixels, whether by moist or dry particles, the marking of dust as cloud is not totally wrong, but it should be flagged appropriately. The SAF cloud mask also has problems over desert areas, especially in the morning, often wide stretches are masked as cloudy. A difficulty the SAF and FUB cloud mask have is that both very often mask coastlines as cloudy. This is probably due to a ratio test between  $VIS_{006}$  and  $VIS_{008}$ , over clouds this ratio is near one, but this is also true for coastal pixels (see chapter 6.8 for details). The IMK cloud mask does not use this test, as the number of additionally found clouds is low, but the problems that arise along coastlines are huge.

Over all the IMK cloud mask seems to have a solid performance, that can withhold the comparison with other MSG cloud masks. Therefore the use of the IMK cloud mask as a validation data set for the CLM is possible.

For the validation of the CLM results the area of southwest Germany and the bordering

Eastern part of France was chosen. The middle range mountains of the Vosges, the Black Forest and the Swabian Alb are included, as well as the Rhine valley, the river Danube and Lake Constance. Data for the months from March to October 2005 were used.

The agreement between CLM and IMK cloud mask data is not very good. It is at 77,5% for all days of the period and at only 72.0% for convective days. Over the Black Forest, the Vosges Mountains and near Lake Constance the agreement is best. In the Rhine Valley and along the Danube the lowest agreement is reached. The agreement changes significantly from month to month, with a high in April of 86.9% and a low in July of only 63.8%.

The agreement during the day is better than during the night. Although the IMK cloud mask has some problems at night, identifying too many clouds, the CLM has much more clouds than the IMK cloud mask, up to 27.7% clouds only appearing in the CLM data.

The overall performance of the CLM in terms of modelling the cloud cover correctly is not very good. One reason for this is that the CLM might only have slight shift in time and/or space. This can result in a very bad agreement, especially in convective situations where clouds are broken up and do not have a great horizontal extend. One way to avoid this, is to go from a pixel based comparison to an analysis based on segments.

In the process of segmentation, neighbouring pixels with a similar spectral characteristic are grouped together to form a segment. Other than pixels, segments do not have a single spectral value, but statistical information, such as mean, standard deviation, minimum and maximum values. Additionally a Segment also has form parameters like size, length/width or curvature. New neighbourhood information is available and can also be very helpful in analysing the image. Depending on the purpose different sized segmentation levels are created. This adds a 'vertical hierarchy' to the segments, enabling further analysis. These segments, built up out of the individual pixels are the basis of the object based image analysis (OBIA).

In this thesis the object based image analysis was used to analyse MSG data especially for convective days. A set of rules was developed to identify different convective clouds, such as Cumulonimbus, Cirrus or different sized Cumuli clouds.

Another use was the comparison between the cloud mask data and the CLM data, this time on an object basis. Especially for convective days a better validation of the CLM data is possible. In some cases the amount of clouds within an object is similar in the two data sets. But just a small spatial shift leads to very bad agreement in the above described methods. Comparing them on an object basis the result is a lot better.

However, the performance of the CLM does not increase dramatically. Although in some convective cases the CLM is not so bad, in other situations, where the pixel based

agreement is good, the object based comparison reveals that the modelled clouds are totally different than those in the MSG data. Therefore a better analysis is possible, but the results do not necessarily increase.

In this thesis an automated cloud mask for MSG was developed, that delivers at least equally good results as other available cloud detection schemes. The performance of the CLM modelling clouds, especially for convective situations was evaluated. An object based cloud analysis for MSG was developed and the CLM was validated using objects.

# Chapter 12

## Literature

ACKERMAN, A., 1997, Remote sensing aerosols using satellite infrared observations. *Journal of Geophysical Research*, **102**, 17069 - 17079.

ASNER, G.P., HICKE, J.A., LOBELL, D.B., 2003. Per-pixel analysis of forest structure. Vegetation indices, spectral mixture analysis and canopy reflectance modeling. In: *Remote Sensing of Forest Environments. Concepts and Case Studies*. Wulder, M.A., Franklin, S.E. (Eds.), pp. 209 - 254 (Kluwer Academic Publishers).

BAKER, C.B., QUAYLE, R.G., WANLIN, W., 1995, The influence of night time cloud cover on the observed minimum temperature in China. *Atmospheric Research*, **37**, 27 - 35.

BARRY, R.G. and CHORLEY, R.J., 1987, *Atmosphere, Weather & Climate, fifth edition* (London & New York: Routledge)

BARTHLOTT, Ch., CORSMEIER, U., MEISSNER, C., BRAUN, F., KOTTMEIER, Ch., 2006, The Influence of mesoscale circulation systems on triggering convective cells over complex terrain. *Atmospheric Research*, **81**, 150 - 175.

BEHRENDT, A., WULFMAYER, V., KOTTMEIER, Ch., CORSMEIER, U., CRAIG, G., HAGEN, M., BARTHLOTT, Ch., 2007, Die Feldmesskampagne COPS. DMG-Mitteilungen, Vol. **3**, 2-4.

BLASCHE, T. and HAY, G.J., 2001, Object-oriented image analysis and scale-space: theory and methods for modeling and evaluating multiscale landscape structure. *Int. Archives Photogrammetry and Remote Sens.*, **34**, part 4/W5, pp. 22-29.

CAMPBELL, J.B., 2002, *Introduction to Remote Sensing* (London and New York: Taylor & Francis).

CARSLAW, H.S., and JAEGER, J.C., 1959, *Conduction of heat in solids* (Oxford University Press, Amen House, London, Great Britain).

CASTILLA, G., HAY, G.J. and RUIZ-GALLARDO, J.R., 2008, *Size-constrained Region Merging (SCRM): An Automated Delineation Tool for Assisted Photointerpretation*, *Photogrammetric Engineering & Remote Sensing*, **74**, No. 4, 409 - 419.

CERMAK, J., BENDIX, J., 2008, A novel approach to fog/low stratus detection using Meteosat 8 data. *Atmospheric Research*, **87**, 279 - 292.

CORSMEIER, U., 2008, Interaction of boundary layer and land surface based processes with mesoscale convection Initiation: COPS IOP 9c. *6th COPS-Workshop, Universitt Hohenheim, 27.02.-29.02.2008*.

CRACKNELL, A.P. and HAYES, L.W.B., 1991, *Introduction to Remote Sensing*(London, New York, Philadelphia: Taylor & Francis).

DASH, P., GÖTTSCHE, F.-M., and OLESEN, F.-S., 2002, Potential of MSG for surface temperature and emissivity estimation: considerations for real-time applications. *International Journal of Remote Sensing*, **23**, 4511-4518.

DOMS, G. and SCHÄTTLER, U., 2002, A description of the nonhydrostatic regional model LM Part I: Dynamics and Numerics. *COSMO NEWSLETTER*, **2**, 225 - 235.

DWD, 2005, European Meteorological Bulletin, Deutscher Wetterdienst.

DWD, 1990, *Internationaler Wolkenatlas, 2. Auflage (2. edition)* (Deutscher Wetterdienst, Zentralamt, Offenbach am Main, Germany)

EUMETSAT, 2006, Eumetsat webseite ([http://www.eumetsat.int/Home/Main/What\\_We\\_Do/Satellites/Meteosat\\_Second\\_Generation/Space\\_Segment/SP\\_1119959405658?l=en](http://www.eumetsat.int/Home/Main/What_We_Do/Satellites/Meteosat_Second_Generation/Space_Segment/SP_1119959405658?l=en)).

EUMETSAT, 2007, Meteosat-8/MSG 1 - Spectral Response. Eumetsat webseite ([http://www.eumetsat.int/Home/Main/What\\_We\\_Do/Satellites/Meteosat\\_Second\\_Generation/Space\\_Segment/SP\\_1138096039033?l=en](http://www.eumetsat.int/Home/Main/What_We_Do/Satellites/Meteosat_Second_Generation/Space_Segment/SP_1138096039033?l=en))

FIEDLER, F., PRENOSIL, T., 1980, Das MESOKLIP-Experiment. Mesoskaliges Klimaprogramm im Oberrheintal. *Wiss. Ber. Inst. Meteorol. und Klimaforsch., Universitt Karlsruhe, Karlsruhe*.

GÖTTSCHE, F.M., OLESEN, F.S., 2008, Modelling the effect of optical thickness on diurnal cycles of land surface temperature. *Remote Sensing of Environment* - submitted.

GÖTTSCHE, F.M., OLESEN, F.S., 2002, Multi-scale segmentation of satellite data into image objects and knowledge-based detection and classification of clouds. *The 2002 EUMETSAT Meteorological Satellite Conference (Dublin, Ireland, 2.-6.9.2002)*.

GÖTTSCHE, F.M., OLESEN, F.S., 2001, Modelling of diurnal cycles of brightness temperature extracted from METEOSAT data. *Remote Sensing of Environment*, **76**, 337 - 348.

- HALL, D.K., RIGGS, G.A., SALOMONSON, V.V., 1995, Development of Methods for Mapping Global Snow Cover Using Moderate Resolution Imaging Spectroradiometer Data. *Remote Sensing of Environment*, **54**, 127 - 140.
- HALLER, M., 2005, Simulation einjähriger Klimazeitreihen in Süddeutschland mit dem regionalen Klimamodell CLM. Diploma thesis, Universität Karlsruhe, Karlsruhe.
- HAY, G.J., CASTILLA, G., WULDER, M.A. and RUIZ, J.R., 2005, *An automated object-based approach for the multiscale image segmentation of forest scenes*, *International Journal of Applied Earth Observation and Geoinformation*, **7**, 339 - 359.
- HAY, G.J., MARCEAU, D.J., DUBÉ, P. and BOUCHARD, A., 2001, A Multiscale Framework for Landscape Analysis: Object-Specific Analysis and Upscaling. *Landscape Ecology*, **16**, 6, 471 - 490.
- Houghton, J.T., Genkins, G.J. and Ephraums, J.J., 1990, *Climate Change: The IPCC Scientific Assessment* (Cambridge University Press, Cambridge).
- HUCKLE, R. and OLESEN, F.S., 2008, Multi Annual Cloud Analysis from METEOSAT Data Using Object Based Image Analysis (OBIA) for Climate Model Validation. *The 2008 EUMETSAT Meteorological Satellite Conference (Darmstadt/ Germany, 08.-12.09.2008)*
- HUCKLE, R. and OLESEN, F.S., 2007, Multi annual cloud analysis from Meteosat data. *General Assembly European Geosciences Union (EGU) (Vienna, Austria 2007)*.
- HUCKLE, R., 2004, Bestimmung der Strahlungstemperatur der Erdoberfläche während der VERTIKATOR Messtage. Term paper (Seminararbeit), Universität Karlsruhe, Karlsruhe.
- HUNT, G.E., 1973, Radiative properties of terrestrial clouds at visible and infra-red thermal window wavelengths. *Quart. J. Royal Meteorological Society*, **99**, 346 - 369.
- INOUE, T., 1987, A Cloud Type Classification With NOAA 7 Split-Window Measurements. *Journal of Geophysical Research*, **92**, 3991 - 4000.
- KABSCH, E., OLESEN, F. and PRATA, A. J., 2008, Validation of Land Surface Temperatures (LSTs) derived from MSG/SEVIRI with the Evora, Portugal ground-truth station measurements. *International Journal of Remote Sensing*, **29**, 5329 - 5345.
- KASKAOUTIS, D.G., KAMBEZIDIS H.D., NASTOS P.T., KOSMOPOULOS P.G., 2008, Study on an intense dust storm over Greece. *Atmospheric Environment*, **42**, 6884 - 6896.
- KASPERBAUER, M.J., 1987, Far-Red Light Reflection from Green Leaves and Effects on Phytochrome-Mediated Assimilate Partitioning under Field Conditions. *Plant Physiol*, **85**, 350-354.

- KOCH, C., 2004, Klassifikation von Wolken durch Struktur- und Kontextanalyse. Diploma thesis, Universität Karlsruhe, Karlsruhe.
- KÜCKEN, M., HAUFFE, D., 2002, *The Nonhydrostatic Limited-area Model LM (Lokal-Modell) of DWD with PIK extensions, Part III: Extensions User Guide* (Potsdam-Institut für Klimafolgenforschung, Potsdam).
- LILLESAND, T. M. and KIEFER, R. W., 1994, *Remote Sensing and Image Interpretation 3rd Edition* (John Wiley and Sons, New York).
- LIN, J.D., 1980, On the force-restore method for prediction of ground surface temperature. *Journal of Geophysical Research*, **85**, 6, 3251-3254.
- LINKE, J., McDERMID, G., McLANE, A.J., LASKIN, D.N, 2008, Methods for tracking landscape change in an object-based environment: towards a framework for reliable monitoring (Oral Presentation). *GEOBIA 2008 Conference - Pixels, Objects, Intelligence. Calgary, Alberta. August 5 - 8 2008*.
- LIU, K.N., 2002, *An Introduction to Atmospheric Radiation* (San Diego, London: Academic Press).
- LIU, K.N., 1986, Influence of Cirrus Clouds on Weather and Climate Processes: A Global Perspective. *Monthly Weather Review*, **114**, 1167 - 1199.
- LOPEZ COTIN, L.F., 2005, *User Manual for the PGE01-02-03 of the SAFNWC / MSG: Scientific part* (SAFNWC, Meteo-France).
- JIN, M., DICKINSON, R.E., 1999, Interpolation of surface radiative temperature measured from polar orbiting satellites to a diurnal cycle. *Journal of Geophysical Research*, **104**, D2, 2105 - 2116
- MESCHEDE, D., 2006, *Gerthsen Physik* (Berlin, Heidelberg: Springer Verlag).
- MEISSNER, C., 2008, High-Resolution sensitivity studies with the regional climate model COSMO-CLM. PhD dissertation, Universität Karlsruhe, Karlsruhe.
- MEISSNER, C., KALTHOFF, N., KUNZ, M., ADRIAN, G., 2007, Initiation of shallow convection in the Black Forest mountains. *Atmospheric Research*, **86**, 42 - 60.
- MEISSNER, C., 2004, Modellierung der Konvektionsentwicklung unter Einfluss unterschiedlicher Oberflächeneigenschaften. Master Thesis (Diplomarbeit), Universität Karlsruhe, Karlsruhe.
- MINNIS, P., AYERS, J.K., PALIKONDA, R., PHAN, D., 2004, Contrails, Cirrus Trends, and Climate. *Journal of Climate*, **17**, 1671 - 1685.
- OLESEN, F.S. and GRASSL, H., 1985, Cloud detection and classification over oceans at night with NOAA-7. *International Journal of Remote Sensing*, **6**, 1435-1444.

OU, S.C., LIU, K.N., BAUM, B.A., 1996, Detection of Multilayer Cirrus Cloud Systems Using AVHRR Data: Verification Based on FIRE II IFO Composite Measurements. *Journal of Applied Meteorology*, **35**, 178191.

PRICE, J.C., 1989, Quantitative aspects of remote sensing in the thermal infrared. In *Theory and applications of optical remote sensing*, Ghassem Asrar (Editor), pp. 578-603 (John Wiley and Sons, Inc., USA).

REUTER, M., 2005, Identification of cloudy and clear sky areas in MSG SEVIRI images by analyzing spectral and temporal information. PhD dissertation, Freie Universität Berlin, Berlin.

ROJAS, M. and SETH, A., 2003, Simulation and sensitivity in a nested modelling system for South America. Part II: GCM boundary forcing. *J. Clim.*, **16**, 24542471.

SAUNDERS, R. and Kriebel, K.T., 1988, An improved method for detecting clear sky and cloudy radiances from AVHRR data. *International Journal of Remote Sensing*, **9**, 123 - 150.

SCHEPANSKI, K., TEGEN, I., LAURENT, B., HEINOLD, B., and MACKE, A., 2007, A new Saharan dust source activation frequency map derived from MSG-SEVIRI IR-channels. *Geophys. Res. Lett.*, **34**.

SCHMETZ, J., GOVAERTS, Y., KÖNIG, M., LUTZ, H-J., RATIER, A. and TJEMKES, S., 2002, *A Short Introduction to Meteosat Second Generation (MSG)* (EUMETSAT, Darmstadt).

SCHMID, J., 2005, The SEVIRI Instrument. EUMETSAT website ([http://www.eumetsat.int/Home/Main/Publications/Technical\\_and\\_Scientific\\_Documentation/Technical\\_Notes/SP\\_1124282611560?l=en](http://www.eumetsat.int/Home/Main/Publications/Technical_and_Scientific_Documentation/Technical_Notes/SP_1124282611560?l=en)).

SCHMIDT, A., 2008, Zeitreihen der Landoberflächentemperatur abgeleitet aus METEOSAT-7 Satellitendaten. PhD dissertation, Universität Karlsruhe, Karlsruhe.

STERN, N., 2006, *The Economics of Climate Change* (Cambridge University Press, Cambridge).

STRAHLER, A.N., 1965, *Introduction to physical geography* (New York, J. Wiley).

VOGEL, B., GROSS, G., WIPPERMANN, F., 1986, MESOKLIP (first special observation period): observations and numerical simulation - a comparison. *Boundary Layer Meteorology*, **35**, 83 - 102.

de WILDT, M.R., SEIZ, G., GRUEN, A., 2007, Operational snow mapping using multitemporal Meteosat SEVIRI imagery. *Remote Sensing of Environment*, **109**, 29 - 41.

WMO, 1957, *International cloud atlas (abridged edition)*, 62pp.

# Danksagung

An dieser Stelle möchte ich all jenen herzlich danken, die durch Rat und Tat zum Gelingen dieser Arbeit beigetragen haben. Insbesondere danke ich:

- Herrn Prof. Dr. H. Fischer für die Vergabe der interessanten und aktuelle Themenstellung, die Übernahme des Hauptreferates, die Durchsicht der Arbeit und die konstruktiven Verbesserungsvorschläge.
- Herrn Prof. Dr. Ch. Kottmeier für die freundliche Übernahme des Korreferates und interessanten Diskussionen während meiner Promotion.
- Herrn Folke Olesen und Herrn Gerd Schädler für die engagierte Betreuung, die fachliche Unterstützung, die ständige Diskussions- und sehr große Hilfsbereitschaft.
- Herrn Andreas Schmidt und Herrn Frank Göttsche für die Unterstützung und große Hilfsbereitschaft in den vergangenen drei Jahren.
- Allen Mitgliedern der IMK-MSA Arbeitsgruppe für die zahlreichen interessanten Gespräche, Diskussionen und das angenehme Arbeitsklima.
- Den Mitgliedern der Arbeitsgruppe Wasserkreislauf und Klimamodellierung für die Bereitstellung der CLM Daten.
- Dem Institut für Weltraumwissenschaften der Freien Universität Berlin für die Bereitstellung der Wolkenmaske.
- Ein ganz besonderer Dank gilt schließlich meiner Familie auf deren Unterstützung ich mich jederzeit verlassen konnte.